The Liquid Structure of Haloalkanes

Thesis submitted in accordance with the requirements of the university of Liverpool for the degree of Doctor in Philosophy by

Katherine Ann Mort

April 1998

To my parents and husband.

Abstract

This project has been concerned with deriving the intermolecular structure of liquid haloalkanes. Neutron diffraction experiments have been performed to produce experimental pair distribution functions. The molecular liquids investigated by this method have been trifluoromethane at 153 K, difluoromethane at 153 K, 1,1,1,2-tetrafluoroethane and 1,1,2,2-tetrafluoroethane, both at 200 K, 250 K and 300 K. The scattering data for the methane derivatives, and for the ethane derivatives at 200 K, have been fully analysed and a structure factor and pair distribution function for each is presented.

Molecular dynamics simulations have been performed to reproduce the experimental pair distribution functions, and internal energies of a variety of halomethanes. Although the initial work on the fully halogenated methanes was performed by Dr. C. D. Hall, the analysis of that work has been completed in this project. The intermolecular pair distribution function for bromotrifluoromethane and chlorotrifluoromethane has been reproduced by the simulations and the orientations of the molecules analysed. The pair distribution function for dichlorodifluoromethane has been simulated and the interpretation of the liquid structure performed with different conclusions to Dr. C. D. Hall being reached. The intermolecular structure of trifluoromethane has been simulated and, together with a reanalysis of the measurements made by Hall et al. on deuterated trifluoromethane, has led to a full interpretation of the liquid-state structure for this fluid. Finally attempts have been made to simulate the structure of difluoromethane but, as yet, a full interpretation has not been possible.

Acknowledgements

I would like to thank my family, particularly my parents, who looked after me and supported me throughout my time as a PhD student and without whom I probably would never been able to manage. I'd also like to thank my long suffering husband for his patience and understanding, and for allowing our wedding to be postponed for three years whilst I did my research.

Special thanks go to Kathy Johnson for all her help on both the academic side and when I wanted to throw the towel in. Thanks also go to David Cooper for all his help on the simulation and computer side of the project.

I'd like to thank the team at ICI, and particularly Andrew Burgess for all his help in the neutron scattering and simulations. Thanks are also due to Alan Soper and Spencer Howells from the Rutherford Appleton Laboratory for their help with the neutron scattering experiments.

I'd like to thank the EPSRC and ICI for funding the research

Table of Contents

Chapter One

Chapter Two

Chapter Three

Chapter Four

Chapter Five

Chapter Six

Chapter One

Liquid Structure

1.1 Introduction

The structure of a physical sample is normally taken to mean the spatial distribution of the atoms or molecules in the sample. In the case of a solid this means the positions of the equilibrium sites of the atoms, which are largely time independent. However, for a liquid, the component molecules or atoms possess enough energy to move around the sample. Thus their positions are largely time dependent and hence there is no equilibrium position. Clearly then some method is needed to define the structure in a liquid that takes this into account. If a snap shot of the liquid is considered, then it is possible to work out the distribution of the atoms in this snapshot. The structure is usually defined in terms of the two-particle, or pair distribution function, g(r), which is a continuous function describing the probability of two atoms being a distance r apart. Considering a series of snapshots of the liquid over time, and averaging the pair distribution function over all these snapshots, leads to a resultant pair distribution function that can be considered to describe the average liquid structure, i.e. a time-independent description of the structure of the liquid.

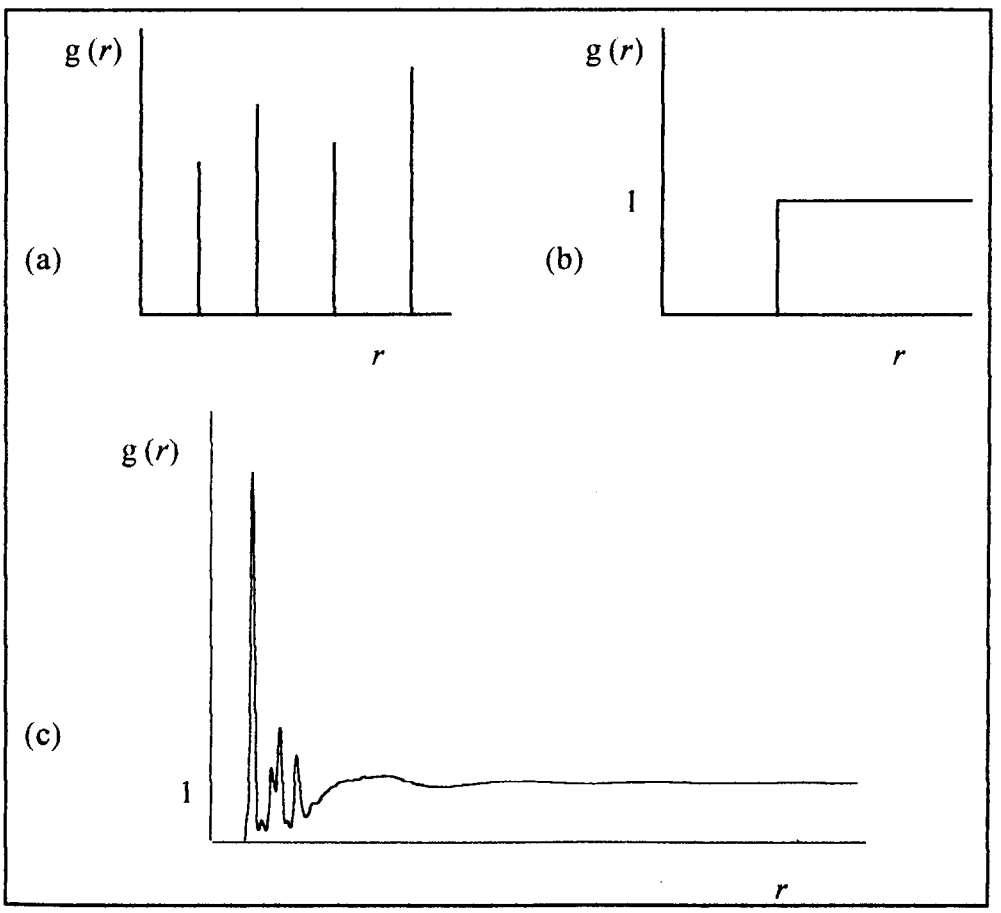

Figure 1.1 General pair distribution functions for (a) crystalline solid, (b) ideal atomic gas, and (c) molecular liquid.

For a crystalline solid, the pair distribution function consists of sharp peaks at the lattice spacings with nothing in-between (see figure 1.1). The pair distribution function for an ideal atomic gas would be zero within the distance of closest approach and would then step up to 1 and continue as a straight line. This shows the complete randomness of the ideal gas structure. A monatomic liquid would show a smooth curve rising to a maximum at a distance that is approximately twice the atomic radius and then oscillates about 1 with decreasing amplitude with increasing r. This indicates that the liquid shows short range structure, but averages out to randomness at long range. The pair distribution function is normalised to the ideal gas structure so that a value of 1 indicates the probability of finding two atoms with

that separation in a completely random system. A value less than 1 indicates a lower probability and a value greater than 1 indicates a higher probability.

Assuming that for a polyatomic molecular liquid, the pair distribution function is that for any *atom* in the sample, there will be sharp peaks at the start due to the intramolecular structure, followed by oscillations in the intermolecular region. Whereas for a monatomic liquid, the pair distribution function fully describes the liquid structure, for a polyatomic molecular liquid there is no inherent information about the relative orientations of the molecules. However, if the total pair distribution function is considered to be made up of a series of partial pair distribution functions, then each of these partial pair distribution functions describes the probability of finding two defined *atoms* at a distance r from each other. Knowing all the possible partial pair distribution functions for a liquid leads to an insight into how the molecules in the liquid interact and orientate themselves to each other.

Neutron diffraction experiments can be performed to obtain a *Structure Factor*, commonly referred to as $S(Q)$. This $S(Q)$ can be Fourier transformed to obtain the pair distribution function (see chapter two). The nature of neutron scattering means that the scattering from different elements, and isotopes of the same element, is different. It is possible, therefore, to perform isotopic substitution on molecules, for example D for H, and hence manipulate the data to obtain the partial pair distribution functions. However, frequently isotopic substitution is not possible or is prohibitively expensive and so some other means of extracting this data is needed.

In this project we have performed neutron scattering experiments to obtain an experimental pair distribution function, and then tried to reproduce this pair

distribution function by simulating the liquid using molecular dynamics. By using molecular dynamics we are able to obtain the partial pair distribution functions directly. If the simulation can reproduce the experimental pair distribution functions as well as matching the internal energy, then it can be considered to be a reasonable portrayal of the liquid and hence be used to understand the structure of the liquid.

1.2 Previous Work In The Simulation Of Liquids

A number of simulations have been performed in the past that have compared computer simulations with neutron diffraction data. Yarnell et al. [1] investigated liquid Argon near its triple point by performing neutron diffraction experiments. He then compared the experimental structure factor with that given by a molecular dynamics simulation using a Lennard-Jones effective pair potential. The agreement between the simulation and the experimental data was excellent. He also compared the pair distribution function with both the Lennard-Jones molecular dynamics simulation and a Monte Carlo simulation based on the BFW potential [2]. He found that the agreement between the experiment and simulation was good, and that the two simulations were almost indistinguishable.

Evans [3] compared the results of computer simulations, using the Lennard-Jones potential with fractional charges, of trichloromethane with the partial pair distribution functions derived from a number of neutron diffraction experiments [4,5,6,7,8,9,10]. The pair distribution functions from his simulations were similar but detailed agreement was not obtained. He attributed the failings to the fact that the pair distribution function obtained holds no information about orientation and only describes the structure in terms of the separation of the atoms. He also took account of the fact that the instrument precision was 1 %, and when coupled with the

problems analysing the neutron data, can lead to disagreement between neutron diffraction data.

Kneller and Geiger[11] compared the results of two molecular dynamics simulations, using a Lennard-Jones potential and an exp-6 potential, with the neutron diffraction results for dichloromethane from work by Jung et al.[12] Although there were a few dissimilarities between the experiment and simulation this was attributed to problems in the neutron data reduction.

Tetrachloromethane has proven to be a controversial problem with researchers. Gubbins [13] claims that the structure depends upon the long range electrostatic term, the octopole-octopole interaction. However other groups [14,15,16,17] claim that there is no such dependence. Eglestaff et al. [15] believe the molecule arranges itself in the 'apollo' or 'rocket' arrangement (see figure 1.2).

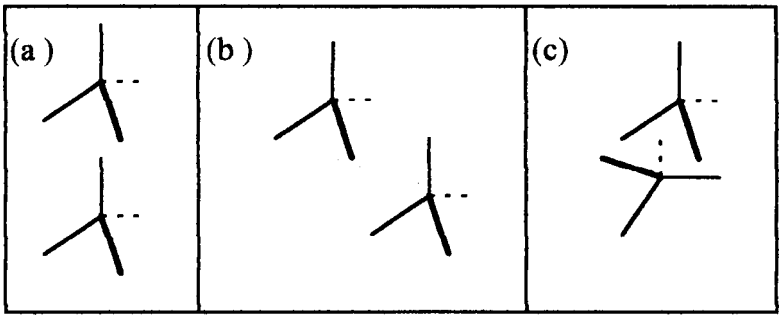

Figure 1.2 Proposed structures of trichloromethane. (a) apollo or rocket, (b) straddle, (c) interlocking

Lowden and Chandler [16] thought that the molecule arranged itself in a interlocking fashion (shown in figure 1.2(c)). McDonald et al. [17] discounted this interlocking type structure, but felt that the rocket structure was important. They also proposed the arrangement in figure 1.2(b) that is referred to as the straddle arrangement.

J. Böhm et al. investigated a variety of different liquids using molecular dynamics simulations [18,19]. The simulated structure factors were compared with diffraction data. These included chloromethane, acetonitrile, carbon dioxide and carbon disulphide, which gave good agreement with the experimental data although the peak heights were underestimated, dichloromethane, which exhibited a discrepancy in the height of the first peak and its shoulder for which they were unable to account, and trichloromethane, which varied in agreement to the experimental data according to the isotopic constitution of the molecule.

Ohba and Ikawa [20] compared two computer simulations with x-ray diffraction data. The simulations both used Lennard-Jones potentials but one also incorporated a fractional charge model. On comparison of the centre-of-mass pair distribution function it was found that both simulations were essentially the same and agreed with the experimental data. However the fractional charge simulation had angular correlations between the centres-of-mass whereas the uncharged model didn't. It can be taken from this paper the importance of reproducing the charge distribution in a molecular simulation as it can effect the underlying structure.

1.3 Literature Review

The rest of this chapter will constitute an overview of some recent work completed. Of particular interest is the use of simulation techniques to establish liquid structure. Unfortunately there are few comparative studies of neutron diffraction and molecular dynamics but other work to establish liquid structure has been performed using the reverse Monte Carlo method. Although this method has not been used in this study, as part of the aim was to produce intermolecular pair potentials as well as derive the liquid structure, it is a useful technique for

establishing the liquid structure and can lead to insight into the way the molecules are orientating themselves, and hence help in choosing suitable parameters for the pair potentials. It is also worthwhile comparing the success of the two simulation methods in predicting the structure of the liquid.

1.3.1 Orientational Correlation-Function for Molecular Liquids [21]

Author : A K Soper

As indicated earlier, the availability of isotopic substitution in neutron diffraction means that the partial pair distribution functions can be obtained directly from experiment. Recent work by A. K. Soper [21] has shown how these measured partial structure factors (the data obtained by neutron diffraction experiments that is then transformed into the pair distribution function, see chapter two) can be used to generate a detailed view of the local intermolecular orientational distribution function. Using the measured structure factors for liquid water, the corresponding maps of the orientational distribution function were derived. He was able to show that, whilst the molecules have a high probability to arrange themselves according to the directionality of the hydrogen bonds , there are also a range of other local orientations that are compatible with the neutron data. This evidence goes against past speculation that water forms short-lived "ice-like" clusters at ambient temperature and pressure.

The method shown gives a powerful tool to aid in the analysis of neutron data of liquids. However, in order to be able to utilise it, the partial structure factors must be available. This is only possible in molecular liquids where isotopic substitution is possible to be able to eliminate various distributions in the experimental data. The

molecules we are interested in do not have this ability and hence the method of molecular dynamics simulation was chosen.

1.3.2 Empirical Potential Monte Carlo Simulation of Fluid Structure [22]

Author : A. K. Soper

This paper uses Monte Carlo simulations to develop pair potential parameters in a similar method to the way in which potentials have been developed in our own project, that is changing the parameters in an iterative manner in order to reproduce the experimental data. The work not only compares to experimental neutron data, but, because pair potentials are included in the simulation, also compares the results to thermodynamic data. This is because there is only one unique solution that will reproduce all the experimental data and hence the simulation results can be taken as a good representation of the liquid.

The author uses a site-site Lennard-Jones potential (see equation 1.1) together with the simple point charge extended (SPCE) model of water.

$$U_{ij} = 4\varepsilon_{ij}\left[\left(\frac{\sigma_{ij}}{r_{ij}}\right)^{12} - \left(\frac{\sigma_{ij}}{r_{ij}}\right)^{6}\right] + \frac{q_i q_j}{4\pi\varepsilon_o r_{ij}} \qquad 1.1$$

Where U_{ij} is the effective pair potential between atoms i and j, ε_{ij} and σ_{ij} are the Lennard-Jones parameters, r_{ij} is the separation of the two atoms, q_i and q_j are the partial charges on i and j respectively, and ε_o is the permittivity of free space. The simulation is driven by equilibrating the energy distribution, unlike reverse Monte Carlo methods which are driven by equilibrating the value of chi^2, which measures how close the fit to the experimental structural data is. The Monte Carlo method allows a random walk through a wide range of configurations to find the minimum

energy. The parameters are altered until the pair distribution functions match the experimental distribution functions obtained by neutron scattering. The resulting pair distribution functions are compared to those obtained from neutron scattering. The total, and partial pair distribution functions are available from neutron scattering experiments and so the accuracy of the simulation structure can be ascertained.

The empirical potentials derived show qualitative similarities with the true SPCE potential, although there are quantitative differences. Although the experimental pair distribution functions are reproduced, the internal energy and pressure are not.

1.3.3 A Transferable Potential Model For The Liquid-Vapour Equilibria Of Fluoromethanes.[23]

Authors: S. C. Potter, D. J. Tildesley, A. N Burgess and S. C. Rogers.

This paper is concerned with the development of intermolecular potentials by performing molecular dynamics simulations of coexisting liquid-vapour phases on fluoromethanes to obtain orthobaric curves. The molecules investigated were difluoromethane, trifluoromethane and tetrafluoromethane. By comparing with experiment the authors have derived a force field for these molecules which consists of a site-site 12-6 Lennard-Jones potential supplemented with point charges at the atomic sites, to model the coulombic interactions. The structure, intramolecular forcefield, and point charges were obtained by performing *ab initio* molecular orbital calculations using the GAMESS [24] package with a TZVP basis set. Although the bonds in the simulation were constrained to the equilibrium values, the bond angles were allowed to vibrate. The bending constant was calculated from the change in energy produced by distorting the bond angle by five per cent. Two types of

molecular dynamics simulations were performed: two phase simulations to calculate the coexisting densities, and fully periodic bulk simulations of both coexisting phases to estimate the enthalpy of vaporization and the coexisting pressures. In the simulation of the two phase system, the long range corrections have been ignored. The two phase simulations were produced by taking a bulk fluid and running the simulation until the fluid had reached equilibrium. The periodic cell was then surrounded by two empty cells in the z direction and the system allowed to come to equilibrium, defined by no net drift in the coexisting densities. This equilibrated system was then allowed to run for five blocks of 1000 timesteps at constant energy. The orthobaric densities were fitted for each block and the standard deviation in the block averages gave an estimate of the error in the coexisting densities. The Lennard-Jones parameters were fitted to the data for difluoromethane, and then applied to trifluoromethane and tetrafluoromethane.

The model obtained reproduces the coexistence curve for difluoromethane reasonably well, although at the lower temperatures both the coexisting densities are greater than the experimental values. Despite various adjustments to the potential parameters the authors were unable to improve on this fit and they suggest that this problem is due to an inability of the potential to account for polarization effects, which are important in the liquid phase. The bulk liquid structure was compared to our own neutron pair distribution function obtained during the course of this project. Although the essential features are reproduced the simulation fails to reproduce the positions and heights of the maxima and produces a liquid that is too ordered compared with experiment. This is a problem we have also seen with our own simulations to this neutron structure.

The fitted Lennard-Jones parameters were transferred directly to trifluoromethane. The reproduction of the coexisting densities is good, to within three per cent of the experimental values. The model also reproduces the neutron pair distribution function, again obtained from this work, with good accuracy, although the position of the maxima are at a slightly lower r than the experiment.

The transferred potential to tetrafluoromethane produces a reasonable fit to the orthobaric curves, although the fit worsens with high temperature. Unfortunately neutron data for tetrafluoromethane has yet to be published and so a comparison to the liquid structure is not possible.

The authors also performed bulk simulations to obtain an estimate of the enthalpy of vaporization and the vapour pressure. Again, trifluoromethane produces the best agreement with the enthalpy experimental data being within the error of the simulation for three of the four temperatures investigated. Difluoromethane consistently underestimates the enthalpy of vaporization whilst tetrafluoromethane overestimates it. The model produces a reasonable agreement with the vapour pressures although it overestimates them for difluoromethane, and underestimates them for tetrafluoromethane, with trifluoromethane again producing the best results.

In conclusion, the authors have produced a working model that transfers between three fluoro-methanes, and reproduces the coexistence curves for each. The model also reproduces the liquid structure for trifluoromethane, but not for difluoromethane. It is interesting to see that success in fitting one type of experimental data does not automatically lead to success in fitting another, particularly the exacting task of fitting the liquid structure, and the converse could be taken as being true. It would be an interesting exercise to implement the parameters obtained in our study into such a two phase simulation to see if the coexistence

densities are reproduced. As can be seen from the above study and our work on halomethanes, the use of simple isotropic potentials may be a limiting factor in the success of reproducing experimental data with these more complicated systems.

1.3.4 Structural Investigation Of Liquid Formic Acid Using X-Ray, Neutron Diffraction, And Reverse Monte Carlo Study [25]

Authors : P. Jedlovszky, I. Bakó, Pálinkás, and J. C. Dore

Although this paper is not a comparison between molecular dynamics simulations and experiment, but rather using reverse Monte Carlo to fit to experimental neutron and x-ray data, it is of interest as a method of using computer simulation to extract the structural information from the experimental results that would otherwise be difficult to obtain.

The authors have performed x-ray and neutron diffraction studies on methanoic acid. They then performed reverse Monte Carlo simulations, fitting simultaneously to two total structure functions resulting from these experiments. This lead to a detailed analysis of the intramolecular structure from the experimental data, and the intermolecular structure from the simulation in association with the experiments.

The reverse Monte Carlo method used in the study was developed by McGreevy and Pusztai [26]. The difference between the reverse Monte Carlo method and that of the ordinary (Metropolis) Monte Carlo method is the difference between measured and calculated structure functions or pair distribution functions of the system are minimized instead of the system's potential energy. The molecules were represented by a flexible group of atoms with co-ordination constraints. The distance of atoms of types A and B in a molecule were described by two co-ordination

constraints. The first constraint means that, within a sphere of radius r_1 around every A atom there are no atoms of B, while the second constraint ensures that every A atom has exactly one B neighbour within a sphere of radius r_2, where $r_2 > r_1$. These constraints were introduced between every pair of atoms which were bonded to each other defining the bond lengths, and between every pair of atoms which were bonded to a common third atom. As the distance from the common neighbour atom were already constrained, a constraint of this type defines a bond angle around this common neighbour. The exception to this definition was that no value for r_2 was used for the acidic hydrogen and either of the oxygens. A third constraint can be added to prevent non-bonded atoms approaching too closely. This makes atoms A singly co-ordinated to atoms B within a sphere of radius r_3 ($r_3 > r_2$). This ensures a space around atom A in which only atoms within the molecule may appear.

The x-ray data obtained by the authors from their experiments was analysed to give the intramolecular structure of the methanoic acid, and this structure was compared to that from previous gas electron diffraction studies [27] and the neutron diffraction experimental data that had previously been reported [28]. The results show a good agreement between both sets of data and the results of the x-ray experiment.

As the geometry of the methanoic acid in the reverse Monte Carlo simulation was defined only by the method above it was necessary that the results from the simulation reproduced the intramolecular structure. This is because a large proportion of the structure factor is due to this intramolecular structure. To ascertain if their simulation was reproducing the intramolecular structure the authors examined the values of three angles: the O=C-O bond angle, the C-O-H bond angle, and the angle between the O-H bond and the O=C-O plane. They found that the

results of these checks on the two bond angles agreed with the findings from their experiments, the distribution for the third angle was broad but still produced a realistic geometry for the molecule.

The neutron diffraction experiments had been carried out on a mixture of hydrogenated and deuterated methanoic acid (HCOOD : DCOOD 0.641 : 0.359) in order to produce an effective coherent scattering length of the acidic hydrogen of zero. They also performed experiments on the pure samples of DCOOD and HCOOD. The reverse Monte Carlo simulation was run to fit the former of these simultaneously with the structure factor from the x-ray experiment. The results of the pure liquid neutron scattering experiments were compared to the results of the simulation.

The fit to the structure factors for the x-ray and neutron experiments by the simulation are quite good, although it would appear that there is possible structure left in the residue. The authors suggest this residue is due to the fact that both experiments produced slightly different intramolecular structures, but the fit assumed both were the same. The comparison between the pair distribution functions for the neutron scattering experiments and the simulation are good, in particular the fit to the peak associated with the hydrogen bond. However the overlap between the intra- and intermolecular structures (approximately 2 - 2.5 Å) is poorly fitted and this is possibly due to the simulation being unable to distinguish the inter and intra separation fitting at this point. However the authors feel that this problem is not so important as to effect the results with respect to the intermolecular structure. Analysis of their reverse Monte Carlo data leads to the prediction that methanoic acid forms two types of hydrogen bond in the liquid phase, one where the carbonyl oxygen is the hydrogen bond acceptor, and another where the hydroxylic oxygen is

the acceptor. This latter type is not found in either the solid or gas phase, but constitutes forty per cent of the hydrogen bonds in this analysis. The average number of the hydrogen bonding interactions per molecule appears to be two. Integration of the peaks leads to an estimation of the co-ordination number of the molecule to be between 11 - 13. This is interesting because although the molecule is hydrogen bonded it still forms a closely packed liquid, instead of a more open structure. This could be explained by the cluster analysis of the reverse Monte Carlo simulation. Here they found that, unlike water, methanoic acid does not form a continuous space filling hydrogen bonded network, but instead contains small hydrogen bonded oligomers built up of just a few molecules, i.e. it prefers to form small branched chains than cyclic structures.

In conclusion the paper presents a very thorough structural analysis of liquid methanoic acid using the output from a reverse Monte Carlo simulation, fitted to x-ray and neutron data. However it should be born in mind that these types of simulations have certain problems:

There is no inherent intermolecular potential included in the simulation and so the only information that can be verified is the outputted structure factors and pair distribution functions. This would mean that the conclusions drawn are a possible answer, but that there may be others that would equally well fit the data. Studies on water [29] show that the configuration produced by reverse Monte Carlo simulations are not uniquely related to the pair correlation functions that are used in the fitting. This is why molecular dynamics, with its dynamical information, can provide more confidence in the validity of the solution obtained. There is the added advantage that the final solution also contains a pair potential that can then be used to investigate other properties.

A large percentage of the information contained within the structure factors is due to the intramolecular structure, which is already known, and the more interesting intermolecular structure lies beneath this. This means that in fitting this data care must be taken that the model reproduces the intramolecular structure well otherwise the simulation will waste a good number of moves trying to compensate for the inadequacies of the structure, instead of fitting the intermolecular region. Another problem associated with reverse Monte Carlo simulations is that moves are accepted according to the fit to the structure. This does not necessarily drive a true random walk through possible configurations, and the final result can sometimes depend on the original starting positions of the simulation.

1.3.5 Effective Potentials for Liquid Simulation Of the Alternative Refrigerants HFC-32: CH_2F_2 and HFC-23: CHF_3 [30]

Authors : M. Lísal and V. Vacek.

The authors have constructed a density-dependent semiempirical effective pair potential for difluoro- and trifluoromethane which reproduces the liquid thermodynamic properties. They modelled the molecules as rigid with interaction centres at the atomic sites. This geometry was obtained from the gas-phase monomers. The van der Waals interactions were described using the Halgren Buf *n* - *m* potential [31] which has the general form:

$$U = \varepsilon \left[\frac{(1+\delta)\, r_{\min}}{r + \delta r_{\min}} \right]^{(n-m)} \left[\frac{(1+\gamma) r_{\min}^{\,m}}{r^m + \gamma\, r_{\min}^{\,m}} - 2 \right] \qquad 1.2$$

where ε is the well depth, $r_{\min}$ is the minimum-energy distance, δ and γ are the shape parameters and r is the interatomic distance. A choice of $n = 12$, $m = 6$, and $\gamma = \delta = 0$ gives the 12 - 6 Lennard-Jones function. However the choice in the paper is $n = 14$

and $m = 7$ with $\gamma = 0.12$. The reasons this potential form was chosen was it contains only one energy and one length parameter (ε and r_{min}). However the potential is finite as $r \rightarrow 0$, which avoids the strong divergence found in the Lennard-Jones potential. It reproduces a dispersion power-series expansion (r^{-6}, r^{-8}, r^{-10}) for distances up to a few times r_{min}. The adjustable parameter, δ, controls the magnitude of the dispersion power-series and influences only very slightly the distance and magnitude of the dispersion. Because the Axilrod-Teller interaction can be absorbed into the pair potential when the C_6 coefficient of the dispersion energy $-C_6 / r^6$ varies linearly with the density [32], they introduced a linear density-dependence of the shape parameter δ.

The electrostatic potential was modelled by the Coulombic potential

$$U_c = \frac{q_a q_b e^2}{4\pi\varepsilon_0 r_{ab}} \qquad 1.3$$

where q_a and q_b are the atomic charges, e is the electron charge, and ε_0 is the permittivity of free space.

An account is taken within the potential for the energy needed to create the effective dipole μ^{eff} from the gas phase value μ^{gas}. This enhanced dipole is regarded as acceptable due to the many-body induced polarization effects on the molecule. Thus the energy needed to create the induced dipole moment $\mu = \mu^{eff} - \mu^{gas}$, is given by

$$U_{self} = \frac{\mu^2}{2\alpha} \qquad 1.4$$

where α is the molecular polarizability. The correction for the fluctuation of the dipole moment can also be included, by approximating it to

$$U_{\text{flct}} = \frac{3\,k_B\,T}{2}\left(\frac{\mu^{\text{eff}}}{\mu^{\text{gas}}} - 1\right) \qquad 1.5$$

where k_B is the Boltzmann constant and T is the temperature.

Thus the final form of the potential between two molecules i and j consisting of 5 atoms each is

$$U_{ij} = \sum_{a=1}^{5}\sum_{b=1}^{5}\left(\varepsilon_{ab}\left[\frac{(1+\delta(\rho))\,r_{\min}}{r_{ab}+\delta(\rho)r_{\min}}\right]^{7}\left[\frac{1.12r_{\min}^{\,7}}{r_{ab}^{\,7}+0.12r_{\min}^{\,7}}-2\right]+\frac{q_a q_b e^2}{4\pi\varepsilon_0 r_{ab}}\right)+U_{\text{self}}+U_{\text{flct}} \qquad 1.6$$

The well depths ε and the energy-minimum distances $r_{\min}$ were taken from the AMBER molecular mechanical force field with the interaction between unlike atoms being calculated by the Lorentz-Berthelot mixing rules. The charges were those predicted by Gough et al. [33,34] and were obtained from a fit to the electrostatic potential using an *ab initio* calculation with a 6 - 31G* basis set. This gave a dipole that was approximately nine per cent greater than the gas phase.

The authors determined the linear density-dependence of the shape parameter δ by performing molecular dynamics simulations at constant temperature, volume and number of molecules on the saturated liquid curves and adjusted the parameter to give the best agreement with experimental second virial coefficients.

The authors compare their results of constant pressure molecular dynamics simulations to the latent enthalpy of vaporization and molar volume for the molecules of interest at five different temperatures, and the molar volume. They also compared their constant volume results with the enthalpy of vaporization and experimental values of PV/RT. They reproduce the molar volume and enthalpy well for difluoromethane but the trifluoromethane simulations consistently overestimate

the enthalpy of vaporization. The simulations correctly produced the molar volume, but this is to be expected as δ was obtained from the virial coefficients. Their prediction of the PV / RT is within experimental uncertainty, although several of the calculated values are negative.

The authors analysed the partial pair distribution functions produced by their simulations although they were unable to compare them to the neutron data that is only now available. They assign an interlocking type structure to both types of molecule based on their analysis of these distributions. Unfortunately the structure they propose does not appear to fit their simulation results as it takes no account of the H...H distance which is substantially shorter than their proposed structure will produce.

The paper also compares the partial pair distribution functions from their simulations, with that resulting from a simulation using their energy and length parameters in a Lennard-Jones potential. However it appears from the paper that these were substituted directly into the Lennard-Jones potential, whereas in actual fact the minimum energy distance r_{min} in the Buf potential does not correspond directly with σ, which is the distance at which the potential is zero. The comparison of the plots indicates that the Lennard Jones is more repulsive, and hence gives greater structure at low r than the Buf potential but this would be expected if the minimum energy distance were used instead of σ.

In conclusion, the authors have produced a potential that reproduces thermodynamic data for difluoromethane well, and gives a fair reproduction of the data for trifluoromethane although as mentioned earlier the reproduction of the molar volume would be expected. The poor analysis of the structural information is disappointing as only a proper analysis could be compared to our own conclusions

for trifluoromethane. The comparison of potentials would be interesting if there were more information concerning the Lennard-Jones simulations. On reading this paper we attempted to perform our own simulations, inserting their Buf parameters (modified) into a Lennard-Jones potential and comparing to our neutron data. We found the simulations produced too much structure and the comparisons in the paper would have been helpful in ascertaining if the original potential would have been an improvement over the Lennard Jones structure if we could have been confident that the necessary adjustments to the potential had been made.

1.3.6 Effective Potentials For Liquid Simulation Of The Alternative Refrigerants HFC-134a : CF_3CFH_2 and HFC-125 : CF_3CF_2H [35]

Authors : Martin Lisal and Václav Vacek

This paper has been produced by the same authors as the previous paper. They use the Buf 14-7 potential again and the molecules are treated as semi-rigid, with rotation about the central bond being allowed. Again the parameters were taken from the AMBER force field [33,34], with the shape parameter, δ, being fitted to experimental saturated pressures and saturated-liquid densities, by a series of constant volume and temperature molecular dynamics simulations. The simulations for both molecules reproduce the molar volume, enthalpy of vaporization, and PV / RT with good accuracy.

Again the authors reproduce the structural information from their simulation, and compare the two molecules. Unfortunately our neutron data for HFC-134a is unpublished yet and a comparison with the data would be interesting. The two molecules show a very close similarity in structure, and their C...C distribution is remarkably different to that of ethane in their comparison. The paper also contained

the self-diffusion coefficients calculated from the simulations but unfortunately their is no experimental data to compare to.

In conclusion the authors have managed to reproduce the thermodynamic properties of the two molecules with good accuracy with their potential.

1.3.7 Neutron Diffraction And Molecular Dynamics Study Of Liquid Benzene And Its Fluorinated Derivatives As A Function Of Temperature. [36]

Authors: M. I. Cabaco, Y. Danten, M. Besnard, Y., Guissani, B. Guillot

The authors performed neutron diffraction experiments on deuterated benzene (C6D6), deuterated trifluorobenzene (C6D3F3) and hexafluorobenzene (C6F6). The studies were on the pure liquids at various temperatures between 270 K and 350 K, along the liquid-vapour coexistence curves between melting point and boiling point. The liquids were also simulated using molecular dynamics and the results analysed.

The intermolecular structure factors for benzene and hexafluorobenzene show similar features, although peak heights are different. However the structure factor for trifluorobenzene shows quite marked differences. The intermolecular structure factors were converted into pair distribution functions via a direct Fourier transform. The curves for benzene and hexafluorobenzene are similar, although the positions of the peak heights for hexafluorobenzene are at slightly longer *r*. The distribution function for trifluorobenzene displays peaks at roughly the same position as for hexafluorobenzene but the heights are less pronounced and the general shape are different. The authors explain small oscillations seen in the curves by packing of the molecules. Considering that the pair distribution function was obtained from a

direct Fourier transform of a truncated function with a modification function to reduce the truncation effects, these features could just be a spurious result of the transform and not bare any physical meaning.

Molecular dynamics simulations were performed that used the Williams potential [37,38] placed at atomic sites.

$$U_{\alpha\beta}(r) = B_{\alpha\beta}\exp(-C_{\alpha\beta}r_{\alpha\beta}) - A_{\alpha\beta}(r_{\alpha\beta})^{-6} + q_\alpha q_\beta (r_{\alpha\beta})^{-1} \qquad 1.7$$

where A, B, C are parameters of the potential, $U_{\alpha\beta}$ is the potential energy, α and β are atoms and $r_{\alpha\beta}$ is the distance between them. The partial charges were obtained from *ab initio* calculations, or chosen to reproduce the experimental quadrupole moment of the molecule. The comparison between the experimental intermolecular structure factor and the structure factor calculated from the simulations shows a broad agreement. The simulation reproduces the positions of the first peaks correctly but over estimates the heights. The agreement between experimental and simulated pair distribution functions is better. The agreement for benzene is good, whilst for hexafluorobenzene, and trifluorobenzene is reasonable. The authors feel the reproduction for the trifluorinated species is the worst, but it would seem that this is because the simulation fails to reproduce the small oscillations mentioned earlier. As these could simply be an artifact of the transform then they could be discounted.

Both the neutron diffraction experiments and the molecular dynamics simulations show that the local ordering is only very slightly affected in the temperature range under investigation.

The authors show by the analysis of their results that the orientational local order in liquid benzene is almost isotropic at distances corresponding to the first shell of neighbours. Hexafluorobenzene exhibits maxima for parallel and

perpendicular configurations that occur at distinct r values, with the parallel being predominant at short distances. For 1,3,5-trifluorobenzene, the orientational order of the first shell is strongly anisotropic, and a stacked configuration involving a pair of molecules is observed at short distances of about 4 Å. This finding, together with the value of the co-ordination number found from the simulation data clearly shows the existence of dimers (sandwichlike). The structure of hexafluorobenzene appears to be midway between that for trifluorobenzene and benzene.

In conclusion the authors have produced good experimental structure factors from neutron scattering for the three benzene molecular liquids. They have managed to reproduce this data using molecular dynamics and have analysed their simulation results to show the intermolecular structure in the liquids. The work shows how the combination of molecular dynamics and neutron scattering can be a powerful tool in the analysing of liquid structure.

---

1 YARNELL, J. L., KATZ, M. J., WENZEL, R. G., KOENIG, S. H., 1973, *Phys. Rev. A*, **7**, 2130

2 BARKER, J. A., FISHER, R. A., WATTS, R. O., 1971, *Molec. Phys.*, **21**, 657

3 EVANS, M. W., 1983, *J. Mol. Liq.*, **25**, 211

4 BERTAGNOLLI, H., 1981, *Ber. Buns. Phys. Chem.*, **85**, 644

5 BERTAGNOLLI, H., LEICHT, D. O., ZEIDLER, M. D., CHIEUX, P., 1978, *Mol. Phys.*, **36**, 1769

6 BERTAGNOLLI, H., LEICHT, D. O., ZEIDLER, M. D., CHIEUX, P., 1978, *Mol. Phys.*, **35**, 199

7 BERTAGNOLLI, H., ZEIDLER, M. D., 1978, *Mol. Phys.*, **35**, 177

8 BERTAGNOLLI, H., LEICHT, D. O., ZEIDLER, M. D, 1978, *Mol. Phys.*, **35**, 193

9 BERTAGNOLLI, H., CHIEUX, P., 1980, *Ber. Buns. Phys. Chem.*, **84**, 1225

10 STEINHAUSER, O., BERTAGNOLLI, H., 1981, *Ber. Buns. Phys. Chem.*, **85**, 45

11 KNELLER, G. R., GIEGER, A., 1989, *Molec. Phys.*, **68**, 487

12 JUNG, W. G., ZEIDLER, M. D., CHIEUX, P., 1989, **68**, 473

13 GUBBINS, K. E., GRAY, C. G., EGELSTAFF, P. A., ANANTH, M. S., 1973, *Molec. Phys.*, **25**, 1353

14 BERMEJO, F. J., ENCISO, E., ALONSO, J., GARCIA, N., HOWELLS, W. S., 1988, *Molec. Phys.*, **64**, 1169

15 EGELSTAFF, P. A., PAGE, D. I., POWLES, J. G., 1971, *Molec. Phys.*, **20**, 881

16 LOWDEN, L. J., CHANDLER, D., 1974, *J. Chem. Phys.*, **61**, 5228

17 McDONALD, I. R., BOUNDS, D. G., KLEIN, M. L., 1982, *Molec. Phys.*, **45**, 521

18 BÖHM, H. J., MEISSNER, C., AHLRICHS, R., 1984 *Molec. Phys.*, **53**, 651

19 BÖHM, H. J., AHLRICHS, R., 1985, *Molec. Phys.*, **54**, 1261

20 OHBA, T., IKAWA, S., 1991, *Molec. Phys.*, **73**, 999

21 SOPER, A. K., 1994, *J. Chem. Phys.*, **101**, 6888

22 SOPER, A. K., 1996, *J. Chem. Phys.*, **202**, 295

23 POTTER, S. C., TILDESLEY, D. J., BURGESS, A. N., ROGERS, S. C., 1997 *Molec. Phys.*, preprint, accepted

24 GUEST, M. F., KENDRICK, J., GAMESS, Daresbury Laboratory, Warrington, U.K

25 JEDLOVSKY, P., BAKÓ, I., PÁLINKÁS, G., DORE, J. C., 1995, *Mol. Phys.*, **86**, 87

26 MCGREEVY, R. L., PUSZTAI, L., 1988, *Molec. Simul.*, **1**, 359

27 ALMENNINGEN, a., BASTIANSEN, O., MOTZFELDT, T., 1969, *Acta. Chem. Scand.*, **23**, 2848

28 SWAN, G. I., DORE, J. C., BELLISENT FUNEL, M. C., in preparation; SWAN, G. I., PhD Thesis at the University of Kent at Canterbury.

29 JEDLOVSKY, P., BAKO, I, PALINKAS, G, RADNAI, T, SOPER, A. K., 1996, *J. Chem. Phys.*, **105**, 245

30 LÍSAL, M., VACEK, V., 1996, *Fluid Phase Equil.*, **118**, 61

31 HALGREN, T. A., 1992, *J. Am. Chem. Soc.*, **114**, 7827

32 STENSCHKE, H., 1994, *J. Chem. Phys.*, **100**, 4704

33 GOUGH, C. A., DEBOLT, S. E., KOLLMAN, P. A., 1992, *J. Comput. Chem.*, **8**, 963

34 GOUGH, C. A., PEARLMAN, D. A., KOLLMAN, P. A., 1993, *J. Chem. Phys.*, **99**, 9103

35 LÍSAL, M., VACEK, V., 1997, *Fluid Phase Equil.*, **127**, 83

36 CABACO, M. I., DANTEN, Y., BESNARD, M., GUISSANI, Y., GUILLOT, B., 1997, *J. Phys. Chem. B*, **101**, 6977

37 WILLIAMS, D. E., COX, S. R., 1984, *Acta. Crystallogr.*, **B40**, 404

38 WILLIAMS, D. E., HOUPT, D. J.., 1986, *Acta. Crystallogr.*, **B42**, 286

Chapter Two

Neutron Diffraction

2.1 Introduction

Sources of reference for this chapter have been Dr. C. D. Hall's thesis [1], *Chemical Applications of Thermal Neutron Scattering* by B. T. M. Willis (Oxford University Press)[2] and *Neutron Scattering in Chemistry* by G. E. Bacon (Butterworths)[3].

In 1932 Chadwick performed an experiment in which Beryllium interacted with alpha particles from natural Polonium. From this experiment he produced a low flux of a new particle, the neutron. Even though the flux from this experiment was low it was still sufficient to show, in 1936, that these neutrons could be diffracted by condensed materials. When the first nuclear-fission reactor CP1 (Chicago Pile 1) was developed in 1942 the attainable neutron flux increased seven fold from that produced by Chadwick. Since then spallation sources, such as that at the Rutherford Appleton Laboratory, have been developed. These fire pulses of high energy protons at a target such as Uranium, to produce neutrons as well as other nuclear particles.

2.2 The Theory of Neutron Scattering

2.2.1 The Neutron

The neutron is a subatomic particle with a mass of 1.675×10^{-27} kg, and a spin of 1/2 with a magnetic dipole moment of 1.913 nuclear magnetons. The energy of neutrons can be categorised as three different types:

epithermal, wavelength < 1 Å

thermal, wavelength between 1 Å and 3.5 Å

cold, wavelength > 3.5 Å.

Reactor sources produce neutrons with energies in the thermal and cold regions, spallation sources also produce epithermal neutrons. Diffraction studies are mainly interested with neutrons that possess energy in the thermal range. These neutrons are good at elucidating the structure and dynamics of the condensed phase because:

1. thermal neutrons have wavelengths of the order of interatomic spacings in condensed materials;
2. the energy of thermal neutrons is of the order of the vibrational excitation energies in the material;
3. neutrons are uncharged and can penetrate deeply into bulk samples;
4. the neutron scattering process is dependent upon the nature of the target atom and varies for both the atomic mass and the atomic number;
5. interaction of the neutron's magnetic moment with unpaired electrons in magnetic materials means that neutrons are good at probing magnetism.

2.2.2 Elastic And Inelastic Scattering

Upon collision of a neutron with a target nucleus two processes can occur. Either the neutron will lose some of its energy to the nucleus, in which case the scattering is *inelastic*, or it will retain all of its energy, in which case the scattering is *elastic*. In all collisions both types of scattering occur, but each leads to different information about the target sample. Inelastic scattering gives information on the dynamic effects, such as vibrational states, diffusion and sound modes of the system, whereas elastic scattering leads to information on the shapes, bond distances and the intermolecular / interparticle spacing. Thus it is necessary, when considering an experiment, to design the conditions so that the undesired scattering event is minimised. In the processing of the experimental data the elastic scattering must be separated from the inelastic scattering.

The experiments performed during this project have been elastic scattering and so the theory of neutron scattering presented here will be limited to this type of scattering.

2.2.3 Coherent And Incoherent Scattering

As a neutron possesses spin it can interact with a target nucleus that also has a non-zero spin state. This means that it can either be scattered *coherently* or *incoherently* (regardless of whether the collision is elastic or inelastic). As the name implies, coherent scattering leads to information but incoherent scattering only leads to background 'noise'.

Non-spin nuclei scatter totally coherently, but when the nucleus possesses spin I it can interact with the neutron in one of two ways. A compound nucleus (nucleus + neutron) will take a spin of $(I+1/2)$ when the spins are parallel (coherent),

or I-1/2), when the spins are anti-parallel (incoherent). It is not possible to predict which arrangement of spins will occur [4] however there is a probability of the compound nucleus being either coherent or incoherent

$$p(w_+) = \frac{(I+1)}{(2I+1)} \qquad 2.1$$

$$p(w_-) = \frac{I}{(2I+1)} \qquad 2.2$$

where $p(w_+)$ is the probability of spin being coherent and $p(w_-)$ is the probability of spin being coherent.

2.2.4 Basic Theory of Nuclear Scattering

Considering the particle-wave duality of neutrons it is possible to think of a beam of neutrons being represented by the plane wave $\exp(i\mathbf{k}.\mathbf{r})$, where $\mathbf{r}$ is the position vector and $\mathbf{k}$ the wave vector. The magnitude of $\mathbf{k}$ is $2\pi/\lambda$, where λ is the de Broglie wavelength. Since $\mathbf{k}$ is a vector and λ is a scalar, it is better to use the wave vector of the neutron beam in preference to its wavelength. $\mathbf{k}$ is related to the neutron velocity, $\mathbf{v}_n$ by

$$\hbar\mathbf{k} = m_n\mathbf{v}_n \qquad 2.3$$

where $\hbar = h/2\pi$ and m_n is the neutron mass. This gives the kinetic energy as

$$E = \frac{1}{2}m_n v_n^2 = \frac{\hbar^2 k^2}{2m_n} \qquad 2.4$$

If this plane wave is incident on a particle *fixed* at $\mathbf{r}'$ (see figure 2.1) then the scattered neutrons can be represented by a spherical wave emanating from the point with position vector $\mathbf{r}'$.

It is shown in standard text books [5] that the solution of the Schrödinger wave equation:

$$-\frac{\hbar^2}{2m_n}\nabla^2\psi(\mathbf{r}) + V(\mathbf{r})\psi(\mathbf{r}) = E\psi(\mathbf{r}) \qquad 2.5$$

for a spherically symmetrical potential $V(\mathbf{r})$ at large $|\mathbf{r} - \mathbf{r}'|$ is

$$\psi(\mathbf{r}) = e^{i\mathbf{k}.\mathbf{r}} - \frac{1}{(4\pi)}\frac{2m_n}{\hbar^2}\int\frac{e^{i\mathbf{k}'.(\mathbf{r}-\mathbf{r}')}}{|\mathbf{r}-\mathbf{r}'|}V(\mathbf{r}')\psi(\mathbf{r}')d\mathbf{r}' \qquad 2.6$$

with $d\mathbf{r}'$ being a small volume element.

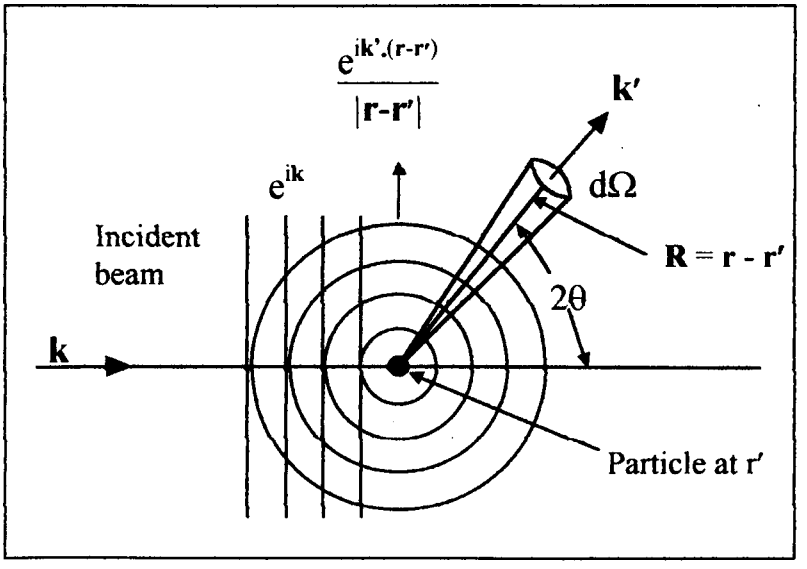

Figure 2.1 Scattering of a plane wave by spherically symmetrical potential field. dΩ is a small solid element within which neutrons are counted (such as in a detector) and 2θ is the angle that the neutron has been scattered from the original direction.

The second term in equation 2.6 represents a superposition of all the spherical waves of wave vector $\mathbf{k}'$ scattered from a source of strength $(2m_n/\hbar^2)V(\mathbf{r}')\psi(\mathbf{r}')$ at $\mathbf{r}'$. Putting the wave function $\psi(\mathbf{r}')$ in this term equal to that of the incident beam gives the first Born approximation:

$$\psi(\mathbf{r}) = e^{i\mathbf{k}\cdot\mathbf{r}} - \frac{1}{4\pi}\frac{2m_n}{\hbar^2}\int \frac{e^{i\mathbf{k}'.(\mathbf{r}-\mathbf{r}')}}{|\mathbf{r}-\mathbf{r}'|} e^{i\mathbf{k}'\cdot\mathbf{r}} V(\mathbf{r}')d\mathbf{r}' \qquad 2.7a$$

which on reduction yields

$$\psi(\mathbf{r}) = e^{i\mathbf{k}\cdot\mathbf{r}} - \frac{1}{4\pi}\frac{2m_n}{\hbar^2}\int \frac{e^{i\mathbf{k}\cdot\mathbf{r}}}{|\mathbf{r}-\mathbf{r}'|} e^{i(\mathbf{k}-\mathbf{k}')\cdot\mathbf{r}} V(\mathbf{r}')d\mathbf{r}' \qquad 2.7b$$

hence

$$\psi(\mathbf{r}) = e^{i\mathbf{k}\cdot\mathbf{r}} - \frac{1}{4\pi}\frac{2m_n}{\hbar^2}\int \frac{e^{i\mathbf{k}'\cdot(\mathbf{R}'+\mathbf{r}')}}{|\mathbf{R}'|} e^{i(\mathbf{k}-\mathbf{k}').\mathbf{r}'} V(\mathbf{r}')d\mathbf{r}' \qquad 2.7c$$

where $\mathbf{r} - \mathbf{r}'$ has been replaced with $\mathbf{R}'$.

If there are n_0 neutrons incident on unit area in unit time, and if $d\Omega$ is an element of solid angle in which the number of neutrons scattered from $\mathbf{r}'$ is counted (such as a detector), then it would be expected that the number counted is proportional both to n_0 and to $d\Omega$. The factor of proportionality is called the *Differential Scattering Cross-Section* and is denoted $d\sigma/d\Omega$. In this case, the plane wave term $\exp(i\mathbf{k}.\mathbf{r})$ is a representation of a wave of unit density and velocity $\hbar\mathbf{k}/m_n$, so that n_0 is $\hbar k/m_n$. The

spherically-scattered wave, $f\exp(i\mathbf{k}'\cdot\mathbf{R}')/|\mathbf{R}'|$, represents a wave of density $|f|^2/R'^2$ and velocity $\hbar\mathbf{k}'/m_n$, where the amplitude f is

$$f = -\frac{1}{4\pi}\frac{2m_n}{\hbar^2}\int e^{i(\mathbf{k}-\mathbf{k}')\cdot\mathbf{r}'}\, V(\mathbf{r}')d\mathbf{r}' \qquad 2.8$$

The number of scattered neutrons per second crossing the area $|\mathbf{R}'|^2 d\Omega$ in the solid angle $d\Omega$ is

$$\frac{|f|^2}{|\mathbf{R}'|^2}\cdot\frac{\hbar k'}{m_n}\cdot|\mathbf{R}'|^2 d\Omega \qquad 2.9$$

and so,

$$\frac{d\sigma}{d\Omega} = \frac{1}{N}\cdot\frac{|f|^2}{|\mathbf{R}'|^2}\cdot\frac{\hbar k'}{m_n}\cdot|\mathbf{R}'|^2 = \frac{k'}{k}\left(\frac{1}{4\pi}\int e^{i(\mathbf{k}-\mathbf{k}')\cdot\mathbf{r}'}\frac{2m_n}{\hbar^2}V(\mathbf{r}')d\mathbf{r}'\right)^2 \qquad 2.10$$

The scattering is elastic for fixed nuclei so the scalar value of the momentum before and after is the same, i.e. $|\mathbf{k}| = |\mathbf{k}'|$. However as momentum is a vector quantity there is a change in momentum at collision. This change is represented by the *Momentum Transfer Wave Vector*, $\mathbf{Q}$:

$$\mathbf{Q} = \mathbf{k} - \mathbf{k}', \qquad 2.11$$

thus the differential scattering cross-section can be written as:

$$\frac{d\sigma}{d\Omega} = \left|\frac{1}{4\pi}\int e^{i\mathbf{Q}\cdot\mathbf{r}'}\frac{2m_n}{\hbar^2}V(\mathbf{r}')d\mathbf{r}'\right|^2 \qquad 2.12$$

The equations 2.7c and 2.12 show that the amplitude of the scattering is proportional to the Fourier transform of the interaction potential between the neutron and the nucleus, $V(\mathbf{r})$, just as in X-ray diffraction, the amplitude scattered coherently

by a single atom is proportional to the Fourier transform of the charge density of the atom.

2.2.5 Scattering from a single nucleus.

The scattering of a beam of neutrons from a single nucleus will depend on the interaction potential $V(\mathbf{r})$ between the neutron and the atomic nucleus which are separated by a distance r. The detailed variation of this potential is unknown but it is extremely short ranged, and its value falls rapidly to zero outside a distance of the order of nuclear dimensions, i.e. greater than 10^{-14} m. Thus the range of the potential is much smaller than the wavelength of the neutron, which will be at the very least 10^{-10} m. Due to this, the term $\exp(i(\mathbf{k}-\mathbf{k}').\mathbf{r}')$ in equation 2.8 hardly deviates from unity before the scattering potential has declined to nothing. Hence the scattering amplitude is

$$f = -\frac{1}{4\pi}\int_{\text{nucleus}} \frac{2m_n}{\hbar^2} V(\mathbf{r})\, d\mathbf{r} \qquad 2.14$$

which to a good approximation is independent of $\mathbf{Q}$. The quantity $-f$ is called the *Scattering Length* of the nucleus, and is denoted by b. The scattering length is specific to the nucleus with a given proton number Z and neutron number N. This means that isotopes of the same element will have *different* scattering lengths. The most marked example of this is in the isotopes of hydrogen as can be seen in table 2.1.

	$b/10^{-14}$ m
^{1}H	-0.374
^{2}H	0.667
^{3}H	0.47

Table 2.1 The scattering lengths of the isotopes of hydrogen.

The negative value for ^{1}H signifies that there is a phase difference of 180° between the neutron wave scattered by the proton compared with waves scattered from other nuclides. If the phase of the scattered neutron from the majority of different nuclides is taken as positive then that for ^{1}H and a few others must be negative.

It is not possible to calculate b with any great accuracy so it has to be determined empirically by experiment. The value of b is dependent on two things, the physical size of the nucleus and the presence of resonance energy levels within the nucleus. These are related in Breit-Wigner formula in equation 2.15.

$$b = \text{potential scattering} + \text{resonance scattering}$$

$$b = R + \frac{\frac{1}{2}\frac{\Gamma_n^{(r)}}{\kappa}}{[E-E_r] + \frac{1}{2}i\Gamma} \qquad 2.15$$

Where R is the nuclear radius, $\Gamma_n^{(r)}$ is the width of the nuclear resonance for re-emission of a neutron, Γ is the total width of resonance, E is the energy of incident neutron, E_r is the energy which would give resonance and $\kappa = 2\pi/\lambda$ is the wave number of the neutron. From this formula it is apparent that b is generally a complex quantity with real and imaginary parts. However the imaginary part is only important

for the few cases where the nuclei have resonances close to thermal energy, for example ^{113}Cd and ^{149}Sm. For the more common case of a remote resonance, the effect of the imaginary part is to make the value of b either larger or smaller than the potential scattering, R, and very slightly dependent on the neutron wavelength. If there are no resonance effects in the nuclei then the above equation indicates that b should equal the nuclear radius. If this is the case then, provided that the nuclear material is of effectively constant density, b should increase as the cube root of the mass number of the nucleus, A.

If, in its naturally occurring state, an element is present as several different isotopes, such as is the case for nickel, the effective value of b, or $\bar{b}$, will be the average value of b among the isotopes, with each isotope weighted according to its relative abundance. Hence

$$\bar{b} = \sum_{r}(w_r b_r) \qquad 2.16$$

where w_r is the fractional abundance of the r^{th} isotope and b_r is the scattering length of the r^{th} isotope.

Earlier it was described how the interaction of the neutron with a nucleus possessing spin produced two possible compound nuclei, (I+1/2, I-1/2). The energy levels of the two possibilities will be different and, if resonance effects are significant, this will result in a difference between the two values of b. The symbol b_+ denotes the scattering length when the spins of the neutron and nucleus are coherent (I+1/2), and b_- when they are incoherent (I-1/2). Thus these spin effects must also be considered in the calculation of the average scattering length $\bar{b}$.

The differential scattering cross-section is isotropic for a single nucleus because b is independent of **Q**. The total cross-section is immediately given by integrating over all solid angles,

$$\sigma_{tot} = \int \frac{d\sigma}{d\Omega} d\Omega = 4\pi b^2 \qquad 2.17$$

There are various tables available that list the scattering cross-sections for the nuclides [6]. It should be noted that in neutron scattering studies samples of macroscopic dimensions are used, so that the relevant cross-sections are usually the bound atom values as discussed above.

In the above discussion it was assumed that the scattering atom was fixed at **r′**, but for the free-atom treatment it is necessary to use centre of mass co-ordinates, replacing m_n in the Scröedinger wave equation (equation 2.5) by the reduced mass

$$\mu = m_n \left(\frac{A}{A+1}\right), \qquad 2.18$$

where A is the ratio of the nuclear and neutron masses. The free-atom scattering length, a, is related to the bound-atom scattering length, b, by

$$b = \left(\frac{A+1}{A}\right) a \,. \qquad 2.19$$

2.2.6 Scattering From Many Nuclei

b_r is the amplitude of the neutron scattered by a single nucleus at a position with position vector **r**. The subscript **r** is used because the scattering length, b, varies irregularly from isotope to isotope, and from one nucleus to another of the *same* isotope if there is non-zero nuclear spin. The phase of the scattered neutrons is $e^{i\mathbf{Q}.\mathbf{r}}$,

so that the differential scattering cross-section for an assembly of many nuclei, all assumed to be stationary, is

$$\frac{d\sigma}{d\Omega} = \left|\sum_{\mathbf{r}} b_{\mathbf{r}} \exp[i\mathbf{Q}\cdot\mathbf{r}]\right|^2 = \sum_{\mathbf{r},\mathbf{r}'} b_{\mathbf{r}} b_{\mathbf{r}'} \exp[i\mathbf{Q}\cdot(\mathbf{r}-\mathbf{r}')] = \sum_{\mathbf{r}} b_{\mathbf{r}}^2 + \sum_{\mathbf{r}\neq\mathbf{r}'} b_{\mathbf{r}} b_{\mathbf{r}'} \exp[i\mathbf{Q}\cdot(\mathbf{r}-\mathbf{r}')]$$

2.20

where $\mathbf{r}'$ indicates the position vector of another nucleus in the sample. The first term in equation 2.20 is $N\langle b_{\mathbf{r}}^2\rangle$, where N is the number of nuclei and the brackets $\langle\rangle$ denote the average value. If there is no correlation between $b_{\mathbf{r}}$ and $b_{\mathbf{r}'}$ and so $\langle b_{\mathbf{r}} b_{\mathbf{r}'}\rangle = \langle b_{\mathbf{r}}\rangle\langle b_{\mathbf{r}'}\rangle = \langle b_{\mathbf{r}}\rangle^2$, and the second term can be written

$$N\langle b_{\mathbf{r}}\rangle^2 \sum_{\mathbf{r}\neq\mathbf{r}'} \exp[i\mathbf{Q}\cdot(\mathbf{r}-\mathbf{r}')] = -N\langle b_{\mathbf{r}}\rangle^2 + N\langle b_{\mathbf{r}}\rangle^2 \sum \exp[i\mathbf{Q}\cdot(\mathbf{r}-\mathbf{r}')] \qquad 2.21$$

where $\mathbf{r} = \mathbf{r}'$ has been restored in the summation. Thus finally

$$\frac{d\sigma}{d\Omega} = N(\langle b_r^2\rangle - \langle b_r\rangle^2) + N\langle b_r\rangle^2 \left|\sum_{\mathbf{r}} \exp[i\mathbf{Q}\cdot\mathbf{r}]\right|^2 \qquad 2.22$$

The term $N(\langle b_r^2\rangle - \langle b_r\rangle^2)$ in equation 2.22 can also be written as $N\langle(b_r^2 - \langle b_r\rangle)^2\rangle$. This indicates that it depends on the mean-square deviation of the scattering lengths from their average value. It is referred to as the *incoherent scattering cross-section*, and is zero for nuclides of zero spin (e.g. ^{12}C, ^{16}O). Both elastic and inelastic contributions to the cross-section are attenuated by the Debye-Waller factor, which arises because interference effects between different atoms on different sites are smoothed out by thermal vibrations. If the effect of the Debye-Waller factor is ignored, that is to continue with the approximation of static nuclei, then the incoherent elastic scattering is isotropic and gives a uniform background to the coherent scattering, represented by the remaining term,

$$N\langle b\rangle^2 \left|\sum_{\mathbf{r}} \exp(i\mathbf{Q}\cdot\mathbf{r})\right|^2, \qquad 2.23$$

in equation 2.22. As can be seen, the coherent scattering cross-section takes into account interference effects, arising from the relative displacements of the nuclei in the assembly. The incoherent scattering cross-section has no phase term and so leads to no information on the structure of the sample.

In a neutron scattering experiment it is necessary to remove the incoherent scattering from the data. Hydrogen, however, exhibits incoherent scattering that is 40 times its coherent scattering. This leads to problems in its data reduction and hydrogenated species need to have data collected over a long period in order to gain sufficient information to analyse.

Returning to equation 2.20 the differential scattering cross-section can also be written as

$$\frac{d\sigma}{d\Omega} = N\langle b_{\mathbf{r}}\rangle^2 + N\langle b_{\mathbf{r}}\rangle^2 \sum_{\mathbf{r}\neq\mathbf{r}'} \exp[i\mathbf{Q}\cdot(\mathbf{r}-\mathbf{r}')] \qquad 2.24$$

Here the first term is *the self scattering term*, and the second the *interference scattering term.* The summation in the interference term is related to the *Structure Factor*, S(Q), by

$$\sum_{\mathbf{r}\neq\mathbf{r}'} \exp[i\mathbf{Q}\cdot(\mathbf{r}-\mathbf{r}')] = S(Q) - 1\,. \qquad 2.25$$

It is this structure factor that is obtained from a neutron scattering experiment. This is related to the pair distribution function, g(r), via a Fourier transform

$$g(r) = 1 + \frac{1}{2\pi^2\rho r}\int_0^\infty Q\{S(Q) - 1\}\sin(Q.r)\,dQ\,, \qquad 2.26$$

where ρ is the number density of the sample. Conversely the pair distribution function can be converted to the structure factor by a Fourier transform:

$$S(Q) = 1 + \frac{4\pi\rho}{Q}\int_0^\infty \{g(r) - 1\} r\sin(Q.r)\, dr \qquad 2.27$$

2.3 Applying Neutron Scattering Theory to Experiment.

In a conventional neutron diffraction experiment, a constant beam of neutrons from a fusion source, is monochromated, collimated, and then fired at the target. The scattering of the neutrons from the target is spherical over a wide range of directions that are defined by the angles θ and ϕ. If the scatterer is isotropic, the intensity of the scattered neutrons is independent of ϕ and hence a detector need only scan through one plane of θ to obtain a complete description of the scattering [7,8] . However, the process of monochromating the beam results in a reduction of the neutron flux. This reduction means that the experiments must run for a long time to acquire good statistics, unless there is a large detector area.

An alternative approach is the Pulsed Time of Flight experiment in which a 'white' collimated beam of thermal neutrons is fired at the target in pulses lasting Δt (Δt is typically less than 1μs), every 1/n seconds (n is in the range 25-50) (see figure 2.2). A bank of detectors is fixed at a distance L away from the target, the detectors being placed at various angles 2θ. The number of neutrons, $I(\theta,t)$, and their time of arrival, t, at the detector are measured.

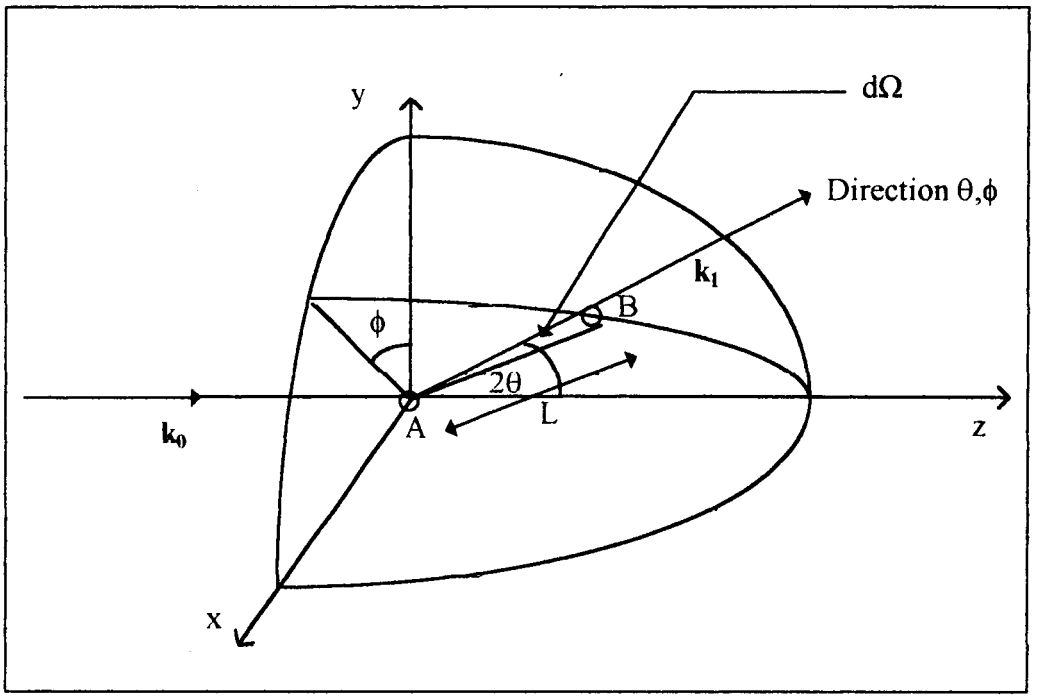

Figure 2.2 The scattering of incident neutrons by the target A. Neutrons are counted in the detector, B, which has a small solid detector angle dΩ. 2θ is the angle of scattering for the neutron.

From either of these methods it is possible to obtain the *momentum transfer wavevector*, **Q**, defined earlier as the change in momentum that has been transferred out of the z-direction into the (θ,ϕ) plane upon collision (see figure 2.3).

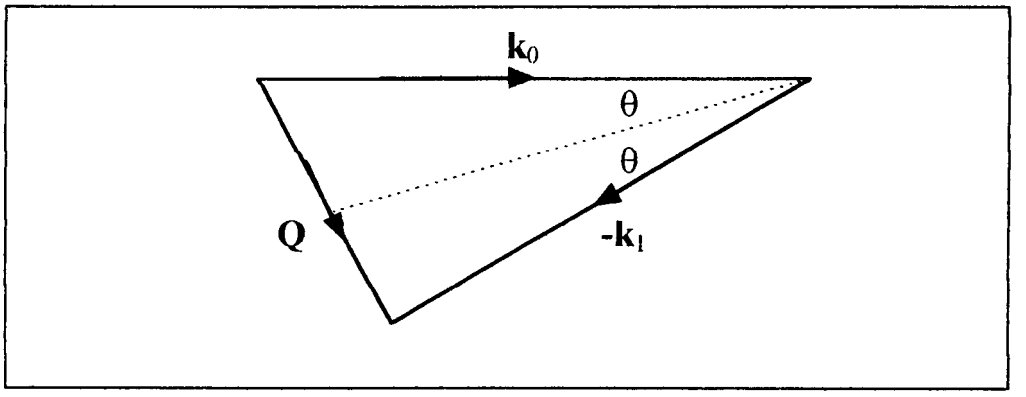

Figure 2.3 The momentum transfer wavevector, Q.

$$\mathbf{Q}=\mathbf{k}_0-\mathbf{k}_1$$

In an elastic scattering event the magnitude of $\mathbf{k}_0$ and $\mathbf{k}_1$ are the same, hence the magnitude of **Q** is given by :

$$Q = 2k_0\sin\theta \qquad 2.28$$

$$k_0 = \frac{2\pi}{\lambda_0} \qquad 2.29$$

$$Q = \frac{4\pi\sin\theta}{\lambda_0} \qquad 2.30$$

where λ_0 is the wavelength of the incident neutron.

In an experiment the intensity of the scattered neutrons in a particular direction is measured and this gives the function I(Q). In the conventional experiment, λ_0 is known, $I(\mathbf{Q}) \equiv I(\theta,\phi)$, $(I(\theta,\phi) = I(\theta))$ and **Q** is calculated by equation 2.30 over the angle range. In the Time-of-Flight experiment $I(\mathbf{Q}) = I(t)$ at each angle. λ is calculated for each time, t ,using the wavelength-time conversion,

$$\lambda = \frac{h}{p} = \frac{h}{mv} = \frac{ht}{mL}, \qquad 2.31$$

where L is the distance from target to detector, m is the mass of a neutron and h is Planck's constant. **Q** can then be calculated using equation 2.30. During a neutron diffraction experiment, the scattered neutrons are counted without analysing their energy and the result is the *Differential Cross-Section*. The differential cross-section of the scattered neutrons, at a detector positioned at angles (θ,ϕ) is defined by:

$$\frac{d\sigma}{d\Omega} = \frac{I(Q)}{N\Psi(Q)d\Omega} \qquad 2.32$$

Where $d\sigma/d\Omega$ is the differential cross-section, N is the number of scattering units, and $\Psi(Q)$ is the incident neutron flux. The differential cross-section is the probability of a scattering event occurring at a chosen angle and is only dependent on **Q**; if the flux doubles then the intensity doubles and $d\sigma/d\Omega$ stays constant.

Since from equation 2.24 and 2.25

$$\frac{d\sigma}{d\Omega} = N\langle b_R\rangle^2 + N\langle b_R\rangle^2 \{S(Q)-1\}$$

it can be seen that the structure factor can be obtained readily from the experiment by removing the self-scattering from the data and dividing by $N\langle b_R\rangle^2$.

2.4 Obtaining The Pair Distribution Function

As seen in equation 2.26 the pair distribution function is related to the structure factor via a Fourier transform. However, because the data from the experiment is available only over a finite range of Q, it is not possible to perform the integration to infinity, and the solution will contain periodic oscillations or 'ringing'. Although it is possible to damp these oscillations by introducing a window function, a better approach to obtaining the pair distribution function was proposed by Soper [9] and referred to as the Minimum Information method.

The basic principle behind the Minimum Information method is to produce the smoothest pair distribution function consistent with the experimental data. Rather than transform the S(Q) into a pair distribution function, a pair distribution function is produced and then converted into an S(Q) via a Fourier transform and compared to the experimental data. This avoids the problem of cut-offs in the Fourier transform, and hence ringing. Peaks and troughs are introduced into the pair distribution function at random and the moves are accepted based on two criteria:

1. The change in the pair distribution function increases the agreement to the experimental data.

2. The change in the pair distribution function reduces the amount of 'noise' in the pair distribution function.

Here the definition of noise is the number of turning points in the pair distribution function. If the criteria are balanced correctly then the pair distribution function produced will have the minimum number of peaks that are consistent with the data. Thus spurious peaks in the pair distribution function that have no physical meaning will be avoided.

2.5 Conclusions

From the information presented in this chapter it is possible to conclude that elastic neutron scattering is a powerful technique for gaining experimental information on the structure of solids and liquids. As can be seen, not only is it possible to derive a pair distribution function for the sample in question, but also, because of the dependence of b on the scattering nucleus, it can utilise isotopic substitution where possible to gain a greater understanding of the orientation of the molecules.

1 HALL, C.D., *Thesis: Neutron Diffraction and Molecular Dynamics Studies of Fluid Halocarbons*, 1992, *University of Liverpool*

2 WILLIS, B. T. M., *Chemical Applications of Thermal Neutron Scattering*, 1973, Oxford University Press

3 BACON, G. E., *Neutron Scattering in Chemistry*, Butterworths

4 MCDONALD, I. R., BOUNDS, D. G., AND KLEIN, M. L., 1982, *Molec. Phys.*, **45**, 521.

5 SCHIFF, L. I., 1955, *Quantum mechanics.*, McGraw-Hill, New York

6 HUGHES, D. J., SCHRARTZ, R. B., 1958, *Neutron Cross-sections*,BNL-325, U.S. Govt. Printing Office, Washington D.C. (and later supplements).

7 BÖHM, H. J., AHLRICH, S. R., 1985, *Molec. Phys.*, **54**, 1261

8 MOUNTAIN, R. D., MORRISON, G., 1988, *Molec. Phys.*, **64**, 91

9 SOPER, A. K., 1990, *Neutron Scattering Data Analysis*, edited by M. W. Johnson (Bristol, UK: Institute of Physics).

Chapter Three

Computer Simulation

3.1 Introduction

Sources of reference for this chapter have been the thesis of C. D. Hall[1], *Computer Simulation of Liquids* by M. P. Allen and D. J. Tildesley [2] (Clarendon Press), the manual for MDMPOL [4], and *Theory of Simple Liquids* by J. P. Hansen and I. R. McDonald [3] (Academic Press). This chapter should be seen as an introduction to the subject of computer simulation and for a more in-depth study it is recommended to read the book *Computer Simulation of Liquids*.

Neutron diffraction provides information about the total distribution of atoms in a liquid, however, for polyatomic molecules, this information is not enough to provide a full analysis of the intermolecular structure, i.e. how the molecules are orientated towards each other. What is needed for a full analysis is to separate the total pair distribution function into the distribution functions for individual pairs of atoms, or its partial pair distribution functions. This information can sometimes be obtained by performing neutron diffraction experiments on isotopically substituted liquids, such as replacing hydrogen with deuterium, however frequently this method is not an option. A more general approach is needed to obtain this information. One method is to try to reproduce the neutron data by simulating the liquid on a computer and then use the computer results to analyse fully the structure of the liquid. This project has utilised molecular dynamics in order to be able to do this.

Initially a modified version of the CCP5 library program, MDMPOL [4] was used to simulate the systems of interest. However in the second year of the project this was changed to using the new molecular dynamics simulation program in the CCP5 library, DLPOLY [5]

3.2 Molecular Dynamics Simulations

Molecular dynamics is a method by which a system is simulated by solving the classical equations of motion. At each step in the simulation the equations of motion are solved for every atom / molecule in the system. The advantages of using this method is that the thermodynamics of the system can be reproduced as well as the liquid structure, providing a method to obtain a unique solution to the problem. Also, the information obtained can be used to predict other properties of the liquid. The disadvantage of this method is that, owing to the large number of calculations performed at every time step, the method is computationally very expensive and only small systems can be investigated at this current time.

3.2.1 Classical Liquids

Molecular dynamics utilises the principles of classical physics in order to simulate the motion of the atoms. However, because the systems examined are of a micro scale, and not a macro scale, it is necessary to validate the use of classical physics as opposed to quantum physics. Consider the de Broglie thermal wavelength Λ:

$$\Lambda = \left[\frac{2\pi\beta\hbar^2}{m}\right]^{\frac{1}{2}} \qquad \beta = \frac{1}{(k_b T)} \qquad 3.1$$

where m is the mass of the atom, k_b is Boltzmann's constant and T is the temperature. To justify a classical treatment of static properties it is necessary that:

$$\frac{\Lambda}{a} << T \qquad a \approx \rho^{-\frac{1}{3}} \qquad 3.2$$

where ρ is the density of the liquid. For molecules it is required, in addition, that:

$$\Theta_{rot} << T \qquad \Theta_{rot} = \frac{\hbar^2}{2I k_b} \qquad 3.3$$

where Θ_{rot} is the characteristic rotational temperature and I is the moment of inertia for the molecule.

Using the classical approximation means that the problem is simplified as the contributions to thermal motion can be separated from those due to interactions between particles.

A major obstacle to the development of an accurate theory of liquids is that there is no idealised model (such as with a perfect gas and harmonic solid) which can be treated exactly. The method that has been widely adopted in the past is to treat the liquid state as an intermediate between the gaseous and solid states, but this is unsatisfactory from a theoretical point of view as it does not take into proper account the geometrical factors. For example, lattice theories tend to overemphasise the solid-like character of the liquids, whereas expansions in powers of density are essentially theories of the imperfect gas and cannot be expected to perform well under triple point conditions. It is better to treat the problem of the liquid state without leaning too heavily on concepts taken over from the theories of dilute gases or solids.

3.2.2 Intermolecular Forces

Consider two atoms, for example Argon, at an infinite distance apart, then the energy of the system, $E_s(\infty)$, is the sum of the energies of the individual atoms, E_1+E_2. This is because the two atoms do not interact and so the main contribution to E_1 and E_2 is the translational kinetic energy of atoms 1 and 2. If the atoms are now brought towards each other there will be an interaction, U, between them. This interaction is dependent upon the distance they are apart, r. The system energy, $E_s(r)$ is now:

$$E_s(r) = E_1 + E_2 + U(r) \qquad 3.4$$

$U(r)$ is the intermolecular pair potential energy function, more commonly referred to as the *Pair Potential*, between the two atoms. It can be thought of as the work required to bring the two atoms together from infinity to a separation r. Taking $F(r)$ to be the force acting between the atoms at separation r then:

$$U(r) = \int_r^\infty F(r)\, dr \qquad 3.5$$

$F(r)$ is by convention taken to be positive when repulsive and negative when attractive. The general form of $U(r)$ and $F(r)$ are shown in figure 3.1. For both functions there is a repulsive wall at short range and an attractive tail at long range. At r_{eq} the potential energy, $U(r_{eq})$, is at a minimum, $-\varepsilon$, and the force acting between the atoms, $F(r_{eq}) = 0$. r_{eq} is the interatomic separation where the attractive and repulsive forces between the two atoms are in equilibrium and hence is the favoured separation of the two atoms. ε is known as the well depth. At a distance $r = \sigma$, the potential energy $U(\sigma) = 0$. This distance σ is roughly equal to the sum of the atomic radii of the interacting atoms.

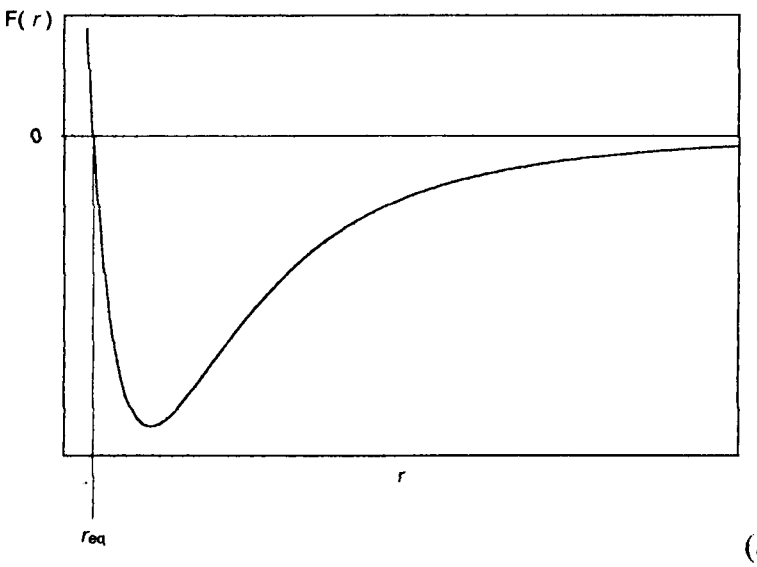

(a)

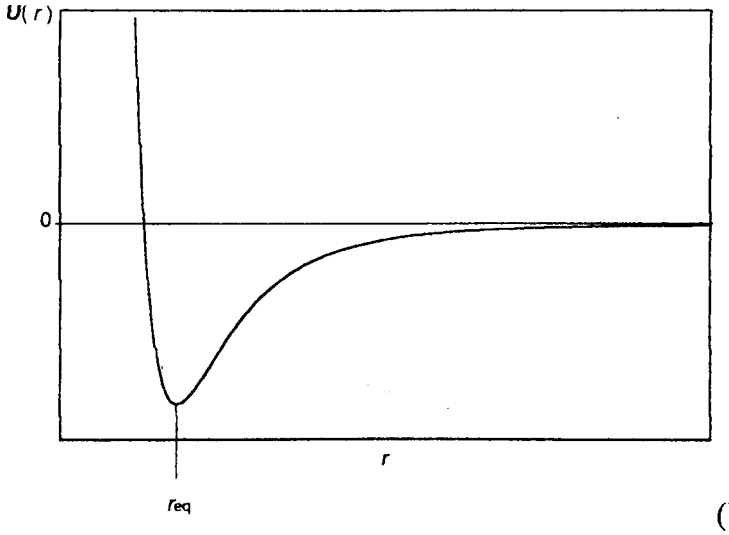

(b)

Figure 3.1 Diagram of Force (F(*r*)) *vs.* separation (*r*) (a) and interatomic potential (U(*r*)) *vs.* separation (b).

The harsh repulsive wall in the pair potential gives rise to the short range order that is displayed in liquids. This repulsion is created by the overlap of the outer-electron shells which produce a reduction in electron density in this overlap region because of the Pauli Exclusion Principle. The reduction in electron density

reduces the masking of the positive charge at the nuclei and hence a repulsive force acts between them. The range of the repulsive force is roughly equal to the nearest-neighbour separation.

The attractive forces that act at longer range vary much more smoothly with distance and play only a minor role in determining the structure of the liquid. They provide instead an essentially uniform attractive background which creates the cohesive energy required to stabilise the liquid.

For a system with N atoms the form of the potential energy is much more complicated. The system energy is the sum of the kinetic energies (ΣE_N) of all the atoms plus the sum of all the potential energies between all the atoms in the system. That is

$$E_s(r) = \sum E_N + \sum \sum U_2(r_i,r_j) + \sum \sum \sum U_3(r_i,r_j,r_k) + \ldots \qquad 3.6$$

Where $U_2(r_i,r_j)$ is the potential energy due to two-body interactions, $U_3(r_i,r_j,r_k)$ is the three-body term etc.

$$E_s(r) = \sum E_N + U(r_i,r_j,r_k,\ldots) \qquad 3.7$$

Consider, as an example of the higher order terms in this equation, the three Argon atoms:

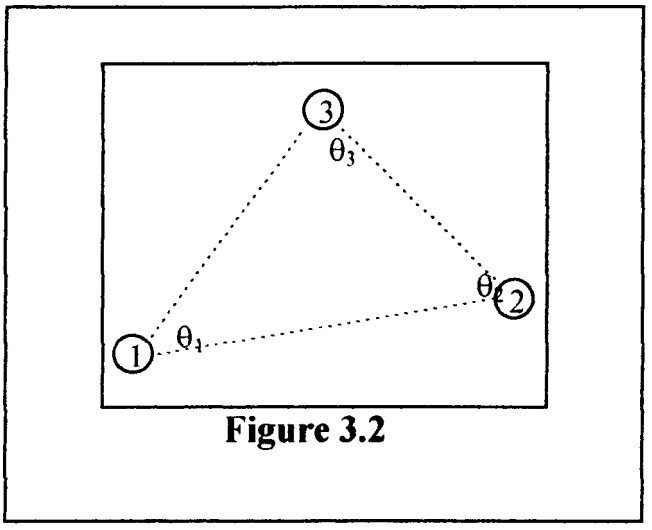

Figure 3.2

The potential $U(r_{12},r_{23},r_{31})$, where r_{xy} is the distance between atom x and atom y, is not the straight addition of the pair potentials $U(r_{12})$, $U(r_{23})$, $U(r_{31})$, but also has an extra term included $U_3(r_{12},r_{23},r_{31})$ which arises from the non-additivity of the potential, i.e.:

$$E_s(r) = \sum E_N + U(r_{12}) + U(r_{23}) + U(r_{31}) + U_3(r_{12},r_{23},r_{31}) \qquad 3.8$$

$U_3(r_{12},r_{23},r_{31})$ may be written [6]

$$U_3(r_{12},r_{23},r_{31}) = v(r_{12},r_{23},r_{31})^{-3}(3\cos\theta_1\cos\theta_2\cos\theta_3 + 1) \qquad 3.9$$

where θ_1, θ_2, θ_3, are the angles of the triangle formed by the atoms and v is the *three-body co-efficient*. This is a small, but significant, contribution to $E_s(r)$

3.2.2.1 Modelling the Pair Potential

In order to calculate the forces acting on the atoms in the simulation it is necessary to model the forces that act between the molecules. An effective pair potential is usually used to reduce the complexity of the calculations. The simplest model for the pair potential is that for a hard sphere (see figure 3.3). This model has

the potential equal to zero at all $r \geq a$, which is the hard sphere radius, and equal to infinity at distances $r < a$

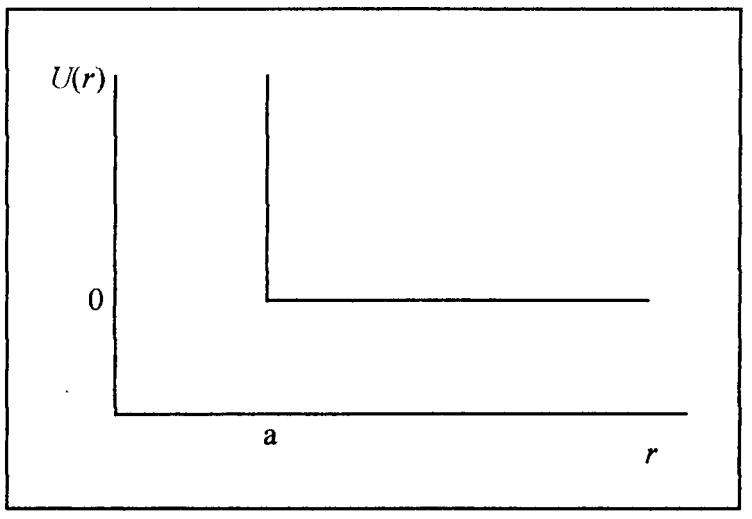

Figure 3.3 Pair potential of hard sphere model.

$$U(r) = \infty \; r < a, \; U(r) = 0 \; r \geq a$$

This simple model is ideal for studying phenomena where the hard core of the potential is dominant. Hard sphere models used in computer simulations (for example [7, 8, 9,]) have shown very clearly that the structure of a hard sphere fluid does not differ in any significant way from that corresponding to more complicated interatomic potentials, at least near crystallisation. However, the hard sphere model has no attractive forces between the atoms and hence, although it does undergo a freezing transition, it does not have a true liquid phase. A simple model that can describe a true liquid phase is given by adding a square attraction well to the hard sphere potential. (see figure 3.4)

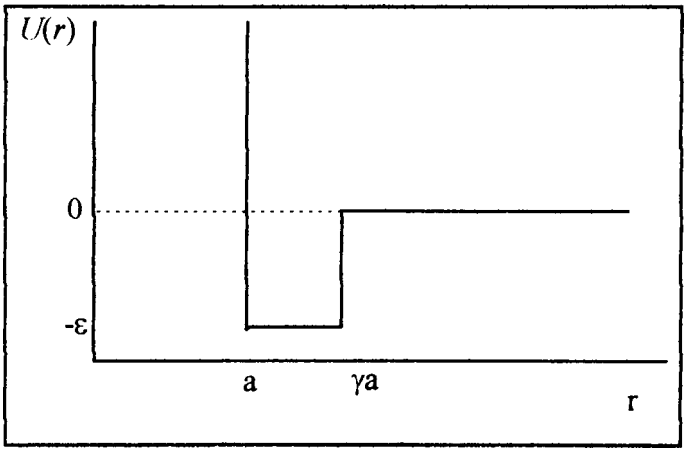

Figure 3.4 Pair potential of square well model. $U(r) = \infty \quad r < a$,

$U(r) = -\varepsilon \quad a \leq r \leq \gamma a$, $U(r) = 0 \quad r > \gamma a$

Both of these potentials, whilst being simple, suffer the problem that they are unrealistic and are discontinuous. A more realistic potential for neutral atoms can be constructed using detailed quantum-mechanical calculations. At large separations the dominant contribution to the pair potential comes from the multipole dispersion forces that arise from the instantaneous electric moments in one atom inducing electric moments in another. These moments arise from fluctuations in the distribution of electrons around the nucleus. All the terms of the multipole series represent attractive contributions to the potential. The leading term, which is the most dominant, varies as r^{-6} and describes the dipole - dipole interactions. Higher order terms represent dipole - quadrupole (r^{-8}), quadrupole - quadrupole (r^{-10}) interactions, and so on. However these higher order terms are small in comparison with the leading term.

The short range repulsive interaction is much more difficult to represent. Various potentials represent it either as an inverse power law, such as r^{-12} in the Lennard-Jones potential, or as an exponential function, such as $e^{(-r/\rho)}$ in the Buckingham potential. (This latter approximation must be supplemented by

requiring that for r less than some arbitrary value $U(r) \rightarrow \infty$.) The behaviour of $U(r)$ in the two limiting cases $r \rightarrow 0$ and $r \rightarrow \infty$ can be represented in a simple potential function of the form:

$$U(r) = 4\varepsilon\left[\left(\frac{\sigma}{r}\right)^{12} - \left(\frac{\sigma}{r}\right)^{6}\right] \qquad 3.10$$

where σ is the collision diameter (i.e. the separation of the particles when $U(r) = 0$) and ε is the depth of the potential well at the minimum in $U(r)$. This is the Lennard-Jones potential (see figure 3.5)

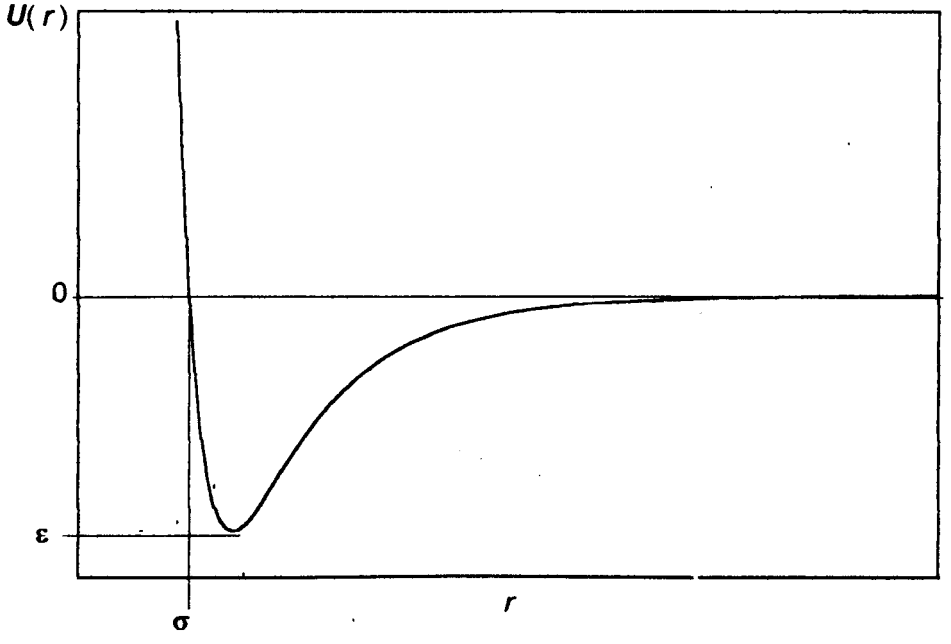

Figure 3.5 Diagram of the Lennard-Jones potential

The Lennard-Jones potential provides a fair description of the interaction between pairs of rare-gas atoms and quasispherical molecules such as CH_4.

All the above potentials refer to an isolated pair of atoms or quasispherical molecules. As indicated before, the use of such pair potentials in the simulation of multi-body systems involves the neglect of many bodied interactions, an

approximation that cannot wholly be justified. Estimates of the magnitudes of the leading, triple-dipole, three body contribution have been made for inert gases in their solid-state face centred cubic lattices [10,11]. It is found that up to 10 per cent of the lattice energy of argon (and more in the case of more polarizable species) may be due to these non-additive terms in the potential and it can be expected that the same order of magnitude holds in the liquid phase. However four-body terms (and higher) are expected to be small in comparison to the two- and three-body terms. The calculation of the three-body term in a computer simulation is very time consuming and is rarely used.[12,13] Maitland and Smith developed a potential [14] that took into account a large amount of experimental data, including molecular beam scattering, spectroscopy of the argon dimer, inversion of the temperature-dependence of the second virial coefficient, and solid-state properties, together with theoretical calculations of the long range contributions. This showed that the argon potential is not of the Lennard-Jones form, but has a deeper bowl and weaker tail. The pairwise approximation can still give a remarkably good description of liquid properties because the average three-body effects can be partially included by defining an 'effective' pair potential.

The description of the interaction between two molecules is a more difficult problem than for spherical particles because the pair potential is a function of both the separation of the molecules and of their mutual orientation. For a system of N molecules, the analysis involves:

1) establishing the intermolecular effective-pair potential between every atom on every molecule
2) allowing for the free rotation of the molecules (energy = RE)

3) estimating the vibration of the atoms in the molecules (energy = VE).

For example, consider two diatomic molecules of HCl :

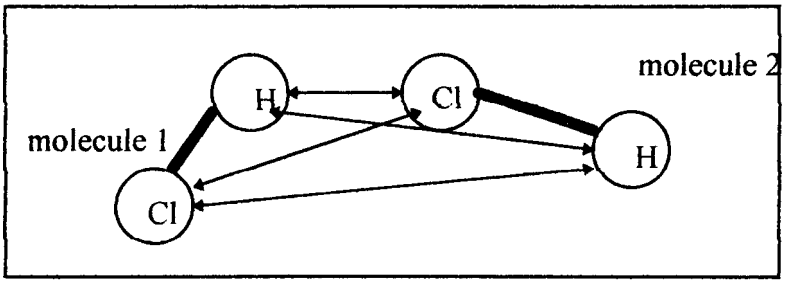

Figure 3.6

There are four atom-atom pairwise interactions. The energy of a molecular system (ignoring the orientational effects) is:

$$E_s(r) = \sum TE + \sum RE + \sum VE + \sum \sum U_{ab}(r_{ab}) \qquad 3.11$$

where TE is the translational kinetic energy, r_{ab} is shorthand for r_{ia} - r_{jb}, where ia is atom i of molecule a and j_b is atom j of molecule b, and $U(r) = \sum \sum U_{ab}(r_{ab})$ is the effective pair-potential.

For a molecule such as CHF_3 there are twenty-five two body potentials to consider. The simulations of such liquids are frequently simplified by making the intramolecular structure rigid in order to avoid calculating the vibrational or internal-rotational energies.

A vast percentage of the computing time necessary for the simulation is spent calculating the forces between pairs of atoms. In order to reduce this time, use is made of a cut-off sphere, with the cut-off radius being less than half the length of the molecular dynamics cell. Together with the cut-off radius, use is made of *neighbour tables*. Although there are different schemes available the basic idea is very simple. In computing the total force acting on particle i, the loop on j is restricted to those particles that, from calculations from earlier timesteps, are known to be relatively

close neighbours of i, with all due allowance being made for the minimum image convention (see later). The necessary information is contained in tables that for each i, list the neighbours j such that $r_{ij} < r_c + \Delta$. The quantity Δ corresponds to a thin shell that covers the cut-off sphere. The tables must be updated at intervals determined by the choice of Δ. If efficient use is made of the tables, then taking N to be the number of atoms in the molecular dynamics box, the number of pair separations that must be calculated at each timestep is reduced from ½ $(N)(N\text{-}1)$ to, N times the number of entries in the neighbour list of a typical particle. This in turn makes the computing time required per step a linear rather than a quadratic function of N.

3.2.3 Equations of motion for atomic systems

As previously stated, molecular dynamics involves the solution of the classical equations of motion for all the particles in the system of interest. Although the technical details of simulating a model with discontinuous potentials and purely impulsive forces, such as the hard sphere potential, differ from those appropriate to models with continuous potentials, nevertheless they are a good starting point in the discussion of molecular dynamics.

The motion of hard spheres is unusual in the respect that the velocities of the particles only change at collisions, and remain constant in-between. The time-evolution of such a system can therefore be treated as a sequence of strictly binary, elastic collisions. The laws of Conservation of Energy and Momentum apply as the particles possess mass. Taking $\mathbf{v}_1$, $\mathbf{v}_2$ to be the velocities of the two spheres before the collision, and $\mathbf{v}_1^*$, $\mathbf{v}_2^*$ to be the velocities of the two spheres after the collision, then the conservation of energy and momentum can be written as:

$$|\mathbf{v}_1^*|^2 + |\mathbf{v}_2^*|^2 = |\mathbf{v}_1|^2 + |\mathbf{v}_1|^2 \qquad \text{Energy} \qquad 3.12$$

$$\mathbf{v}_1^* + \mathbf{v}_2^* = \mathbf{v}_1 + \mathbf{v}_2 \qquad \text{Momentum} \qquad 3.13$$

Hence :

$$\Delta\mathbf{v}_1 \equiv \mathbf{v}_1^* - \mathbf{v}_1$$

$$\equiv -(\mathbf{v}_2^* - \mathbf{v}_2)$$

$$\Delta\mathbf{v}_1 = -\Delta\mathbf{v}_2 \qquad \mathbf{3.14}$$

The projection of the relative velocity onto the vector joining the centres is reversed in an elastic collision

$$\mathbf{v}_{12}^* . \boldsymbol{r}_{12} = (\mathbf{v}_2^* - \mathbf{v}_1^*) . (\boldsymbol{r}_2 - \boldsymbol{r}_1)$$

$$= -(\mathbf{v}_2 - \mathbf{v}_1) . (\boldsymbol{r}_2 - \boldsymbol{r}_1)$$

$$= -\mathbf{v}_{12} . \boldsymbol{r}_{12} \qquad \mathbf{3.15}$$

but the orthogonal components are unaltered. Thus the change in velocity at a collision is:

$$\Delta\mathbf{v}_1 = -\Delta\,\mathbf{v}_2$$

$$\Delta\mathbf{v}_1 = \left[\frac{\boldsymbol{r}_{12} b_{12}}{d^2}\right] \qquad \mathbf{3.16}$$

where $b_{12} = \mathbf{v}_{12} . \boldsymbol{r}_{12}$ and d is the hard sphere diameter. The term on the right-hand side of equation 3.16 must be evaluated at contact.

The algorithm for the calculation of the trajectories consists of first advancing the co-ordinates of all the particles until a collision occurs somewhere in the system, and then calculating the change in velocities of the colliding particles according to the above equations. The procedure is then repeated for as many

collisions as are necessary to yield sufficient statistical reliability for the problem in hand. Since these equations are exact, it follows that the trajectories of the particles can be computed with a precision limited only by round off errors. As the kinetic energy is a conserved quantity, the temperature of the system stays rigorously constant.

When the potentials are continuous, the trajectories of the particles, unlike those of hard spheres, can no longer be calculated exactly. Consider the case of spherically symmetric potentials, the equations of motion are now the $3N$ coupled, second order, differential equations :

$$m\ddot{\boldsymbol{r}}_i(t) = -\nabla_i V_N(\boldsymbol{r}^N) \qquad 3.17$$

where $\boldsymbol{r}_i\ (t)$ are the co-ordinates of particle i at time t. These equations must be solved numerically by finite difference methods, which lead unavoidably to errors in the predicted trajectories of the particles. However it is rarely necessary to use an elaborate algorithm to obtain solutions.

Given that the co-ordinates of a particle i at time t are $\boldsymbol{r}_i\ (t)$ then the co-ordinates at time $t \pm h$ can be found from a Taylor expansion about $\boldsymbol{r}_i\ (t)$:

$$\boldsymbol{r}_i\ (t \pm h) = \boldsymbol{r}_i\ (t) \pm h\, m\dot{\boldsymbol{r}}_i(t) + \frac{h^2}{2!} m\ddot{\boldsymbol{r}}_i(t) \pm \frac{h^3}{3!} m\dddot{\boldsymbol{r}}_i\ (t) + \sigma\ (h^4) \qquad 3.18$$

The central difference prediction for $\boldsymbol{r}_i(t + h)$ is obtained by adding the two expressions in equation 3.18 to give:

$$\boldsymbol{r}_i(t + h) \approx -\ \boldsymbol{r}_i(t - h) + 2\boldsymbol{r}_i(t) + \frac{h^2}{m} \boldsymbol{F}_i(t) \qquad 3.19$$

where $\boldsymbol{F}_i(t)$ is the total force acting on particle i at time t; in general $\boldsymbol{F}_i(t)$ is calculated as a sum of pair forces $\boldsymbol{F}_{ij}(t)$, with $\boldsymbol{F}_{ij}(t) = -\ \boldsymbol{F}_{ji}(t)$. The error of the

predicted co-ordinates is of the order h^4. Subtraction of the two expressions in equation 3.18 yields an estimate for the velocity of the particle i at time t.

$$\dot{\boldsymbol{r}}_i(t) \approx \frac{1}{2h}[\boldsymbol{r}_i(t+h) - \boldsymbol{r}_i(t-h)] \qquad 3.20$$

The error here is of the order h^2. Verlet [15] was the first to use the central difference algorithm and it has been the commonest choice of most later workers. The timestep, h, is taken as being constant. This is quite a strong contrast to the case for the hard spheres where the analogue of h, the time between successive calculations (or the time between collisions), is a quantity that varies throughout the calculation. The length of h is extremely important as this affects the stability of the algorithm. If h is too large then the fluctuations in the energy of the system will increase and eventually an upward drift will occur. However, too small a value of h means that the number of timesteps needed to obtain good statistical results spirals upwards to unwieldy amounts. A good compromise is a value that is an order of magnitude smaller than the mean collision time.

Despite its simplicity, the central-difference algorithm is apparently as stable as a variety of higher-order schemes [11,16,17] that have been proposed, including a number of so-called predictor-corrector methods.[18,19] On the other hand, higher-order algorithms are sometimes useful in obtaining estimates for the particle velocities that improve on the approximation in equation 3.19. At the start of a molecular dynamics simulation the particles are placed at arbitrarily chosen sites $\boldsymbol{r}_i(0)$. A corresponding set of co-ordinates at an earlier time $\boldsymbol{r}_i(-h)$ is then typically obtained by allocating, to the particles, random velocities drawn from a Maxwell-Boltzmann distribution appropriate to the temperature of interest. The velocities are chosen such that the net linear momentum is zero. The rest of the calculation is

performed as a loop over time. At each step the time is increased by h, the total force acting on each particle is computed, and the particles are advanced to their new positions. In the initial few steps of the simulation the temperature tends to drift from the value at which it was originally set. This is because the initial configuration usually has too high a potential energy and, as the simulation is advanced, this potential energy is converted to kinetic energy thus raising the temperature. Hence it is necessary, in the early stages, to occasionally rescale the velocities to bring the temperature back to the desired value. Once the temperature has stabilised (a period referred to as the *Equilibration Period*), the system is allowed to evolve undisturbed, with both potential and kinetic energies fluctuating around steady mean values.

3.2.3.1 Equations of motion for molecular systems

The above methods are easily extended to molecular systems if the molecules are treated as consisting of independent atoms bound together by continuous intramolecular forces. However this is not a very good way to proceed. Apart from the problem of treating the vibrational motion classically, the choice of timestep is dictated by the timescale of the vibrations rather than the slower, but more interesting translational and rotational motions. This would mean that the number of timesteps needed to allow the system to evolve sufficiently would have to be much greater, making the computational time for a simulation extremely long. In general, therefore, it is much more economic to work with rigid molecules, even though the dynamical problem is much more difficult. The conventional approach to the solution of the equations of motion of a rigid body involves the separation of the internal and centre-of-mass co-ordinates. Consider a linear molecule with centre of

mass co-ordinates r_i and polar angles (θ_i, ϕ_i) relative to a laboratory-fixed frame of reference. In terms of these co-ordinates the equations of motion of the molecule are:

$$\ddot{\boldsymbol{r}}_i = \frac{1}{m}\boldsymbol{F}_i \qquad 3.21$$

$$\ddot{\theta}_i = \sin\theta_i \cos\theta_i \dot{\phi}_i^2 - \frac{1}{I}\sum_{j\neq i}^{N} \frac{\partial U(i,j)}{\mathrm{d}\theta_i} \qquad 3.22$$

$$\ddot{\phi}_i = -2\cot\theta_i \dot{\theta}_i \dot{\phi}_i - \frac{1}{I\sin^2\theta_i}\sum_{j\neq i}^{N} \frac{\partial U(i,j)}{\mathrm{d}\phi_i} \qquad 3.23$$

where m is the molecular mass and I the moment of inertia. The angular derivatives of the pair potential $U(i,j)$ are related to the torque acting on the molecule [20]. The motion of the centre-of-mass can be handled by the same central-difference algorithm that is used in the atomic case. The problem lies in obtaining solutions to the coupled rotational equations 3.21 and 3.23 because 3.23 has a singularity when $\sin\theta_i = 0$. This problem can be overcome by redefining the laboratory frame whenever the singularity is approached.

The most recent and successful method for dealing with the rotational motion of rigid molecules involves the use of quaternion parameters [21]. Evans recognised the fact that singularity-free equations could not be obtained using just three independent variables and so suggested the use of four quaternion parameters as generalised co-ordinates. These quaternions have the property of having well-behaved equations of motion. The four quaternions are linked by one algebraic equation, so that there is only one 'redundant' variable.

A quaternion **Q** is a set of four scalar quantities

$$\mathbf{Q} = (q_0, q_1, q_2, q_3) \tag{3.24}$$

and it is often useful to think of the last three elements (q_1, q_2, q_3) as constituting a vector. The quaternions satisfy the constraint

$$q_0^2 + q_1^2 + q_2^2 + q_3^2 = 1 \tag{3.25}$$

The way in which such a quaternion may represent the orientation of a rigid body is discussed by Goldstein [22]. The four scalar quantities are defined in terms of the Euler angles θ, ϕ, ψ which are defined in Figure 3.7.

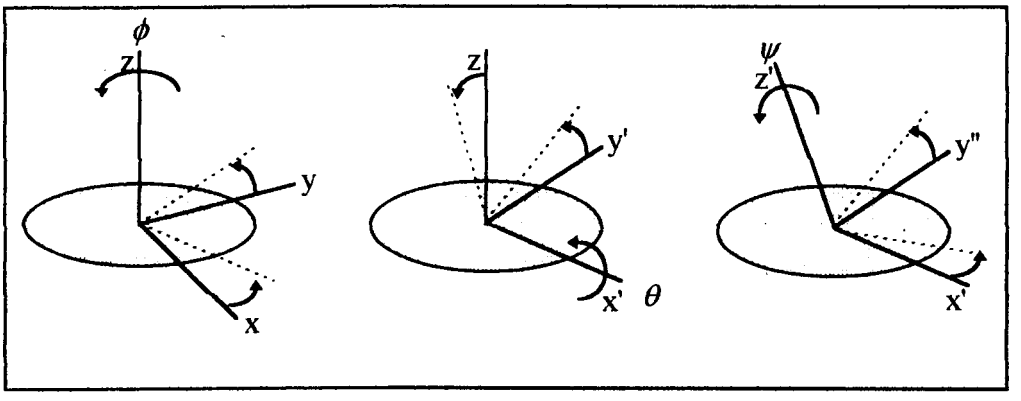

Figure 3.7 Definition of Euler angles

Using this convention, it is most convenient to define the scalars as

$$q_0 = \cos\tfrac{1}{2}\theta \cos\tfrac{1}{2}(\phi + \psi)$$

$$q_1 = \sin\tfrac{1}{2}\theta \cos\tfrac{1}{2}(\phi - \psi)$$

$$q_2 = \sin\tfrac{1}{2}\theta \sin\tfrac{1}{2}(\phi - \psi)$$

$$q_3 = \cos\tfrac{1}{2}\theta \sin\tfrac{1}{2}(\phi + \psi) \tag{3.26}$$

Using this definition the rotation matrix is

$$\mathbf{A} = \begin{pmatrix} q_0^2 + q_1^2 - q_2^2 - q_3^2 & 2(q_1q_2 + q_0q_3) & 2(q_1q_3 - q_0q_2) \\ 2(q_1q_2 - q_0q_3) & q_0^2 - q_1^2 + q_2^2 - q_3^2 & 2(q_2q_3 + q_0q_1) \\ 2(q_1q_3 + q_0q_2) & 2(q_2q_3 - q_0q_1) & q_0^2 - q_1^2 - q_2^2 + q_3^2 \end{pmatrix} \tag{3.27}$$

The quaternions for each molecule must satisfy the equations of motion

$$\begin{pmatrix} \dot{q}_0 \\ \dot{q}_1 \\ \dot{q}_2 \\ \dot{q}_3 \end{pmatrix} = \frac{1}{2} \begin{pmatrix} q_0 & -q_1 & -q_2 & -q_3 \\ q_1 & q_0 & -q_3 & q_2 \\ q_2 & q_3 & q_0 & -q_1 \\ q_3 & -q_2 & q_1 & q_0 \end{pmatrix} \begin{pmatrix} 0 \\ \omega_x^b \\ \omega_y^b \\ \omega_z^b \end{pmatrix} \qquad 3.28$$

where the equations for the components of ω in the body-fixed frame are

$$\dot{\omega}_x^b = \frac{\tau_x^b}{I_{xx}} + \left(\frac{I_{yy} - I_{zz}}{I_{xx}} \omega_y^b \omega_z^b \right)$$

$$\dot{\omega}_y^b = \frac{\tau_y^b}{I_{yy}} + \left(\frac{I_{zz} - I_{xx}}{I_{yy}} \omega_z^b \omega_x^b \right)$$

$$\dot{\omega}_z^b = \frac{\tau_z^b}{I_{zz}} + \left(\frac{I_{xx} - I_{yy}}{I_{zz}} \omega_x^b \omega_y^b \right) \qquad 3.29$$

Where I_{xx}, I_{yy}, I_{zz} are the three principal moments of inertia and τ_x, τ_y, and τ_z are the components of the torque acting on the molecule. The superscript b indicates the body-fixed system. The equations of motion, equations 3.28 and 3.29, using the matrix **A** in equation 3.27 to transform between space-fixed and body-fixed co-ordinates, contain no singularities. They are a system of first-order differential equations which may be solved by the Gear predictor-corrector method.[23,24]

3.2.4 The Periodic Boundary Condition and the Minimum Image Convention.

In order to simulate a liquid as realistically as possible with only N particles use is made of the *periodic boundary condition*. The liquid is viewed as an infinite periodic assembly of cells (usually cubic in shape), referred to as the molecular

dynamics cell, each of which contains N particles. The contents and dynamics within each cell are identical at any given instant in time and within this constraint the particles are free to move from cell to cell. Particles leaving a cell are replaced by identical particles with identical dynamical properties (see figure 3.8) entering the opposite face. Thus the periodic boundary condition enables the simulation of a pseudo-infinite liquid that is free of surface effects and requires only the study of a single cell and its contents.

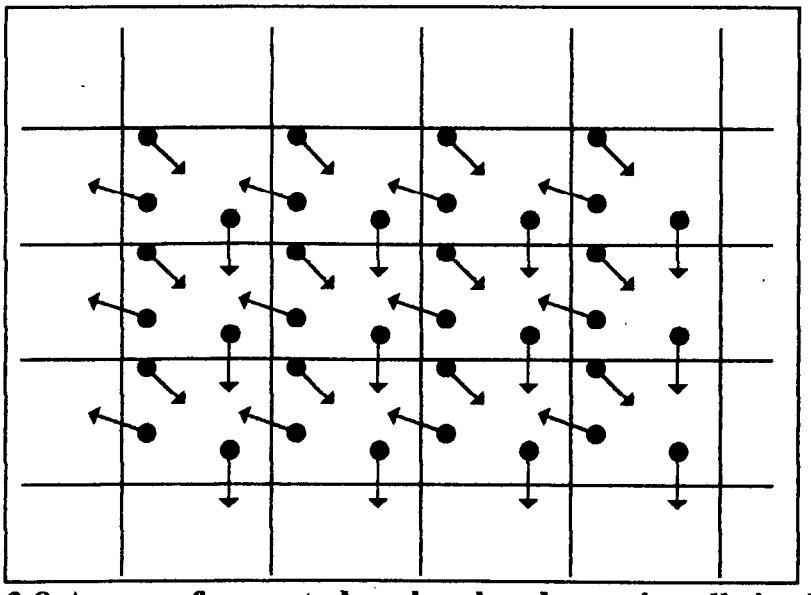

Figure 3.8 Array of repeated molecular dynamic cells in the periodic boundary condition.

If the periodic boundary condition is being implemented then it is also necessary to use the *minimum image convention.* This decrees that the interaction between pairs of particles in the molecular dynamics cell is replaced by the interaction between the closest images of particles in the three dimensional periodic system (see figure 3.9)

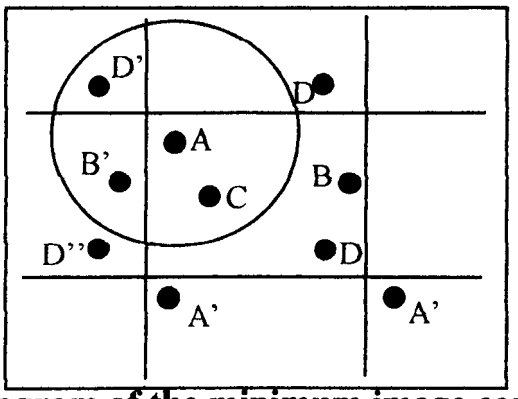

Figure 3.9 Diagram of the minimum image convention.

From figure 3.9 it can be seen that the interactions between particle A and particles B, C, D are replaced with the 'nearest image' interactions, i.e. A with B', C , D'. The circle shown represents the interactions truncation radius, that is the cut-off radius. This requires for consistency, and to prevent the introduction of artificial correlations into the system, that the force law employed be truncated to zero value at a particle separation no greater than half the width of the molecular dynamics cell. However in a system where long range forces are evident, the minimum image convention must be abandoned for these forces.

3.2.5 The Fractional Charge Model

Many molecules, whilst being electrically neutral, contain an uneven distribution in the electron cloud giving rise to dipoles, quadrupoles etc. In order to simulate these materials some method is needed to represent the coulombic forces due to these partial charges in the simulation. This involves two problems.

1) Some reasonable representation of the electrostatic multipole associated with each molecule must be found.

2) Some means of summing the long range influences on each molecule is needed, since these influences extend beyond the domain of a single molecular dynamics cell and its immediate neighbours.

The simplest solution to the first requirement is to place, at each Lennard-Jones site, (usually the atomic centres of the constituent atoms in the molecule), a small charge such that the sum of all the charges on the molecule comes to zero. This is referred to as the *fractional charge model.* The charges should be chosen to give some representation of the electronic distribution on the molecule. This distribution can be found by performing *ab initio* molecular orbital calculations on the molecule, and then a Mulliken population analysis. However it must be noted that such calculations are performed on an isolated molecule. In a liquid the presence of other charged atoms close by will influence the electronic distribution. Also, these charges are really a condensation of the multipoles onto each atomic site and take no account of the actual distribution of charge across each individual atom. Taking both these points into consideration, the charges obtained from a Mulliken population analysis should only be seen as a guide, it is preferable to consider the charges to be quantities that can be varied in order to fit experimental data. From experience we have found that the final charges on each atom are substantially less than that given by the population analysis.

A better method for representing this charge distribution is to use some method to describe the multipoles within the molecule. This could be done by including point multipole moments at the centre of charges [25]. These multipoles can either be equal to the known values calculated on an isolated molecule, or 'effective' values chosen to reproduce the experimental data and liquid structure. However such a multipole expansion is not rapidly convergent. An alternative for

ionic and polar systems, is to use a set of fictitious 'partial charges' that are distributed about the molecule in a 'physically reasonable way' so as to reproduce the known multipole moments [26]. A further improvement on this is to distribute fictitious multipoles in a similar way [27]. However the coding to include these in the molecular dynamics routines that have been used in this project was still under development and so unavailable.

The second requirement is difficult to tackle. A brute force solution would be to increase the size of the molecular dynamics cell to hundreds of nanometers in length so that the screening by neighbours would diminish the effective range of the potential. However this solution is impracticable as the time required to perform the simulation, with no use of neighbourhood tables, is approximately proportional to N^2 ie. to L^6 where L is the cell box length. An alternative is spherical truncation of the potential, but again this is unworkable because the resulting sphere around a given ion could be charged, since the number of cations and anions need not balance at any one instant. The basic minimum image method corresponds to cutting off the potential at the surface of a cube surrounding the ion in question. This cube would be electrically neutral. However the drawback is that similarly charged ions will tend to occupy positions in opposite corners of the cube. This would mean that the periodic image structure will be imposed directly on to what should be an isotropic liquid which would lead to a distortion of the liquid structure.

There are two types method of dealing with these long range forces which use well-known ideas from the theory of electrostatics. These are the reaction field methods and the lattice methods, such as the Ewald sum. The former of these methods tends to overemphasise the continuum nature of a polar fluid and require an *a priori* estimate of the relative permittivity, whilst the latter tends to overemphasise

the periodic nature of the model fluid. It is this latter method, in particularly the Ewald sum [28] that has been utilised in this project for dealing with the electrostatic forces. It should be noted, however, that the inherent assumption of long range periodicity is not valid in real liquids and the use of the Ewald sum is only justified as a means of obtaining some account of the long range electrostatic effects. '*Computer Simulations of Liquids*'[2] provides a good account of the Ewald sum but below are the main points.

The potential energy due to the fractional charges can be written as

$$V^{zz} = \frac{1}{2} \sum_{\mathbf{n}}' \left(\sum_{i=1}^{N} \sum_{j=1}^{N} z_i z_j |\mathbf{r}_{ij} + \mathbf{n}|^{-1} \right) \qquad 3.30$$

where z_i and z_j are the charges on atoms i and j respectively, N is the number of atoms in the box, the sum over $\mathbf{n}$ is the sum over all simple cubic lattice points, $\mathbf{n} = (n_x L, n_y L, n_z L)$ with n_x, n_y, n_z integers and L is the box length. This vector represents the shape of the basic box. The prime indicates that $i = j$ is omitted for $\mathbf{n} = 0$. The factor $4\pi\varepsilon_0$ has been omitted in this equation for simplicity of notation, and this corresponds to a non-SI unit of charge. For long range potentials this sum is conditionally convergent, that is, the result depends on the order in which the terms are summed. If the boxes are summed in order of their proximity to the central box (i.e. the first term is $|\mathbf{n}| = 0$, the second $|\mathbf{n}| = L$, etc.), then as further terms are added, the system is developed into an infinite system of roughly spherical layers. When this approach is adopted, then the nature of the medium surrounding the sphere, particularly its relative permittivity, ε_s, must be specified. This is because the results for a sphere surrounded by a good conductor, such as a metal ($\varepsilon_s = \infty$), and for a sphere surrounded by vacuum ($\varepsilon_s = 1$) are different [29]

$$V^{zz}(\varepsilon_s = \infty) = V^{zz}(\varepsilon_s = 1) - \frac{2\pi}{3L^3} \left| \sum_i z_i \mathbf{r}_i \right|^2 \qquad 3.31$$

This equation applies in the limit of a very large sphere of boxes. In the vacuum, the sphere has a dipolar layer on its surface: the last term in equation 3.31 cancels this. For the sphere in a conductor there is no such layer.

At any point in a simulation, the distribution of charges in the central cell constitutes the unit cell for a neutral lattice which extends throughout space. In the Ewald method, each point charge is surrounded by a charge distribution of equal magnitude and opposite sign, which spreads out radially from the charge. This distribution is conveniently taken to be Gaussian

$$\rho_i^z(\mathbf{r}) = z_i \kappa^3 \exp(-\kappa^2 r^2)/\pi^{3/2} \qquad 3.32$$

where the arbitrary parameter κ determines the width of the distribution, and $\mathbf{r}$ is the position relative to the centre of the distribution. This extra distribution acts like an ionic atmosphere, to screen the interaction between neighbouring charges. The screened interactions are now short-ranged, and the total screened potential is calculated by summing over all the molecules in the central cube and all their images in the real space lattice of image boxes.

A charge distribution of the same sign as the original charge, and the same shape as the original distribution $\rho_i^z(\mathbf{r})$ is also added. This cancelling distribution reduces the potential to that due to the original set of charges. The cancelling distribution is summed in reciprocal space. The formula includes the interaction of the cancelling distribution centred at $\mathbf{r}_i$ with itself, and this self term must be subtracted from the total. The final potential is

$$V^{zz}(\varepsilon_s = 1) = \frac{1}{2}\sum_{i=1}^{N}\sum_{j=1}^{N}\left(\sum_{|\mathbf{n}|=0}^{\infty}{}' z_i z_j \frac{\mathrm{erfc}(\kappa|\mathbf{r}_{ij}+\mathbf{n}|)}{|\mathbf{r}_{ij}+\mathbf{n}|}\right.$$

$$+\left(\frac{1}{\pi L^3}\right)\sum_{\mathbf{k}\neq 0} z_i z_j \left(\frac{4\pi^2}{k^2}\right)\exp\left(\frac{-k^2}{4\kappa^2}\right)\cos(\mathbf{k}.\mathbf{r}_{ij})\Bigg)$$

$$-\left(\frac{\kappa}{\pi^{1/2}}\right)\sum_{i=1}^{N} z_i^2 + \left(\frac{2\pi}{3L^3}\right)\left|\sum_{i=1}^{N} z_i \mathbf{r}_i\right|^2 . \qquad 3.33$$

Here erfc (x) is the complimentary error function

$$\mathrm{erfc}(x) = \left(\frac{2}{\pi^{1/2}}\right)\int_x^{\infty} \exp(-t^2)\mathrm{d}t \qquad 3.34$$

which falls to zero with increasing x. Thus is κ is chosen to be large enough, the only term which contributes to the sum in real space is that with $n = 0$, and so the first term reduces to the normal minimum image convention. The second term is a sum over reciprocal vectors $\mathbf{k} = 2\pi\mathbf{n} / L^2$.

3.3 Calculating The Pair Distribution Function

'Computer Simulation of Liquids' by Allen and Tildesley[2] provides a very good description of the pair distribution function and how to incorporate it into a molecular dynamics simulation. However the salient points are presented below.

Although the pair distribution function is a continuous function, an approximation can be made by using a binning method to calculate the probability function. Consider the simple case of Argon atoms in the liquid phase at any one instant. (figure 3.10)

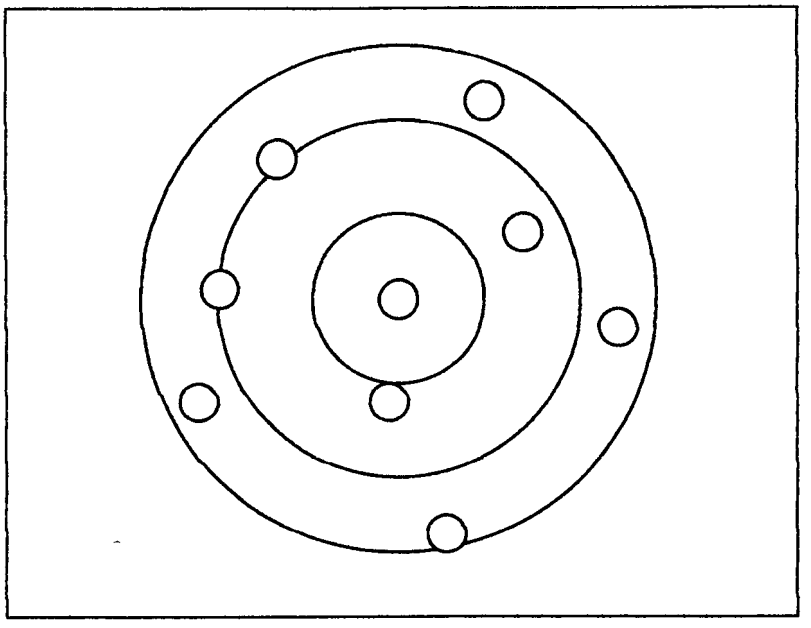

Figure 3.10 A two dimensional distribution of Argon atoms

The figure shows a distribution in two dimensions for simplicity but in reality this would be a number of concentric spheres.

The g(r) is derived from this distribution in five steps:

1) One of the atoms is arbitrarily chosen and spheres of radius r are drawn around it in increments of dr (the binwidth of a histogram).
2) The number of atoms n(r) within the shells between each sphere (of thickness dr) is counted and placed in the histogram bins.
3) n(r) is divided by the number density, ρ, and the volume of the sphere, $4\pi r^2 dr$.
4) Steps 1 - 3 are repeated for all other atoms adding the results into the appropriate bins.
5) The totals in the bins are divided by the total number of atoms N.

This is equivalent to using:

$$g(r) = \frac{\langle n(r) \rangle}{4\pi\rho r^2 dr} \qquad 3.35$$

This procedure is repeated at every n^{th} timestep to achieve a time averaged picture of the structure in a simulation run.

3.3.1 Partial Pair Distribution Functions

The total pair distribution function can be considered to be a sum of all the partial pair distribution functions. Consider the molecule CHF_3, the number of individual interactions between the two molecules can be calculated as below.

	C	H	F	F	F
C	α	β	χ	χ	χ
H	β	δ	ε	ε	ε
F	χ	ε	ϕ	ϕ	ϕ
F	χ	ε	ϕ	ϕ	ϕ
F	χ	ε	ϕ	ϕ	ϕ

Thus for any two molecules of CHF_3 there will be:

1 C...C interaction (α)

1 H...H interaction (δ)

2 C...H interactions (β)

6 C...F interactions (χ)

6 H...F interactions (ε)

9 F...F interactions (ϕ)

This makes a total of 25 possible interactions. However it is not possible to distinguish between the individual fluorines on each molecule. Thus if the partial pair distribution function for each type of pair were calculated then there would only

be 6 distinct partial pair distribution functions. In order to sum these to create the total pair distribution function then each partial pair must be weighted according to the number of interactions there really are of that type:

$$g_{total}(r) = \sum_{x} \frac{N_{xy}}{N} g_{xy}(r) \qquad 3.36$$

Where $g_{total}(r)$ is the total pair distribution function, $g_{xy}(r)$ is the partial pair distribution function for the pair xy, N_{xy} is the number of interactions for pair xy and N is the total number of interactions possible. Thus, for trifluoromethane the sum would look like:

$$g_{total}(r) = \frac{1}{25} g_{CC}(r) + \frac{1}{25} g_{HH}(r) + \frac{2}{25} g_{CH}(r) + \frac{6}{25} g_{CF}(r) + \frac{6}{25} g_{HF}(r) + \frac{9}{25} g_{FF}(r)$$

3.3.2 Comparing To Pair Distribution Functions From Neutron Scattering

The pair distribution functions obtained from neutron scattering experiments are *'neutron weighted'*. This means that the partial pair distribution functions have an extra factor referred to as the *scattering length, b* (see section 2.2.5). In order for the total pair distribution function from a simulation to be compared to that from a neutron scattering experiment, the neutron weighting must be taken into account. This is done by summing the partial pair distribution functions according to equation 3.37.

$$g_{total}(r) = \frac{\sum N_{xy}\, b_x\, b_y\, g_{xy}(r)}{(\sum N_x\, b_x\,)^2} \qquad 3.37$$

N_x is the number of atoms in one molecule and b_x is the scattering length of atom x.

3.4 Establishing The Intermolecular Structure

Once the partial pair distribution functions have been obtained then some method is needed to extract the necessary information about molecular orientation. The peaks in the functions indicate the most likely separations for a pair of atoms in the liquid. Integration of the pair distribution functions leads to information about the number of atoms around a central atom. For example, integration of the sharp, intramolecular peaks indicates the number of bonds in the molecule. Integration of the first shell of the total pair distribution function gives the co-ordination number of the liquid:

$$Z \equiv 4\pi n \int_0^{r_m} g(r) r^2 \, dr \qquad 3.38$$

$$n^2 = \frac{N(N-1)}{V^2} \qquad 3.39$$

Z is the co-ordination number, n is the conditional probability density of finding a molecule a distance r from the centre of a given molecule, N is the number of molecules, V is the volume occupied by N molecules and r_m is the value of r where the integrand is at its first minimum. Examination of this co-ordination number in the total pair distribution function leads to information on the density of packing, i.e. whether the liquid is close packed or of a more open structure. Performing this integration on the peaks in the partial pair distribution function leads to information about how the molecules are arranging themselves towards one another. Using a molecular modelling package it is possible to build structures of molecules that fit the information provided. Whilst these images of the structure are static they nevertheless provide an insight into the most probable arrangement of the molecules

in the liquid. This in turn leads to a better understanding of the properties of that liquid.

3.5 Conclusions

Molecular dynamics simulations provide a solution to the problem of understanding what is happening within a liquid at the molecular scale and the results of such simulations can be compared to experimental data, and hence provide further information about that data than would be observed by conventional experimental techniques.

---

1 HALL, C.D., *Thesis: Neutron Diffraction and Molecular Dynamics Studies of Fluid Halocarbons*, 1992, *University of Liverpool*

2 ALLEN, M. P., TILDESLEY, D. J., 1989, *Computer Simulation Of Liquids*, Clarendon Press

3 HANSEN, J. P., McDONALD, I. R., *Theory Of Simple Liquids*, Academic Press

4 MDMPOL, CCP5 molecular dynamics program, SMITH W., FINCHAM D., (modified by COOPER D. L., for our purposes).

5 FORESTER, T. R., SMITH, W. 1994, DLPOLY: a molecular dynamics program for the simulation of polyatomic molecular liquid mixtures, CCP5 Program Library (Manchester, UK: Daresbury Laboratory).

6 BERMEJO, F. J., ENCISO, E., ALONSO, J., GARCIA, N., HOWELLS, W. S., 1988, *Molec. Phys.*, **25**, 1353.

7 ALDER, B. J., WAINWRIGHT, T. E., 1959, *J. Chem. Phys*, **31**, 459

8 ALDER, B. J., WANWRIGHT, T. E., 1960, *J. Chem. Phys.*, **33**, 143

9 O'DELL, J., BERNE, B. J., 1975, *J. Chem. Phys.*, **63**, 2376

10 AXILROD, B. M., TELLER, E., 1943, *J. Chem. Phys.*, **11**, 299

11 DORAN, M. B., ZUCKER, I. J.,1971, *J. Phys.*, **C4**, 307

12 BARKER, J. A., FISHER, R. A., WATTS, R. O., 1971, *Mol. Phys.*, **21,** 657

13 MONSON, P. A., RIGBY, M., STEELE, W. A., 1983, *Mol. Phys.*, **49**,893

14 MAITLAND, G. C., SMITH, E. B., 1971, *Mol. Phys.* **22**, 861

15 VERLET, L., 1967, *Phys. Rev.*, **159**, 98

16 FINCHAM, D., HEYES, D. M., 1982, *CCP5 Quarterly*, **6**, 4

17 HEYES, D. M., SINGER, K., 1982, *CCP5 Quarterly*, **6**, 11

18 GEAR, C. W., 1966, The numerical integration of ordinary differential equations of various orders. Report ANL 7126, Argonne National Laboratory.

19 GEAR, C. W., 1971, *Numerical initial value problems in ordinary differential equations*. Prentice-Hall, Englewood Cliffs, NJ

20 BAROJAS, J., LEVESQUE, D., QUENTREC, B., 1973, *Phys. Rev.*, **A7**, 1092

21 EVANS, D. J., 1977, *Molec. Phys.*, **34**, 317

EVANS, D. J., MURAD, S., 1977, *Molec. Phys.*, **34**, 327

22 GOLDSTEIN, H., (1980). *Classical Mechanics* (2nd edn.). Addison-Wesley, Reading, MA

23 GEAR, C.W. 1966, *The numerical integration of ordinary differential equations of various orders*, Report ANL 7126, Argonne National Laboratory

24 GEAR, C. W., 1971, *Numerical initial value problems in ordinary differential equations*, Prentice-Hall, Englewood Cliffs, NJ

25 STREETT, W. B., TILDESLEY, D.J., 1977, *Proc. R. Soc. Lond.*, **A355**, 239

26 MURTHY, C. S., O'SHEA, S. F., MCDONALD, I. R., 1983, *Mol. Phys.*, **50**, 531

27 PRICE, S. L., STONE, A. J., ALDERTON, M., 1984, *Mol Phys.*, **52**, 987

28 EWALD, P., 1921, *Ann. Phys.*, **64**, 253

29 DE LEEUW,S. W., PERRAM, J. W., SMITH, E. R., 1980, *Proc. R. Soc. Lond.*, **A373**, 27

Chapter Four

Molecular Dynamic Experiments

4.1 Introduction

Before discussing the results of the simulations that have been performed in this project it is beneficial to understand how these results were achieved. It is desirable for anyone continuing this work to begin where it has finished, rather then to retread over ground already covered. Bearing this in mind a section has been included that gives an overview of the program utilised in the project, that is DLPOLY [1], and the effect of varying the various parameters that can be manipulated in the program. The users manual for DLPOLY [1] has been used as a source for the information concerning the program and its use. This section should only be regarded as an overview, and if more detailed knowledge is needed then it is strongly recommended to read this manual.

4.2 How to use DLPOLY

DLPOLY [1] is a molecular dynamics simulation package developed by W. Smith and T. R. Forester under the encouragement of the Engineering and Physical Sciences Research Council (EPSRC). The aim of the program is to provide a simulation program that extended the techniques of molecular dynamics to the simulation of macromolecules, polymers, ionic systems and solutions on a distributed memory parallel computer.

4.2.1 Setting up a start up configuration

As with all simulations, some method is needed to create the starting positions of all the molecules in the molecular dynamics cell. DLPOLY contains within it a program that generates a lattice configuration, *Genlat*. This will produce an array of the molecules in a format such that DLPOLY can use. For the systems studied in this project it was necessary to calculate the volume occupied by one molecule, and produce a single cell of this volume containing one molecule. As the systems were to be simulated in a cubic cell, this was relatively straight forward, with the unit cell being cubic. The co-ordinates of the molecule must be entered in fractional co-ordinates *of this single cell*. The program takes this single cell and repeats it to fill the molecular dynamics cell. The repetitions along each side are defined by the user, and to obtain a cubic cell these values must be equal. For example, consider the molecule CCl_2F_2, then the input for Genlat would be as below:

Header: CCl2F2 at 153 K

Number of basis atoms: 5

*Unit Cell Vector **a**: 4.88 0 0*

*Unit Cell Vector **b**: 0 4.88 0*

*Unit Cell Vector **c**: 0 0 4.88*

Integer multiples of unit vectors: 5 5 5

Name and co-ordinates of atoms:

Cl 0.0000 0.5943 0.0000

Cl 0.0000 0.0000 0.0000

F 0.4225 0.2971 0.0368

F 0.1637 0.2971 0.3913

C 0.1637 0.2971 0.1195

This would set up a cubic deck 5 x 5 x 5 i.e. 125 molecules. The box length for the molecular dynamics cell would be 24.402 Å and the volume would be 1.453×10^4 Å^3. The program is run interactively and produces a file called LATTICE containing the configurational details. This must be copied into a file called CONFIG. (Note: as with all unix systems, the capitalisation is important.)

4.2.2 The CONTROL file

This file contains the control variables needed for running a DLPOLY job. There are various options contained within this file and a good explanation of them is found in the user manual. In this section some of the important options used in this project are explained.

temperature 153

This is fairly self explanatory. The temperature is entered in Kelvin, and DLPOLY uses this to select a range of initial velocities for the start of the run, and for rescaling during the equilibration period.

timestep	5.0E-3 ps
steps	50000
equilibration steps	40000
scale every	5
multiple timestep	1 steps

These define the simulation length and the equilibration period. *Timestep* sets the length of the timestep to *n* ps. This value is very important. As explained in Chapter Three, if the timestep is too short than the number of steps needed for the simulation to yield good results become very large, and hence the time taken for the simulation to complete becomes too large. If the timestep is too long than the energy will tend to drift instead of staying constant. The value shown provided constant total energy of the system, whilst keeping the runtime at a reasonable level. *Steps* is the *total* number of steps in the simulation, and *equilibration steps* is the number of steps that the simulation will spend equilibrating at the start of the simulation. Data are collected during the non-equilibration time, which is (*steps* - *equilibration steps*.) To ensure that data are collected *steps* must be greater than *equilibration steps*. Starting from a lattice configuration a large number of timesteps are needed to bring the liquid to equilibration. At least 80,000 steps were required for the molecules in this project. This was ascertained by performing a simulation from the lattice structure and comparing the pair distribution function and total energy regularly until there was no change. However, if several runs are going to be made as forcefield

adjustments are implemented then, provided the input deck is from a previous equilibrated run, the number of timesteps can be reduced to a much lower value, for example 4,000. A reasonable number of timesteps are needed during data collection to ensure good statistics, and usually a minimum of 5000 are required. *Scale every* indicates how frequently the velocities of the molecules are rescaled during the equilibration period to ensure that the temperature stays at the required value. *Multiple timesteps* specifies the number of timesteps that elapse between partitions of the full Verlet neighbour list into primary and secondary atoms. In all the simulations in this project this has been set to one.

cut-off 10.3

delr 0.2

Cut-off is the radius of the cut-off sphere, outside of which the force due to the pair potential is set to zero. This should be no greater than half the length of the molecular dynamics cell. *Delr* sets the Verlet neighbour list shell width. The list is updated whenever two or more atoms have moved a distance of more than *delr*/2 from their positions at the last update of the Verlet list.

rdf sampling every 10 steps

print rdf

Rdf sampling indicates the interval between calculations of the pair distribution function. This calculation requires a reasonable amount of computational time, so instead of calculating it at every step, the cell is sampled at regular intervals. The command *print rdf* informs the program to print the averaged partial pair distribution functions at the end of the OUTPUT file when the simulation is completed.

ewald sum 0.32 6 6 6

Ewald sum indicates that the program is to use the Ewald sum for the electrostatics using the four parameters α, *k1*, *k2*, *k3*. α is the Ewald convergence parameter ($Å^{-1}$), *k1* is the maximum k-vector index in the x-direction, *k2* is the maximum k-vector index in the y-direction, *k3* is the maximum k-vector index in the z-direction. The Ewald sum is explained in section 3.2.5. The *k* vector indicies in each direction is taken to be an arbitrary value, for example 8, 8, 8. α should lie in the region of 0.32 for the simulations in this project, but can be chosen by performing a series of single step simulations, changing α each time, and plotting the Coulombic energy versus α. The plot should show a plateau which indicates that both the reciprocal and real space sums are converged. The smallest value for α is picked for which the sums are converged, and the values of *k* are systematically reduced until they are the lowest value that still gives the energy within the accuracy desired.

ensemble nve

This command tells the program what type of ensemble is to be simulated. NVE indicates that the number of molecules in the box, the volume and the total energy of the system are to be kept constant. This ensemble was chosen for all the simulations described in this thesis.

Once a simulation has finished it is possible to restart using one of two commands:

restart

restart scale

Restart restarts the job from the end point of the previous run. In order to do this the final configuration is copied into the CONFIG file using the command.

gopoly copy.

This copy command also renames the REVIVE file, containing statistics arrays from the previous simulation, REVOLD. The previous number of timesteps performed is carried over and so the number of timesteps defined by *steps* must be greater than the last. Note that no extra equilibration is performed using this command, and so it should not be used when the potential parameters have been changed. *Restart scale* also needs to have the new CONFIG file copied over via the above command line. However with this command the simulation starts from zero timesteps again and an equilibration period will be performed if one is specified. The number of timesteps are not carried over and so an adjustment to the *steps* value is not necessary. When varying the parameters in a force field it is more useful to use the latter command so that the system can equilibrate with the new forces on the atoms.

4.2.3 The CONFIG file

This file contains the dimensions of the unit cell, the key for the periodic boundary conditions, the atomic labels, co-ordinates and, if the file has been written after a simulation, the final velocities and forces. If the initial configuration has been set up using Genlat then the LATTICE file will be in the correct format for the CONFIG file and can simply be renamed. This initial configuration will not contain the velocities of the atoms and these will be selected from a Maxwell-Boltzmann distribution suitable for the temperature specified in the CONTROL file.

4.2.4 The FIELD File

The FIELD file contains the information pertaining to the force field in the simulation. It contains the partial charges on the atoms, the vibrational forces and any constraints used in defining the molecules. It also contains the parameters for the

intermolecular potential. There are a wide variety of options when defining the various parts of the force field and for the full range refer to the DLPOLY manual.

Although DLPOLY contains force fields to simulate the vibrations within a molecule it soon became clear that it was better to model the molecule as rigid. This was because the transference of energy between the vibrations and the rest of the system was poor. To overcome this it would have been necessary to greatly reduce the timestep for the simulation due to the small time period for the oscillations. This would vastly increase the number of timesteps needed to attain equilibrium and collect data, and hence the physical time taken to run a simulation and obtain results.

The file is divided up into three sections: general information, molecular descriptions, and non-bonded interactions.

4.2.4.1 General Information

The first record in the file is the title which must be followed by the *units* directive. Both these are mandatory. The energy units are described by additional keywords. The choice of energy unit also determines the choice of units used for length, time etc. The energy unit defined by *internal* (10 J mol^{-1}) was used in this project, which is the unit DLPOLY uses internally. This means that the unit of length is defined in Å and the unit of time in ps. Consequently all energy units in the input and output are given in 10 J mol^{-1}.

4.2.4.2 Molecular Details

It is important that the order of specification of molecular types and their atomic constituents in the FIELD file follows the order in which they appear in the CONFIG file. If this does not happen then the program will fail.

The entry of the molecular details begins with the mandatory directive:

molecules n

where n is an integer specifying the number of different *types* of molecule appearing in the FIELD file. For a pure liquid this value is 1. Once this directive has been encountered DLPOLY enters the *molecular description* environment in which only molecular description keywords and data are valid. These define :

1 the name of the molecule (for reference purposes)

2 the number of these molecules in the cell

3 the names, masses and charge of each constituent atom in the molecule.

4 the vibrational details, and / or constraints within the molecule, or whether the molecule is completely rigid.

Once the atoms have been named, they are referred to in the rest of the intramolecular descriptions by integers that indicate their position in the atomic definition list. This means a value of 1 means the first atom in the list, 2 the second etc. These indices are used in the definition of bonds, angles and dihedrals. It is important to define **all** the molecular structure as DLPOLY uses these definitions to create an *excluded atoms list*. These are the atoms that have a separate potential, or constraint defined for them and thus do not need to be included in the calculation of the intermolecular potential. Any separations that are not defined will have a Lennard-Jones potential applied between them using the intermolecular parameters that are defined at the end of the file. As such, because the distances are smaller then σ, a large positive value will be seen, leading to errors in the reported value of the energy.

Finish. This directive is entered to signal the end of the details for the molecule. The entries for the second molecular type may now be entered, beginning with the name

and ending with *finish*. The cycle is repeated until all the types of molecules indicated by the *molecules* directive have been entered.

There are various other option available in the molecular description that we have not made use of. For more information refer to the user manual.

4.2.4.3 Non-bonded Interactions

The rest of the entries in the FIELD file are concerned with non-bonded interactions. These are identified by atom types as opposed to specific atomic indices. Again there are various different potentials available, both effective pair, and three body potentials. We have made use of the effective pair potential represented by the Lennard-Jones potential

$$U(r) = 4\varepsilon\left[\left(\frac{\sigma}{r}\right)^{12} - \left(\frac{\sigma}{r}\right)^{6}\right] \qquad 4.1$$

where ε is the depth of the potential well and σ is the distance at which the pair potential is zero.

Any pair potential not specified in the field file is assumed to be zero. The pair potentials are implemented between any pair of atoms that have not already been defined in the molecular descriptions.

The field file must be closed with the directive

close

which signals the end of the force field data. Without this directive DLPOLY will abort the job.

4.2.5 The REVOLD file

This file contains statistics arrays from a previous job. It is only required if the current job is a continuation of a previous run (i.e. if the *restart* directive is present in the CONTROL file).

4.2.6 The HISTORY file

The HISTORY file contains the atomic co-ordinates, velocities and forces. Its principal use is for off-line analysis. This file is created only if the directive *traj* appears in the CONTROL file. To date we have made no use of this facility so a detailed analysis of it shall not be included. More information is available in the DLPOLY manual.

4.2.7 The OUTPUT file

As its name implies this file contains the main output results from the simulation. It also contains regular summaries of the statistical data, reported at intervals determined by the directive *print every* in the command file. Thus the simulation can be monitored to ascertain the simulation progress during a run. The file consists of seven sections: header, simulation control specifications, force field specification, summary of the initial configuration, simulation progress, summary of the statistical data, sample of the final configuration, and the pair distribution functions. These sections are written at various stages of the job. The OUTPUT file is always created when DLPOLY is run.

4.2.7.1 Header

This gives the version number of DLPOLY, the number or processors used and a title for the job as specified in the CONTROL file.

4.2.7.2 Simulation control specifications

This section reproduces the input from the CONTROL file. Some values may be reset if illegal values were specified.

4.2.7.3 System force field specification

This reproduces the FIELD file. A warning line is printed if the system is not electrically neutral. This warning will appear immediately before the non-bonded short-range potential specifications.

4.2.7.4 Summary of the initial configuration

This section states the periodic boundary specification, the cell vectors and volume and the initial configuration of 20 atoms in the system. For periodic systems this is followed by the long range corrections to the energy and pressure.

4.2.7.5 Simulation progress

The header for this is printed at the top of every page. The manual gives a description of each statistical variable in the list. The energy terms are given in the internal units, that is 10 $Jmol^{-1}$. However this means per mole of the molecular dynamics cell. To obtain the energy per mole of species (or molecule for a pure liquid) it is necessary to divide this figure by the number of molecules in the cell.

At each timestep that printout is requested the instantaneous values of the statistical variables are given in the appropriate columns. Immediately below these

three lines of output the rolling averages of the same variables are given. The working number of timesteps for rolling averages is controlled by the directive *stack* in the CONTROL file.

4.2.7.6 Summary of statistical data

This section of the output file contains the number of timesteps, the averages and the root mean squared deviations for each of the statistical variables. The statistics only refer to the production portion (i.e. the non-equilibration portion) of the run Also provided in this section is an estimate of the diffusion coefficient for the different species in the simulation, which is determined from a *single time origin* and is therefore very approximate. There is an estimate of the average pressure tensor provided.

4.2.7.7 Sample of final configuration

This section of the output file contains the positions, velocities and forces of the 20 atoms used for the sample of the initial configuration.

4.2.7.8 Radial (pair) distribution functions

If the commands *rdf* and *print rdf* are included in the CONTROL file then the OUTPUT file will contain the *partial* pair distribution functions of all the atoms in the simulation. First the number of timesteps, i.e. configurations used for collection of the histograms is stated. Then each function is given in turn. For each function a header line states the atom types ('a' and 'b') represented by the function. Then r, $g(r)$, and $n(r)$ are given in tabular form. Output is given from two entries before the first non-zero entry in the $g(r)$ histogram. The pair distribution function excludes

information about the intramolecular structure, assuming that all the intramolecular separations have been defined in the *molecular description* section of the FIELD file. $n(r)$ is the average number of atoms of type 'b' within a sphere of radius r around an atom of type 'a'.

In order to be able to analyse, display, sum and neutron weight these partial pair distribution functions a program has been written to extract the relevant information from the OUTPUT file. This program has been set up as part of DLPOLY and can be run by typing :

gopoly rdfedit

at the command prompt.

4.2.8 The REVCON file

REVCON contains the data for the restart configuration file. The file is written every *ndump* timesteps in case of a system crash during execution and at the termination of the job. A successful run of DLPOLY will always produce a REVCON file, but a failed job may not produce the file if an insufficient number of timesteps have elapsed. *ndump* is defined in the source code but can be altered and the whole program recompiled. REVCON is identical in format to the CONFIG input file.

4.2.9 The REVIVE file

This file containes the accumulated statistical data. It is updated whenever the REVCON file is updated.

4.2.10 The STATIS file

This file contains the instantaneous values of statistical variables, defined in the manual, that have been appended to the file, at intervals determined by the *stats* directive in the CONTROL file, during the simulation. No use was made of this file in this project.

4.3 Choosing a suitable intermolecular potential

All the molecular dynamics simulations in this study have used a site-site Lennard-Jones potential augmented with fractional charges at the atomic positions. The Lennard-Jones sites also coincide with the atomic positions. It is the selection of suitable potential parameters and charges that determine the success of the simulation.

4.3.1 Lennard-Jones Potential Parameters

The Lennard-Jones potential has the form shown in equation 4.1. ε_{ab} and σ_{ab} are adjusted to obtain different simulation results. In the past it has been usual to chose the values of these parameters for the like - like interactions such as C...C and F...F, and to use a mixing rule to calculate the like - unlike interactions, such as C...F, for example the Lorentz-Bertheholt mixing rules:

$$\varepsilon_{ab} = (\varepsilon_{aa}\varepsilon_{bb})^{\frac{1}{2}}$$

$$\sigma_{ab} = \frac{1}{2} (\sigma_{aa} + \sigma_{bb}) \qquad 4.2$$

These mixing rules provide a reasonable starting point for the cross parameters but we have found that an improvement to the fit to the experimental data can be obtained by allowing the cross parameters to vary.

As the choice of the potential parameters is an empirical fitting exercise then their values will change from run to run as they are adjusted to improve the reproduction of the experimental data. However reasonable values must be chosen at the start for the first simulation. The value for σ can be estimated from the sum of the Van der Waals' radii although the value obtained in this way will, in general, be too large. The best method for obtaining starting values for the parameters is to look over past simulations to see what values have been used. Although the values for the parameters will not necessarily be the same from one molecular type to another, they will usually be similar, particularly in the value of σ. The value of ε takes into account the polarizability of the atoms and should have a higher value for the more polarizable atoms.

It is useful to have some indication of how an adjustment in the parameters will effect the output of the simulation. The value of σ has the greatest effect on the local structure. An increase in σ leads to greater ordering and hence the peak heights of the individual pair distribution function will increase. The position of the first peak maxima will move to slightly longer r , although this effect may not be as noticeable as the change in peak height.

Altering the value of ε has a much more subtle effect on the structure. Frequently no change is perceptible with only small changes in value. However the changes do effect the energy and so ε can be used to produce fine adjustments to the value of the configurational energy.

As the mixed interactions are adjusted separately from each other, an alteration in the value of σ for one pair will only effect the pair distribution of another pair by a 'knock-on' effect. That is, if the alteration makes one interaction

more favourable, then by necessity another interaction must become less favourable. This must be born in mind when trying to increase or decrease a peak height in an individual pair distribution function.

However the contribution of the Lennard-Jones potential to the general shape of the total pair distribution function is limited. Adjustments really only result in slight changes in peak heights and positions unless large changes are made to σ. The general structure in most methane derivatives that have no significant dipole is determined by volume minimisation and so the changes to σ simply alter the way the molecules fit together. In molecules with a reasonable dipole, such as trifluoromethane, the fractional charges can dramatically alter the shape of the pair distribution function.

4.3.2 Fractional Charges

At each Lennard-Jones potential site there is a fractional charge. These are used to represent the charge distribution within the molecule. As such it is a very simple model, and consequently can only be expected to be a rough representation. As a starting point the fractional charges are obtained from a Mulliken Population analysis of an *ab initio* molecular orbital calculation on an isolated molecule. When these values are used in a molecular dynamics calculation the energy is normally greater than the experimental value and total pair distribution is too structured. In the past modellers have kept the values of these charges set at the Mulliken values and altered the Lennard-Jones parameters until the energy was correct. However this usually results in far too much structure in the pair distribution function. During the course of this project comparisons of the coulombic potential using fractional charges were compared with the potential produced by the distributive multipoles

obtained from *ab initio* molecular orbital calculations on the molecule. It was found that the decay of the coulombic potential took longer than for the distributive multipoles over distance. Considering that the calculation for the Mulliken population analysis is performed on an isolated molecule, rather than a molecule in a liquid, and given that the fractional charges are point charges rather than disperse charges, it seems reasonable to consider the fractional charges as being a variable quantity for the purpose of fitting the structure and energy. If this is done then not only can the energy be reproduced, but close fitting to the pair distribution function can also be seen. For molecules that only possess a small dipole, such as bromotrifluoromethane and chlorotrifluoromethane, the charges have little effect on the shape of the pair distribution function and the optimum values are quite low. The polarisation of the large atoms is taken into account by the more discriminating ε in the Lennard-Jones potential. In molecules such as trifluoromethane, the dipole plays a large part in determining the orientation of the molecules in the liquid. As such, both the size of the fractional charges and also their relative values to each other are important. Again the relative values need not necessarily be those produced by Mulliken population analysis, but this provides a good place to start. Unfortunately there is no fixed method of determining the distribution and only trial and error can be used.

4.4 Establishing the general liquid structure

A molecular dynamics simulation must not only reproduce the experimental pair distribution function but also, to feel confident that the simulation is a reasonable portrayal of the liquid at this temperature, the potential energy must

compare favourably with experimentally determined values for the enthalpy of vaporisation. This can be done as follows:

$$\Delta H_v = (\mathrm{PE} + \mathrm{KE} + P.V)_g - (\mathrm{PE} + \mathrm{KE} + P.V)_l \qquad 4.3$$

where the subscripts $_g$ and $_l$ represent the gas and liquid phases respectively, PE and KE are the potential and kinetic energies, P is the pressure and V is the molar volume. The kinetic energies cancel and by assuming ideal gas behaviour, the following relation may be derived:

$$\Delta H_v \approx RT - \mathrm{PE}_l \qquad 4.4$$

The further approximations used to yield equation 4.4 are that $P.V_l$ and Pe_g are both close to zero. For a liquid well below its boiling point equation 4.4 normally holds fairly well but at higher temperatures it is preferable to use equation 4.3 if all the data is available.

Once a successful run has been completed that reproduces satisfactorily the experimental data then the partial pair distribution functions can be analysed to establish the favoured orientation of the molecule in the liquid state. The average pair distances can be read off from the distribution functions together with the width of the distribution. Using this information, and utilising a molecular modelling package to calculate the atomic separations, various arrangements of molecules can be tested to see if they reproduce the peaks in the distribution functions. In this way an arrangement can be discarded if the pair distances are not at, or close to, the pair distances from the experiment. Sometimes there are two or more arrangements that when combined reproduce all the peaks and (more importantly) do not give extra peaks that are not in the distribution functions.

As well as pair distances it is possible to integrate the distribution functions to obtain co-ordination numbers. Although co-ordination numbers usually refer to a solid where the constituents do not move away from each other, it can still have some meaning in the more mobile liquid phase. Here it means the average number of molecules surrounding a molecule (or atoms around an atom) at any given instant. By integrating the total pair distribution function from the simulation from $r = 0$ to the first minimum then it is possible to obtain the co-ordination number for the first shell of molecules. This is equivalent to $n(r)$. The simulation results are used as DLPOLY gives $n(r)$ in the output, and because the intramolecular details are not included in the distribution. By examining the individual pair distribution function for the central atom in the molecule, i.e. C...C in a methane, the value of $n(r)$ at the first minimum is the co-ordination number for the molecule. If this method is also applied to the individual pair distribution functions then the number of closest pair interactions for each molecule can be calculated. Combining all this information means that a detailed picture of the average structure of the liquid can be built up.

4.5 Conclusions

DLPOLY is a flexible routine for performing molecular dynamics simulations. The program allows the user to perform repetitive simulations when adjusting the forcefield parameters without the need to start from a lattice configuration each time, reducing the amount of time necessary to obtain results. The analysis of the output is straightforward and can be used to obtain an insight into the way the molecules are orientating themselves within the liquid phase.

1 T. R. Forester and W. Smith, 1994, DLPOLY: a molecular dynamics program for the simulation of polyatomic molecular liquid mixtures, CCP5 Program Library (Manchester, UK: Daresbury Laboratory).

Chapter Five

Results

5.1 Introduction

Both neutron diffraction and simulation studies have been performed in the course of this project. Although the initial work on the fully halogenated methane derivatives was performed by Dr. C. D. Hall [1] the analysis has been completed in this project. New neutron diffraction measurements have been made on trifluoromethane, difluoromethane, 1,1,1,2-tetrafluoroethane and 1,1,2,2,-tetrafluoroethane and the total pair distribution functions for these molecules established. The intermolecular structure of trifluoromethane has been simulated and, together with a reanalysis of the measurements made by Hall et al. [2], has led to a full interpretation of the liquid-state structure of this fluid [3]. Finally attempts have been made to simulate the structure of difluoromethane but, as yet, a full interpretation has not been possible.

5.2 Trifluoromethane

Neutron diffraction experiments were carried out using the SANDALS facility at Rutherford Appleton Laboratory on hydrogenated trifluoromethane during the course of this project. Deuterated trifluoromethane had already been studied using this facility [2] but the results were reanalysed using the minimum information method of Soper [5]. Molecular dynamic simulations were then performed to attempt to reproduce the pair distribution functions and the internal energy.

5.2.1 Neutron Diffraction Experiment

Trifluoromethane, supplied by BOC at a purity of 99.998%, and deuterated trifluoromethane, supplied by ICI at a purity of > 99%, were studied using neutron diffraction on the SANDALS facility at the pulsed neutron source, ISIS, at the Rutherford Appleton Laboratory. The liquid was contained in a cylindrical, thin-walled pressure vessel, constructed of a null scattering titanium-zirconium alloy. Diffraction data were collected at 153 ± 1 K for both liquids and at 250 ± 1 K for deuterated trifluoromethane. The data were analysed using standard correction routines [4] to obtain the differential cross-sections.

The contribution to the differential cross-section from self-scattering needs to be subtracted before the data from the various detector banks can be merged to obtain a structure factor. The routine to do this calculates the self-scattering by assuming that it can be described by a low order Chebychev polynomial, found by fitting the differential cross-section. A parameter r_{min} is used to define the distance below which there is no contribution to the differential cross-section from the pair distribution function, i.e., $g(r) = 0$. Hydrogen exhibits incoherent scattering that is forty times its coherent scattering level, and so the order of the polynomial and the value chosen for r_{min} can affect the result quite critically. For example figure 5.1 shows the difference between the corrected cross-sections for various selections of parameters.

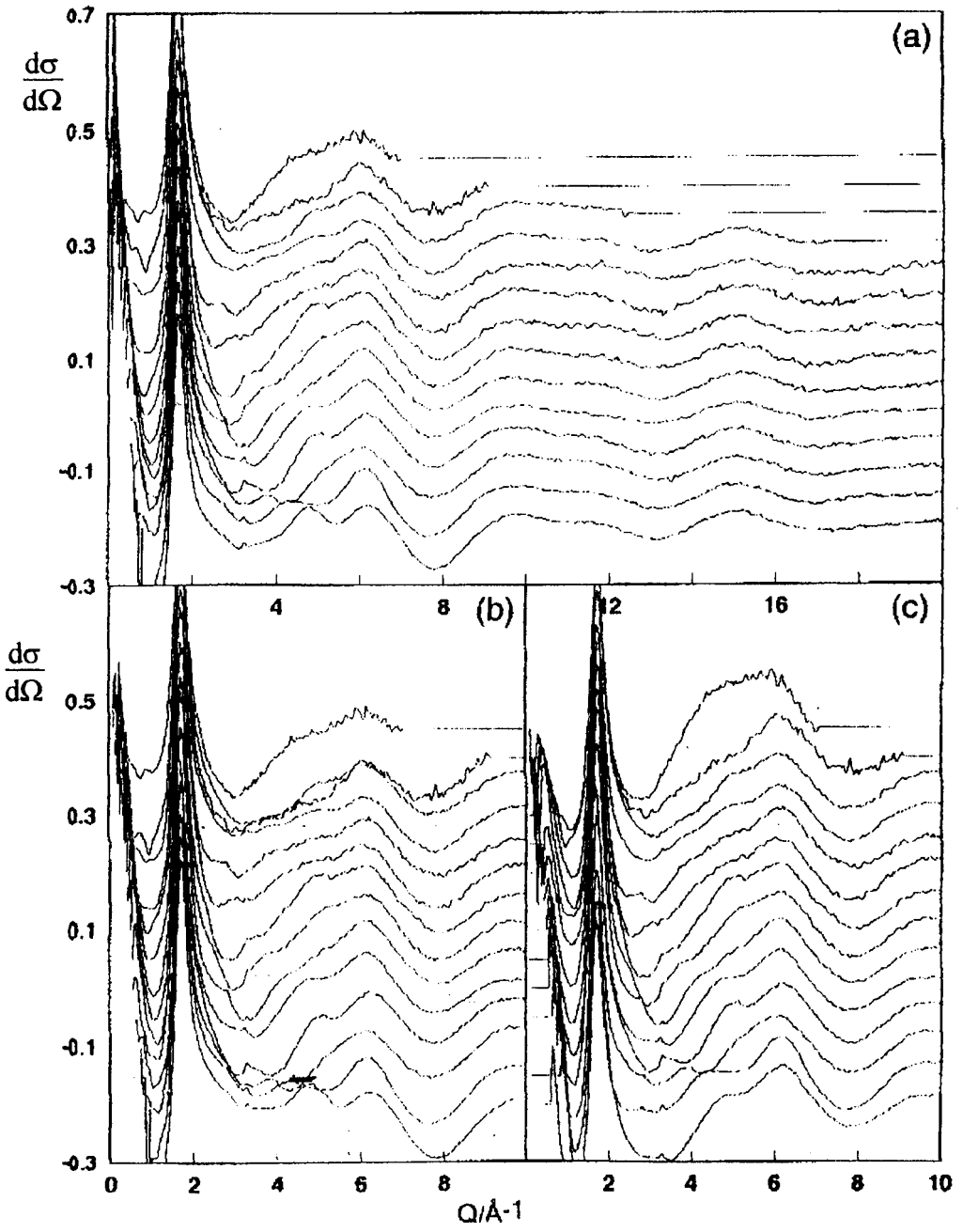

Figure 5.1 Corrected cross-sections obtained from the 14 banks of detectors for trifluoromethane. (a) The final version with r_{min} = 0.9 and Chebychev polynomial of order 3. These results were merged to obtain the final structure factor. (b) The version with r_{min} = 0.5 and Chebychev polynomial of order 3. (c) The version with r_{min} = 0.9 and Chebychev polynomial of order 5.

Each curve should oscillate about zero, but for ease of inspection the results for each bank have been separated by 0.05. The highest angle bank (31.28°) is plotted at the bottom of each figure and the lowest angle bank (3.83°) is plotted at the top. In each plot there is evidence of a small inelastic feature as indicated by a peak that varies position with angle. The merging program should average out the effect of this feature. Above 10 $Å^{-1}$ there was no obvious differences between the analyses. A good subtraction is indicated when the corrected cross-sections for each data bank are as similar as possible. In figure 5.1 it can be seen that a low r_{min} leads to a poor subtraction. Likewise, choosing a polynomial that is too high produces dissimilar cross-sections. Once a good match between the groups is obtained, the data can be merged to produce an S(Q). For the hydrogenated sample it was found that the optimum order of polynomial was 3 and that r_{min} should be set to 0.9 Å.

5.2.1.1 Neutron Diffraction Results

The structure factor, S(Q), obtained from the neutron diffraction experiments are shown in figure 5.2. By convention, these are defined per *atom*. The pair distribution functions shown in figure 5.3, were obtained from the structure factors using the minimum information method of Soper *et al* [5].The intramolecular geometry can be read directly from the position of the sharp peaks at low r, but it is better to attempt to represent the peaks by Gaussians. Data in the region $0.85 < r / Å < 2.5$ were represented by a combination of four Gaussians and a small background term. The positions and heights of all the peaks are allowed to vary freely, but to obtain a reasonable fit it was necessary to fix the width of the F...F peak at 0.1 Å.

The widths of the other peaks were allowed to vary. The results are shown in table 5.1 and are compared with experimental measurements on the isolated molecule.

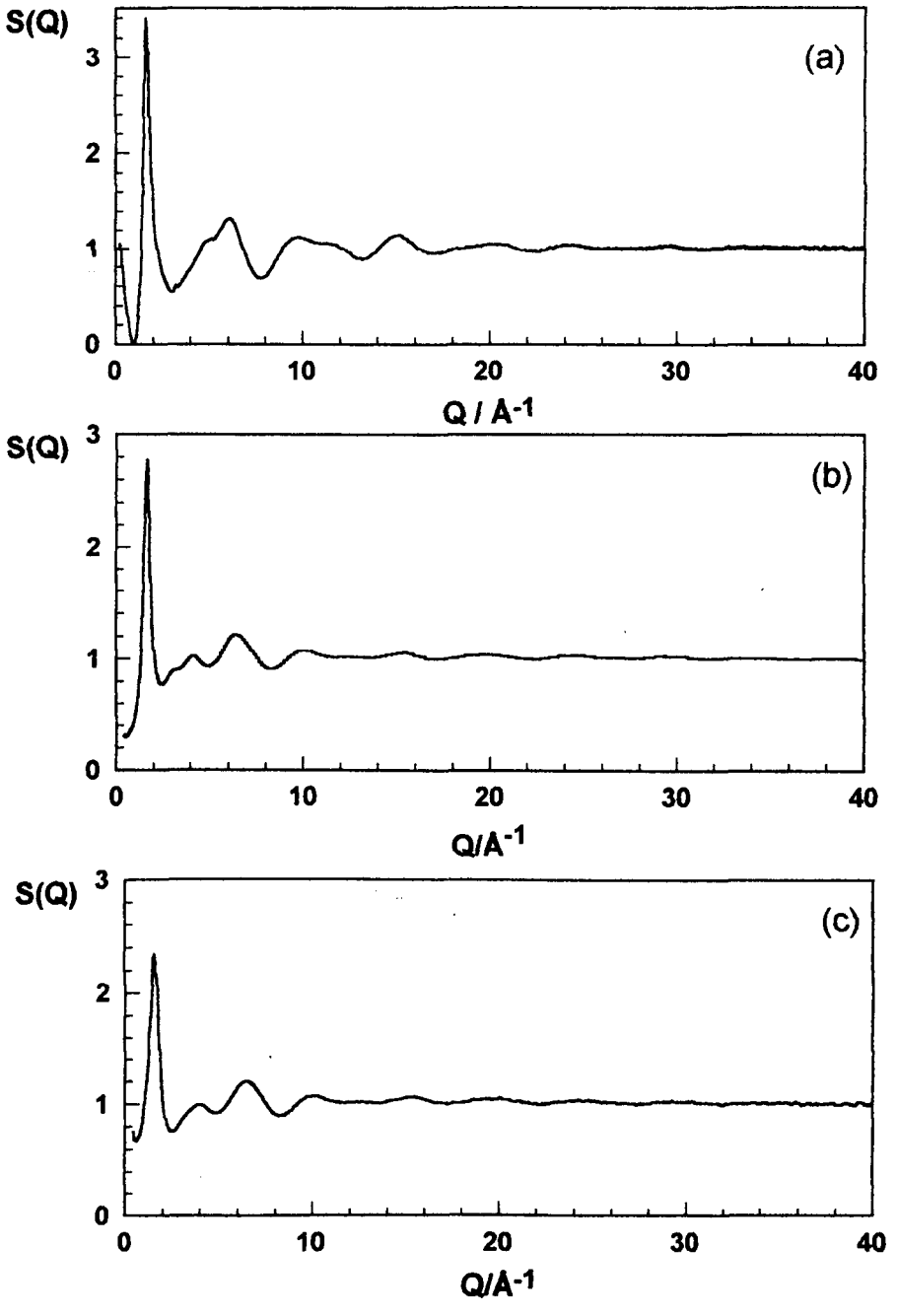

Figure 5.2 Atomic structure factors S(Q) for liquid trifluoromethane: (a) trifluoromethane at 153 K; (b) fully deuterated trifluoromethane at 153 K; (c) fully deuterated trifluoromethane at 250 K.

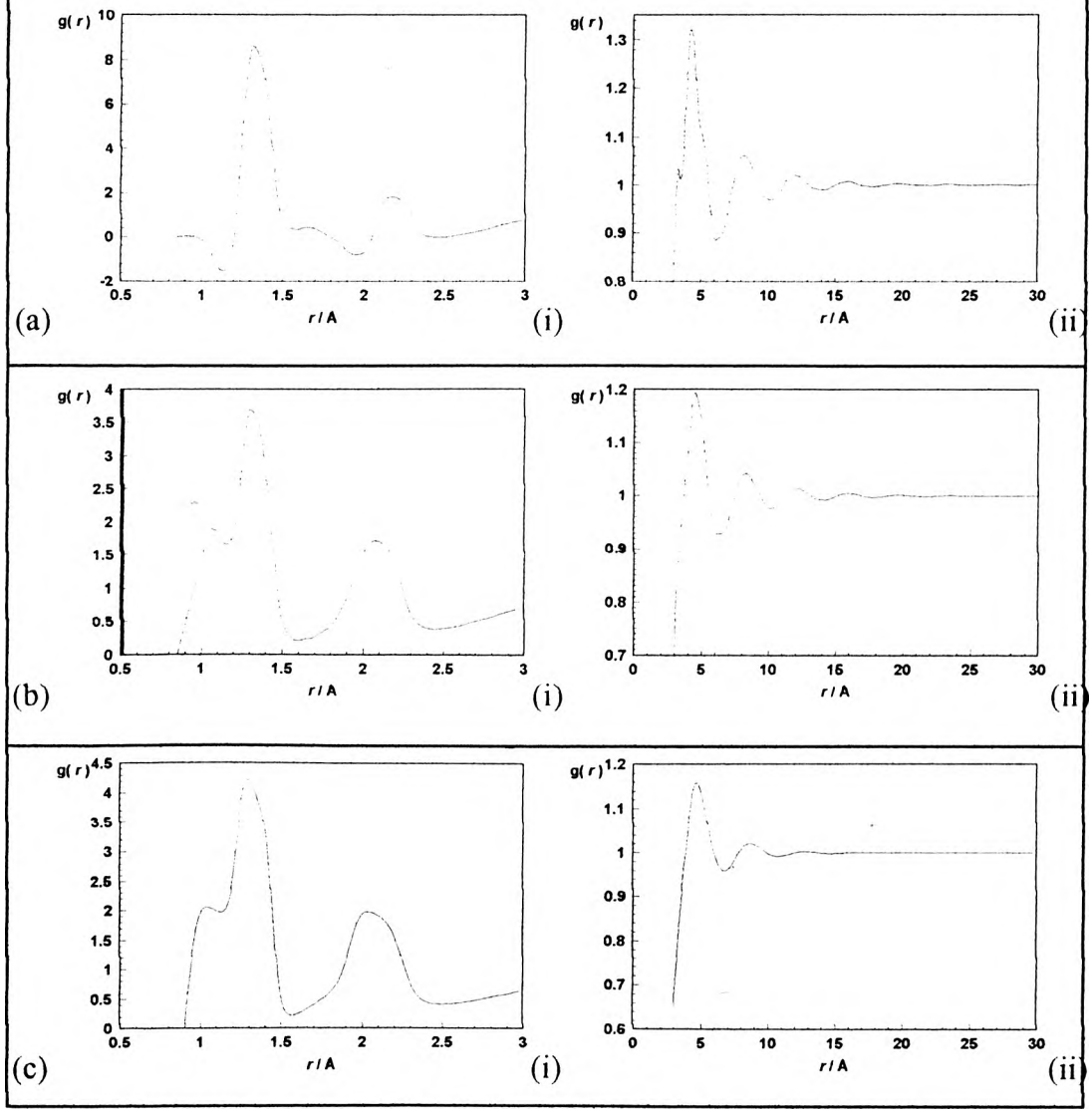

Figure 5.3 Total pair distribution functions g(*r*) for liquid trifluoromethane:(i) range 0.5 - 3.0 Å, (ii) range 0.0 - 30.0 Å, (a) trifluoromethane at 153 K; (b) deuterated trifluoromethane at 153 K; (c) deuterated trifluoromethane at 250 K

	Isolated molecule	Liquid State		
		CDF_3 (153 K)	CDF_3 (250 K)	CHF_3 (153 K)
r_{CH} / Å	1.098	1.061 ± 0.002	1.073 ± 0.002	1.183 ± 0.019
r_{CF} / Å	1.332	1.3290 ± 0.0007	1.3324 ± 0.0009	1.328 ± 0.009
r_{HF} / Å		2.09 ± 0.11	2.06 ± 0.02	2.14 ± 0.01
r_{FF} / Å	2.167	2.09 ± 0.02	2.10 ± 0.01	2.18 ± 0.007

Table 5.1 A comparison between the intramolecular atomic separations in trifluoromethane. The structure of an isolated molecule as determined by microwave spectroscopy [6] is compared with the liquid state structures.

Examination of the pair distribution functions reveals that the liquid is structured out to further than 20 Å at 153 K. The fourth shell is easily visible and the fifth shell is discernible. However, as demonstrated in figure 5.3, at 250 K the liquid displays structure only out to 15 Å, with only the first three shells being visible. This suggests that the liquid is substantially organised, possibly due to Coulombic interactions between the molecules, and that this organisation is reduced at higher temperatures.

After a subtraction of the pair distribution functions according to

$$(\sum N_X b_X)^2 g(r)_{CDF_3} - (\sum N_X b_X)^2 g(r)_{CHF_3}$$

$$= (b_D - b_H)(2b_C\, g(r)_{CH} + (b_D + b_H)\, g(r)_{HH} + 6b_F\, g(r)_{FH}) \qquad 5.1$$

only the C...H, H...F and H...H contributions to the pair distribution function remain. In this equation, N_X is the number of atoms of type X in the molecule, b_X is

the scattering length of atom X, $g(r)_{mol}$ is the pair distribution function of molecule 'mol', and $g(r)_{XY}$ is the partial pair distribution function of atom pair X... Y.

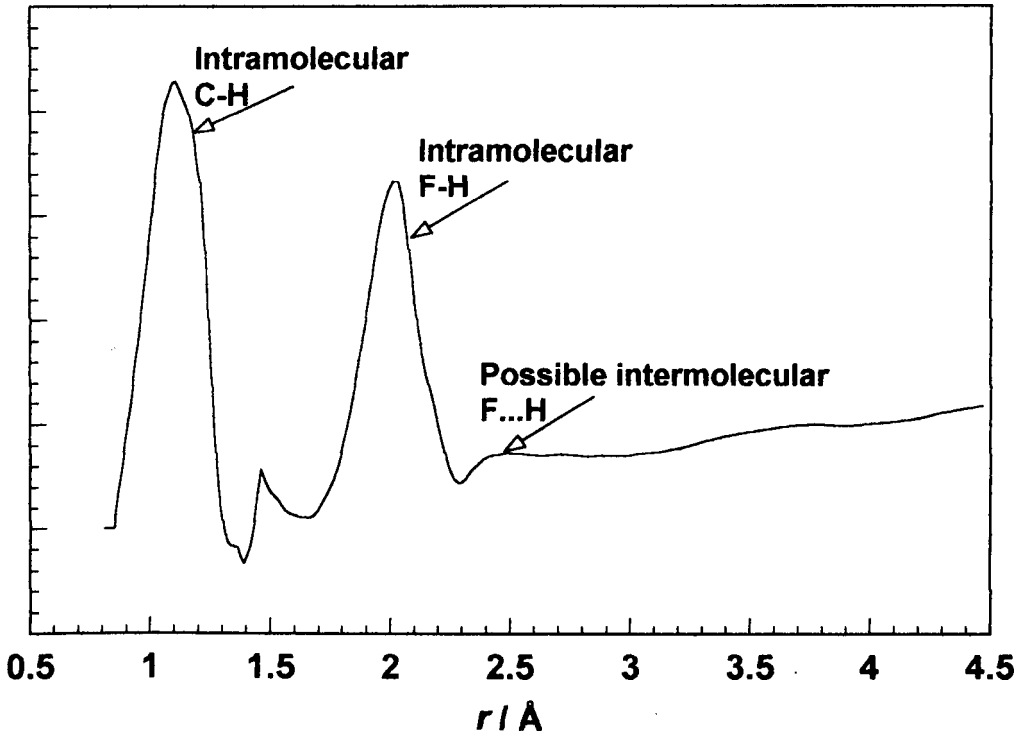

Figure 5.4 A subset of the total pair distribution function obtained from a suitably weighted subtraction of the pair distribution functions obtained for CHF_3 and CDF_3. In the subtraction, contributions from C-F interactions are removed.

Figure 5.4 illustrates the results of this subtraction. Within the intramolecular region, only the C-H bond and H...F distance peaks are left. The C-F bond distance has been subtracted out quite successfully. In the intramolecular region there is evidence of a peak at a distance as low as 2.5 Å. It is thought that this could be a H...F intermolecular peak. If so, this distance is quite short and could indicate the presence of hydrogen bonding between the molecules. No further information about the intermolecular structure can be extracted from the experimental results.

5.2.2 Molecular Dynamics Simulations

Molecular dynamics simulations employing 125 molecules, were performed on IBM RS6000 workstations using the DLPOLY [7] augmented with our own routines for analysing pair distribution functions.

5.2.2.1 Simulation Results

A lattice of 125 molecules was set up in a cubic array. The potential used in the molecular dynamics simulation was varied until the simulation reproduced the pair distribution functions from the neutron scattering experiments and the internal energy calculated from tables. Initially the simulation was performed using CDF_3 molecules and the potential fitted to the deuterated trifluoromethane experimental data at 153 K. Once a fit was obtained the partial pair distribution functions were neutron weighted and summed to reproduce the hydrogenated data and compared to the experimental data for trifluoromethane at 153 K. The simulation was then repeated using CHF_3 molecules and the same potential parameters to ensure that there was no discrepancy in the simulation. It was found that both simulations produced the same results for the pair distribution function and the internal energy. To examine the possibility of cut-off errors in the potential affecting the short-range structure, the simulation was run using 216 molecules in the molecular dynamics cell. After the simulation had equilibrated over 80,000 time steps, no discernible difference was seen in the short range structure of the two simulations up to 11 Å, which is half the box length of the smaller simulation. It was concluded therefore that the 125 simulation was sufficient to reproduce the intermolecular structure up to half its box length.

In order to test the potential produced, CDF_3 was simulated at 250 K using the parameters optimised at 153 K, and the pair distribution function was compared to the corresponding neutron data.

	q
C	0.296
F	-0.151
H	0.157

	ε/Jmol^{-1}	σ/Å
C...C	449.35	3.10
C...F	453.95	3.06
F...F	413.51	2.76
H...F	298.77	2.50
H...C	255.29	2.66
H...H	86.84	2.10

Table 5.2 Potential parameters and partial charges used in the simulation of CHF_3.

Temperature / K	experiment [13] / kJmol^{-1}	simulation / kJmol^{-1}
153	-17.6 ± 0.3	-17.6 ± 0.2
250	-10.3 ± 0.3	-9.74 ± 0.3

Table 5.3 Comparison of experimental internal energy and the configuration energy from the simulation for CHF_3

The final potential parameters used in the simulation are shown in table 5.2. The comparison of the configuration energy of the simulations at 153 K and 250 K with the corresponding internal energy at these two temperatures, is shown in table

5.3. As can be seen, the fitted simulation reproduces the internal energy exactly. The high temperature simulation also reproduces the internal energy reasonably well. Figure 5.5 shows the comparison between the experimental neutron data and the three simulations. As can be seen, the fit to the deuterated data at 153 K is excellent. The comparison between the hydrogenated data and the simulation is reasonably good. There is a discrepancy in the height of the first shoulder, but this region is fitted well in the deuterated data. It could be surmised the discrepancy lies in the neutron data due to the difficulties involved in the analysis of hydrogenated data. If an attempt were made to improve the fit to this region of the data it is found that the fit to the corresponding deuterated data is worse. The comparison between the deuterated data at 250 K and the simulation at this temperature is very good, with only a slight over estimation in the height of the first shell. It would appear, therefore that the potential fitted at 153 K is valid over at least a temperature range of 100 K.

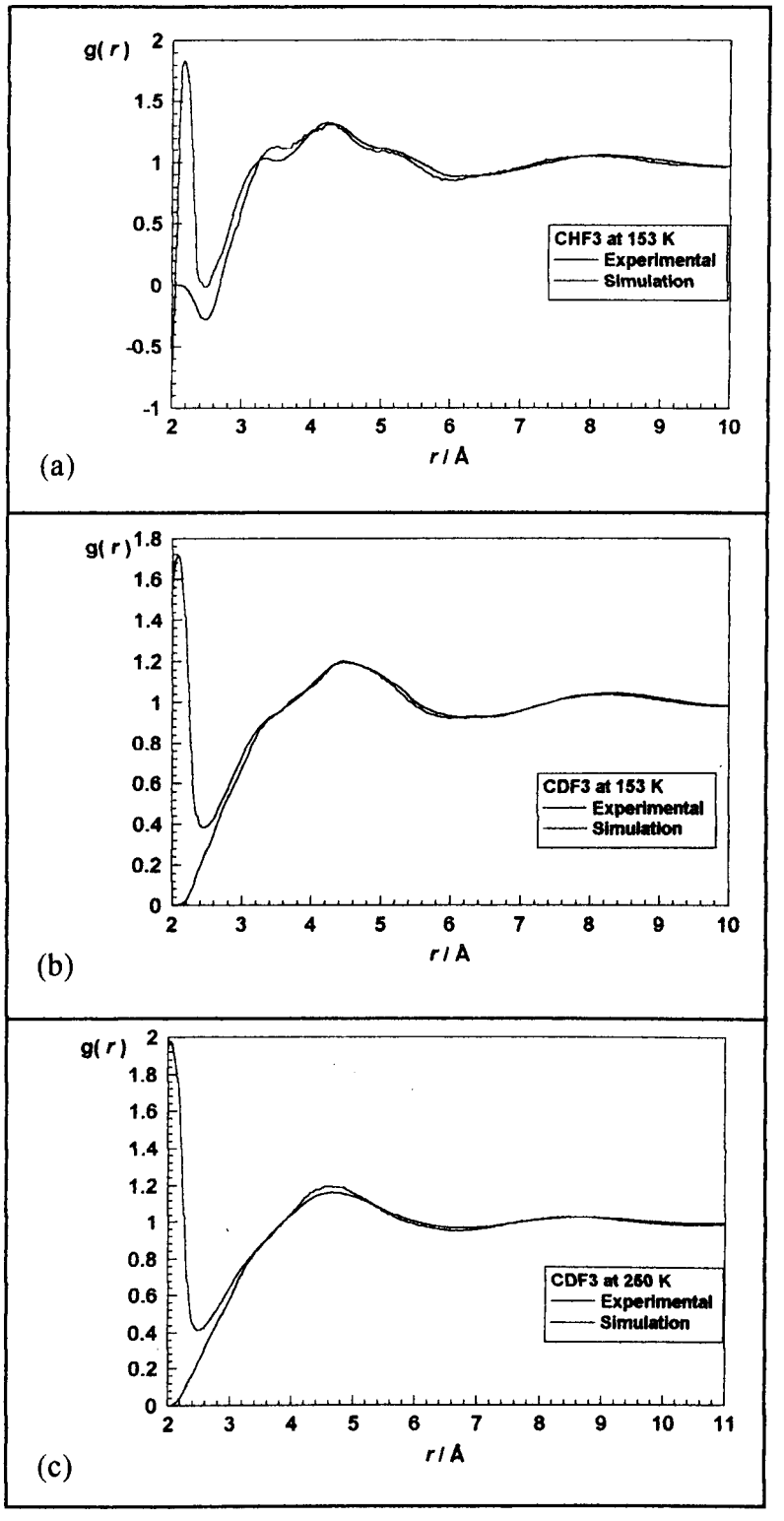

Figure 5.5 Comparison of molecular dynamics simulation pair distribution functions with neutron diffraction data. (a) CHF_3 at 153 K. (b) CDF_3 at 153 K. (c) CDF_3 at 250 K.

5.2.3 Interpretation

In order to extract meaningful information from the partial pair distribution functions it is helpful to have some model of what features one might expect the liquid structure to exhibit. There are two possible orientations of tetrahedral molecules which one would anticipate on the basis of packing arguments. These are namely the 'rocket' or 'Apollo'[8] conformation and the 'straddle'[9] conformation, both depicted in figure.5.6.

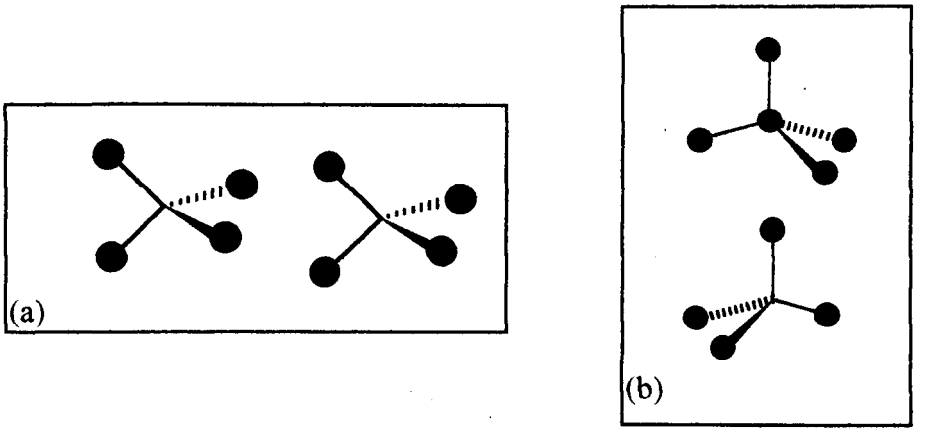

Figure 5.6 Diagram of (a) straddle and (b) rocket arrangement

If the partial pair distribution functions, shown in figure 5.7, from the simulation are summed without neutron weighting, then the resulting pair distribution function can be integrated to give a co-ordination number for the liquid:

$$Z \equiv 4\pi n \int_0^{r_m} g(r)\, r^2\, dr \qquad 5.2$$

In this equation, Z is the co-ordination number, $n^2 = N(N-1)V^2$ is the conditional probability density of finding a molecule a distance r from the centre of a given molecule, N is the number of molecules, V is the volume occupied by N molecules, and r_m is the value of r where the integrand is at its first minimum. Integrating the total pair distribution function from the simulation at 153 K up to $r_m = 6$ Å gave a co-ordination number of approximately twelve. This is the maximum number of molecules that can be fitted around one molecule, and so it appears to indicate a close packed structure. A hydrogen-bonded structure would be expected to be more open, leading to a lower co-ordination number. A value of twelve suggests that the structure is driven by volume minimization. By applying this integration method to the partial pair distribution functions it is possible to obtain an indication of the number of atoms involved in the first peak of each of the distributions, and this is shown in table 5.4. By using this information together with the partial pair distribution functions an attempt was made to try to understand how the molecules were orientating themselves within the liquid phase.

X...Y	Position of Maximum of Peak (Å)	Approximate Co-ordination Number
H...H	4.2	12
H...F	2.6	5
H...C	3.7	3
F...F	3.1	6
F...C	3.6	5
C...C	4.3	12

Table 5.4. The co-ordination numbers for the first peak in each individual pair distribution function. The co-ordination number indicates the number of atoms Y around atom X.

It was found that no single arrangement of two molecules could satisfy all the distances in the partial pair distribution functions. In particular the close H...F distance of 2.6 Å posed great problems. It was found that the straddle arrangement , shown schematically in figure 5.8, satisfied the majority of interactions, except for the low H...F distance. However, when the molecules were placed in a close-packed lattice, with the molecules being placed straddle to each other in each layer, then the rest of the distances, including the short H...F distances were satisfied. Although it cannot be said for certain that this is the way the molecules arrange themselves in the liquid it is the only solution that satisfies all the simulation results, without introducing pair interactions that do not appear in the partial pair distribution functions. Obviously this type of structure is not a permanent arrangement as the

structure of the liquid is dynamic, but it is thought that this is how the molecules prefer to be arranged.

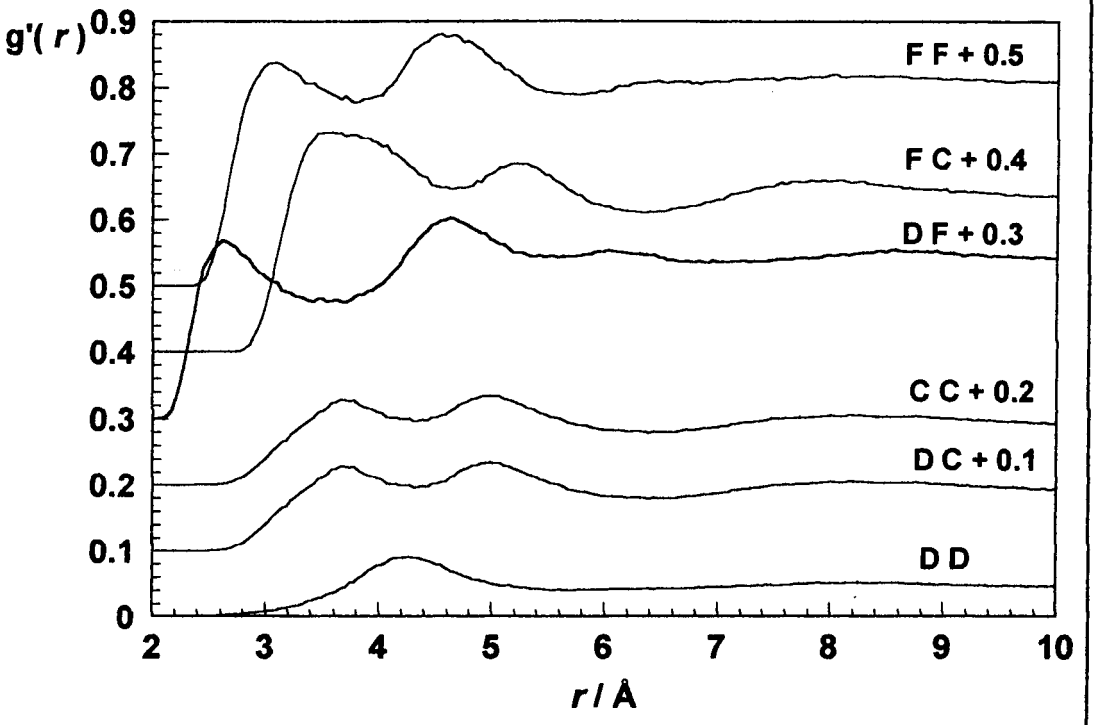

Figure 5.7 Individual pair distribution functions g'(*r*) as obtained from the computer simulation for CDF_3 at 153 K. In the figure each pair distribution has been neutron weighted. The total pair distribution function is obtained by a simple summation of these pair distribution functions. For clarity each curve has been displaced vertically by the amount indicated in the diagram.

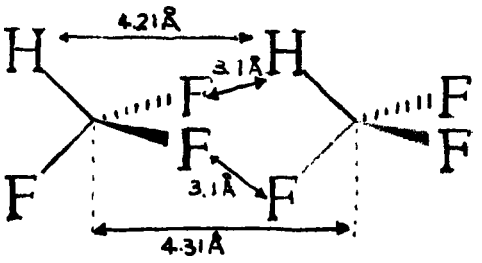

Figure 5.8 Schematic of the proposed structure for trifluoromethane in the liquid phase.

The structure for solid trifluoromethane has been published [10] and the agreement between our proposed liquid structure and the solid state structure is encouraging. It was found that the close non-bonded distances in the solid agree with those found in the liquid phase. In addition, although the unit cell does not contain any straddle arrangements, when the crystal structure is built up by repeating the unit cell it can be observed that the molecules do appear to arrange themselves in this orientation across adjacent cells.

5.2.4 Conclusions

The main conclusion of this work is that the liquid structure of trifluoromethane is driven by coulombic interactions and volume minimisation rather than hydrogen bonding. To justify this statement it is important to define what has been considered as hydrogen bonding. Thus, consider two molecules containing a highly electronegative atom, such as fluorine, and hydrogen. Hydrogen bonding is caused when a lone pair of electrons on fluorine is partially donated to the hydrogen and forms a partial bond between them. The strength of this bond is determined by the degree of displacement of the electron density in the formal bond that the hydrogen is involved with (in the case of trifluoromethane, between the hydrogen

and the carbon) from the hydrogen and onto the other atom. This shift in electron density leaves the hydrogen more able to accept the lone pair from the fluorine. Given this definition, if there is hydrogen bonding in trifluoromethane, the C-H...F bond angle must be close to 180° and, because the lone pairs on the fluorine are in p orbitals, the C-F...H must be close to 90°. In addition the H...F distance would be shorter than expected for non-bonding.

As can be seen in table 5.4 there are five fluorine atoms associated with each hydrogen at an average distance of 2.6 Å. The sum of the van der Waals radii for H...F is 2.55 Å. As a comparison, the hydrogen bonded O...H distance in water is 1.8 Å compared with the sum of the van der Waals radii of 2.6 Å. This alone indicates that there is no hydrogen bonding in this structure. If, in addition, consideration is given to the orientational arrangement of the molecules, there is further evidence of a lack of directional hydrogen bonding. For example, if the C-H...F bond angle is close to 180°, then there must be evidence of a C...F separation of 2.6 Å + 1.1 Å = 3.7 Å. The most dominant C...F peak occurs at a separation of less than this (3.6 Å), which is indicative of an average C-H...F bond angle of 150°. Alternatively, if the C-F...H bond angle is close to 90°, then there must be evidence of a C...H separation close to 2.9 Å. The first C...H peak occurs at a separation much greater than this (3.7 Å), which is indicative of an average C-F...H bond angle of 140°. Finally, although there is significant orientational ordering, as indicated by the similarity between the H...H and the C...C partial pair distribution functions, the molecules are close packed, suggesting that the orientational ordering is due simply to the effect of the Coulombic interactions. Taking this into consideration, together with the lack of evidence of a shift in the

vibrational frequency of the C-H bond [11], then it can be concluded that trifluoromethane does not hydrogen bond in the liquid phase.

5.3 Difluoromethane

Difluoromethane has been studied using neutron diffraction and also by molecular dynamics simulations.

5.3.1 Neutron Diffraction Experiments

Difluoromethane was supplied by ICI at a purity of > 99 %. The liquid was studied using neutron diffraction on the SANDALS facility at the pulsed neutron source, ISIS, at the Rutherford Appleton Laboratory. The liquid was held in a container that has a slab geometry and was constructed of a null scattering titanium-zirconium alloy. The diffraction data were collected at 153 ± 1 K. The data were analysed using standard correction routines [4] to obtain differential cross-sections. Care was taken on the selection of suitable parameters for the Chebyshev polynomial used to subtract the self-scattering from the differential cross-sections.

5.3.1.1 Neutron Diffraction Results

The S(Q) obtained from the experiment for difluoromethane is shown in figure 5.9. This data was then analysed using the minimum information routine of Soper [5] and the pair distribution function obtained is shown in figure 5.10

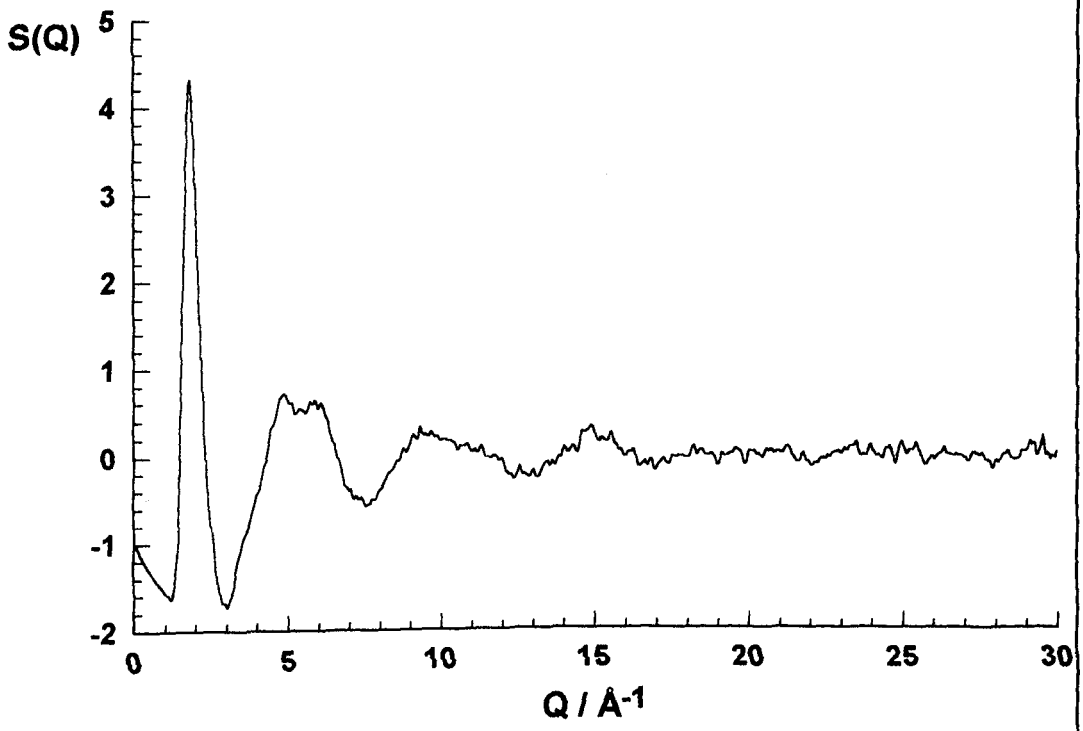

Figure 5.9 S(Q) for difluoromethane at 153 K

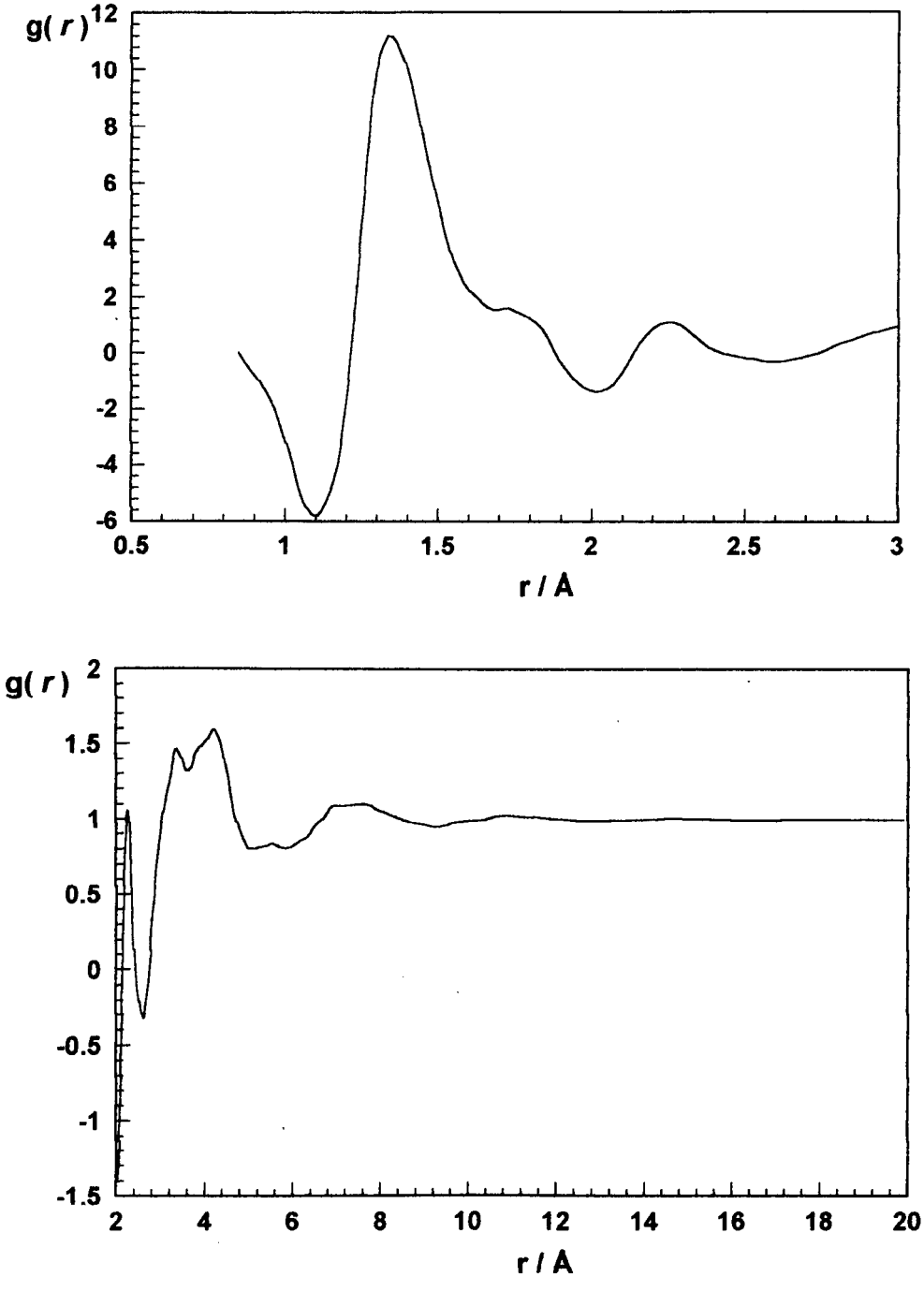

Figure 5.10. Experimental pair distribution function for CH_2F_2 at 153 K

5.3.1.2 Interpretation

As can be seen from figure 5.10, difluoromethane is not as structured as trifluoromethane at 153 K. Only three shells are visible with the long range structure being effectively random beyond approximately 13 Å. It would appear, therefore, that the long range forces are not as strong in difluoromethane as in trifluoromethane. Table 5.5 shows the intramolecular structure of the molecule obtained from the neutron data.

	r / Å
r_{CH}	1.10
r_{CF}	1.32
r_{HH}	1.75
r_{HF}	2.05
r_{FF}	2.25

Table 5.5. Intramolecular structure for difluoromethane from neutron scattering experimental data.

Beyond the intramolecular region of the pair distribution function there is a negative peak at 2.6 Å. This is the H...F intermolecular distance. This distance is too long for a hydrogen bond so it is probable that difluoromethane does not hydrogen bond in the liquid phase. This conclusion is supported by the lack of long range ordering seen in the pair distribution function. It is impossible to assign any other intermolecular distances in the experimental pair distribution function and further interpretation can be obtained by reproducing this distribution function using molecular dynamics simulations.

5.3.2 Molecular Dynamics Simulations

Molecular dynamics simulations employing 125 molecules, were performed on IBM RS6000 workstations using the DLPOLY [7] augmented with our own routines for analysing pair distribution functions.

5.3.2.1 Simulations Results

Unfortunately we have been unable to reproduce the structure from the neutron diffraction data. Figure 5.11 shows a comparison between the latest results and the neutron diffraction data. No structural analysis of this simulation has been done as we have failed to reproduce the neutron data with sufficient accuracy. The intermolecular H...F peak is overestimated, although the difference in height could, in part, be due to the overlap of the intramolecular F...F peak in the experimental data. The shape of the first shell is not reproduced very well, although the second peak is matched by the shoulder of the simulation's first shell. The plateau between the first and second shell is reproduced, and the fit to the second shell is far better than the first shell.

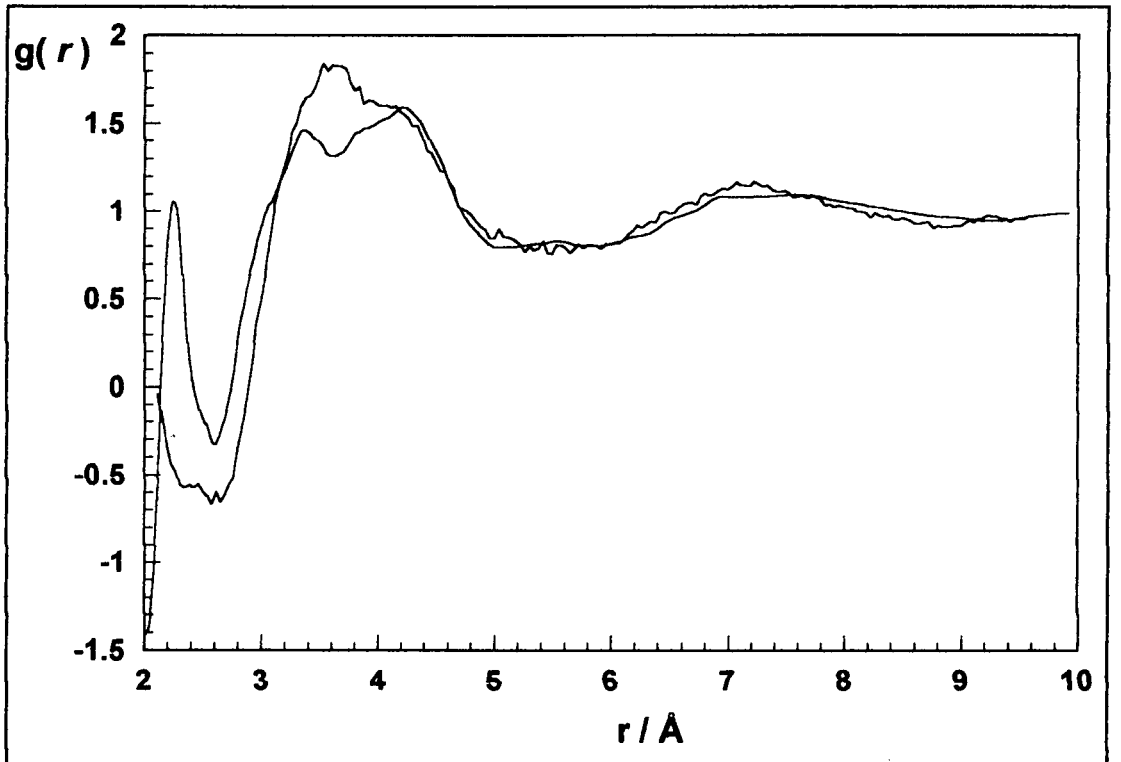

Figure 5.11 Comparison of simulation results with neutron diffraction for difluoromethane at 153 K

It is not clear why the simulations have failed to produce a reasonable fit to the experimental data. Although there are problems with analysing neutron data from hydrogenated samples because of the high incoherence scattering, the neutron experiment had been conducted over a long period to ensure good statistics were obtained. In addition, the care taken in selecting the parameters for the self subtraction would make it seem unlikely that the error in the neutron data could be as large as the difference in the two structures. The Lennard-Jones parameters for the simulation were chosen to reflect those obtained in the successful trifluoromethane simulation. It seems likely that the problem lies with the modelling of the charge distribution and the induced polarisation within the liquid phase. Although the first peak is overestimated in the simulation, because of the presence of the negative scatterer hydrogen in the molecule produces negative peaks in the partial pair

distribution functions, this could be due to the simulation producing the wrong orientation of the molecules and not necessarily due to excessive ordering in this shell. A further neutron diffraction experiment on deuterated difluoromethane may be beneficial in reducing the number of uncertainties in the problem.

5.3.3 Conclusions

Neutron diffraction experiments have been performed on difluoromethane at 153 K. The data have been analysed and a pair distribution function obtained. The intramolecular structure has been obtained but so far molecular dynamics simulations have been unsuccessful in reproducing this pair distribution function, and so the intermolecular structure remains unknown.

5.4 Bromotrifluoromethane

The neutron scattering experiment for this molecule was performed by Dr. C. D. Hall and the results were given in his thesis [1]. However, only a preliminary attempt was made to simulate the structure of the fluid and this project has involved a more extensive look at this with an improved fit to the experimental data. The molecular dynamics simulations were performed on IBM RS6000 workstations using DLPOLY [7] drawn from the CCP5 library. A site-site Lennard-Jones potential was used, augmented by fractional charges at the atomic sites. Initially the fractional charges were extracted from a Mulliken population analysis from *ab initio* calculations performed using the molecular orbital package GAMESS [12]. However, as justified earlier, these values were considered adjustable in order to obtain the best fit to the data. The Lennard-Jones potential parameters were initially taken from previous work [1], but were varied empirically until the neutron weighted

pair distribution function from the simulation reproduced the experimentally-derived pair distribution function in addition to the configuration energy from the simulation reproducing the internal energy calculated from standard enthalpy of vaporisation tables.

5.4.1 Results

The pair distribution function obtained from the neutron diffraction experiments by Dr. C. D. Hall [1] is shown in figure.5.12. The function was plotted to 20 Å to observe the extent of long range structure in the liquid. Although the intramolecular structure can be inferred directly from the positions of the sharp peaks at low *r*, a better method is to fit them using Gaussian distributions and these are shown in table 5.6. As can be seen from figure 5.12 only two shells are visible indicating that the liquid structure randomises quite quickly with distance. This would suggest that there are no strong long-range forces acting within the liquid and the structure is driven by volume minimisation.

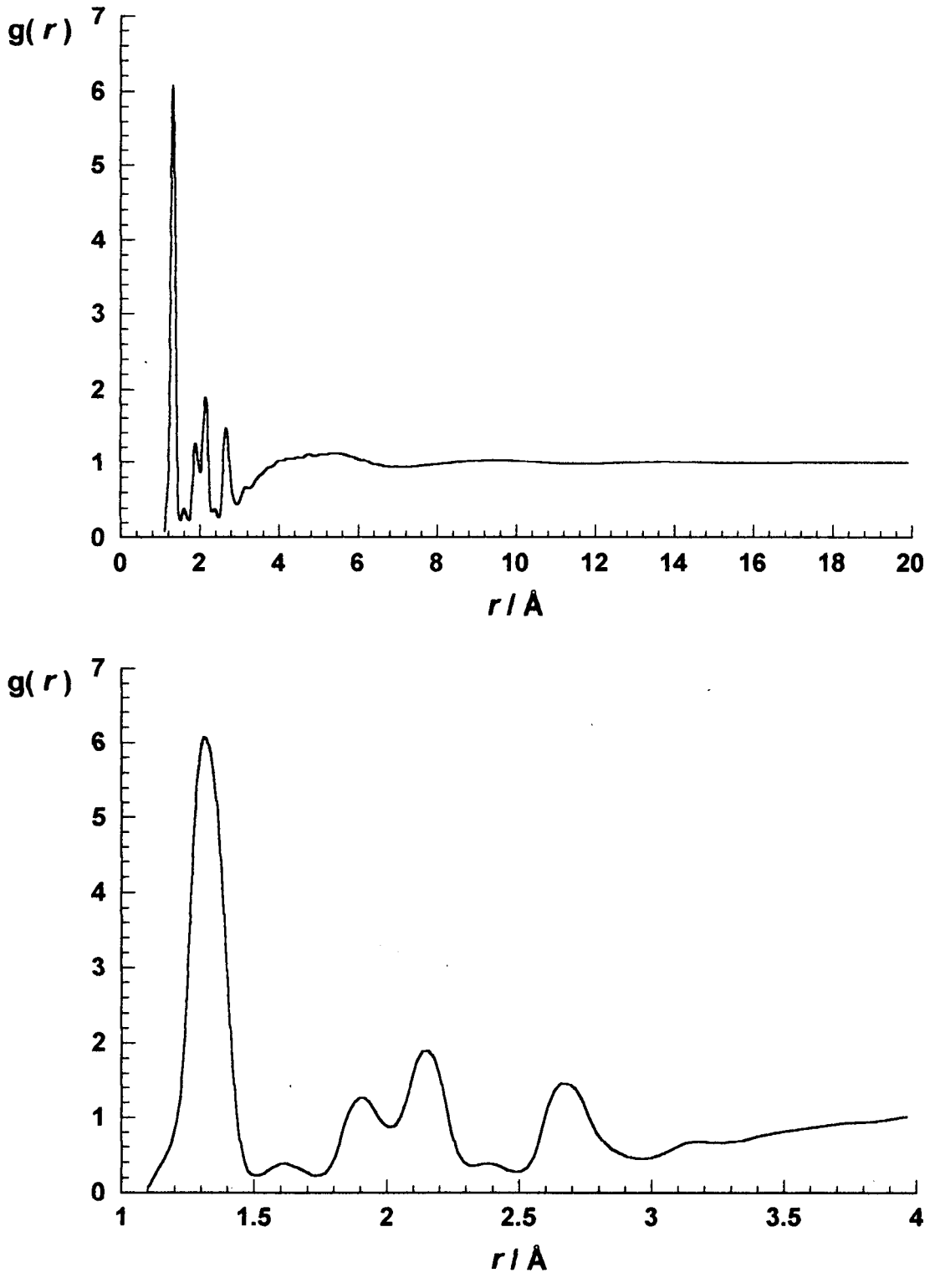

Figure 5.12 Experimental neutron diffraction pair distribution function for $CBrF_3$ at 153 K [1]

	Distance / Å
C-F (bond)	1.328 ± 0.014
C-Br (bond)	1.904 ±0.01
F...F (gem)	2.154 ±0.013
F...Br (gem)	2.676 ±0.011

Table 5.6 Intramolecular structure of $CBrF_3$ derived from experimental neutron scattering.

The comparison between the intermolecular region of the experimental pair distribution function and the neutron weighted pair distribution function from the simulation is shown in figure.5.13. The results from the simulation show only the intermolecular distances and not the intramolecular structure and hence the g(r) at the start of the plot is equal to 0. The comparison between the simulation's configurational energy and the internal energy calculated from enthalpy of vaporisation tables is shown in table 5.7.

experiment [13] / kJmol^{-1}	simulation / kJmol^{-1}
-19.2 ± 0.23	-19.57 ± 0.12

Table 5.7 Comparison between the experimental internal energy and the simulation's configurational energy at 153 K

The fractional charges and Lennard-Jones potential parameters used in the simulation are shown in table 5.8. As mentioned earlier, there is little long range

structure and this is reflected in the fact that the fractional charges are low. The polarisability of the bromine is accounted for in the value of ε, rather than the charges as this reproduces the short range effectiveness of this property better than a point charge on bromine.

	Q
C	0.1460
F	-0.0252
Br	-0.0704

	ε/Jmol^{-1}	σ/Å
C...C	394.8	3.35
C...F	350.28	3.085
F...F	310.8	2.82
Br...F	571.2	3.20
Br...C	643.86	3.485
Br...Br	1050.1	3.62

Table 5.8 Potential parameters and partial charges used in the simulation of $CBrF_3$ at 153 K

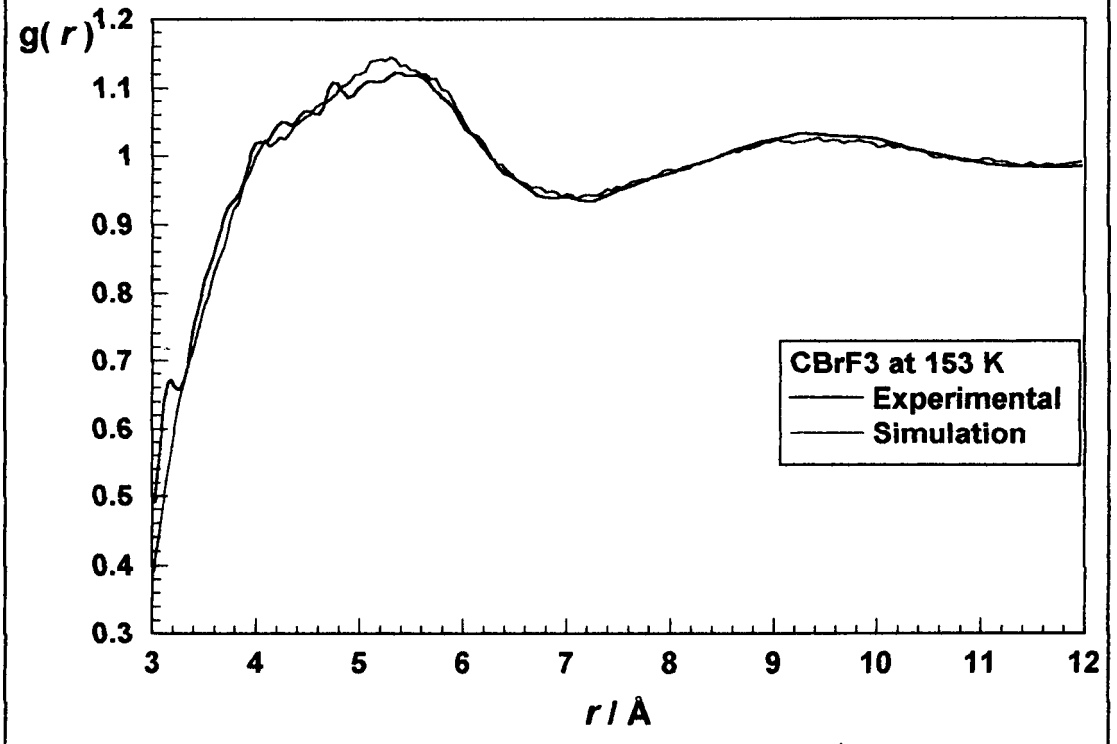

Figure 5.13 Comparison of simulation pair distribution function to neutron experimental pair distribution function.[1]

The simulation reproduces the experimental data very well and can therefore be assumed to be a reasonable representation of bromotrifluoromethane at 153 K. The partial pair distribution functions from the simulation can be analysed to ascertain how the molecules are organised within the liquid phase. The partial pair distribution functions are shown in figure.5.14. These are not true pair distribution functions but have been neutron weighted and number averaged so that a simple summation yields the total pair distribution function.

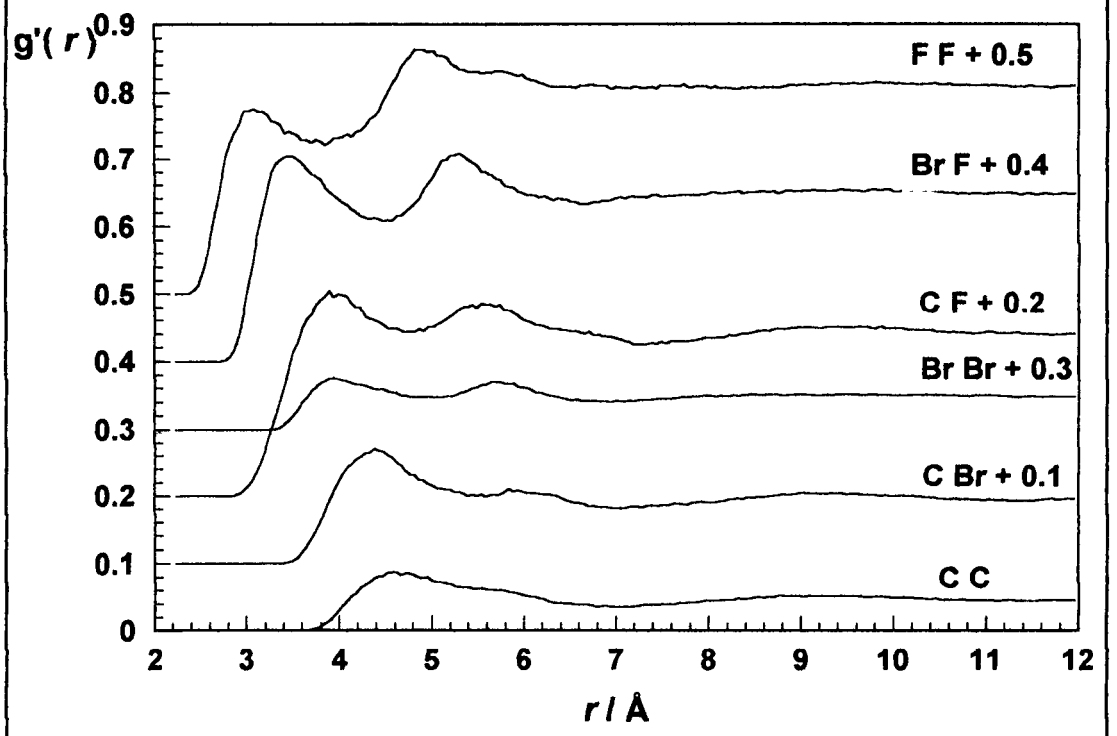

Figure 5.14 The neutron and number weighted partial pair distribution functions for $CBrF_3$ at 153 K. The functions have been separated by 0.1 each to aid clarity.

5.4.2 Interpretation

For bromotrifluoromethane there are eight different possible arrangements of the two molecules and these are illustrated in figure 5.15 and identified as (a) to (h)

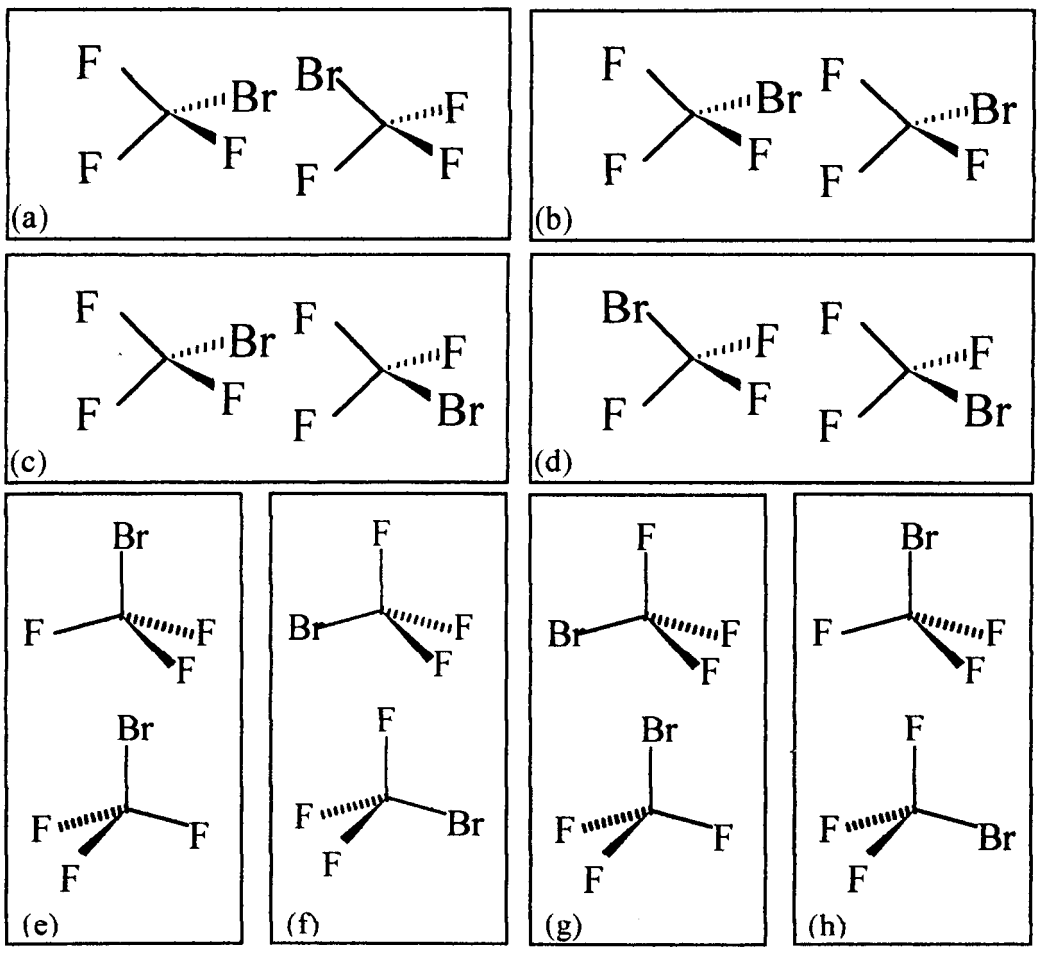

Figure 5.15 Possible arrangements for $CBrF_3$

By considering the positions of the maxima and minima in the pair distribution functions, and by calculating the atomic separations for each arrangement, it is possible to establish which of the arrangements are likely to occur. The C...C distribution shows a maximum at 4.6 Å and a shoulder at 5.8 Å. This would indicate the presence of at least two arrangements. This evidence is supported by the fact that there are two peaks in the Br...Br distribution at 4.0 Å and 5.8 Å. As there is only one bromine atom on each molecule, the two peaks must come from different arrangements. The F...F distribution exhibits peaks at 3.0 Å and 4.9 Å. The

C...Br distribution exhibits peaks at 4.4 Å and 5.9 Å and the C...F peaks are at 3.9 Å and 5.6 Å. The F...Br distributions has maxima at 3.5 Å and 5.3 Å.

The straddle arrangement can achieve closer C...C separations than the rocket as no outer atoms point straight at the other molecule. It would be reasonable, therefore, to assume that the shorter C...C maximum is due to a straddle arrangement and the longer due to a rocket arrangement. If the molecules are arranged as (a) in figure 5.15, with the C...C distance of 4.6 Å, the Br...Br distance is 3.23 Å and the short F...F distance is 3.42 Å. The former is slightly short of the maximum in the distribution, and the latter is slightly long. However it is likely that the molecules will twist to accommodate the much larger bromine atom leading to these distances becoming 4.0 Å and 2.9 Å for Br...Br and F...F respectively. This is in much closer agreement to the distribution functions. The longer F...F separations in this arrangement occur at 4.4 Å, 4.8 Å and 6.3 Å. The first two of these fall within the second F...F peak and the last is in the part of the distribution where no structure is visible. The C...F separations are 3.7 Å and 5.5 Å which agree well with the peaks in the pair distribution functions. The C...Br separation is 4.3 Å which is close to the value for the first maxima in the C...Br distribution. The F...Br separations are 3.5 Å, 4.8 Å and 5.5Å. The first of these is at the maximum for the first peak in the F...Br distribution, the latter two are either side of the maximum for the second peak, but still fall within it.

Many of the separations in the other straddle arrangements, (b) - (d), will be similar to those for (a) so it is only necessary to consider those separations that are different. Arrangement (b) has a separation of 4.6 Å for Br...Br which has a low probability in the distribution. The C...Br separation is 5.8 Å which matches well with the second peak in the pair distribution function. Arrangement (c) has a Br...Br

separation of 6.01 Å. Which, although not at the maximum for the second peak in the Br...Br distribution, has a reasonable probability. The (d) arrangement has no close Br...Br separation, the distance being 7.17 Å. It would therefore appear that, of the possible straddle arrangements, (a) appears to be the most likely.

If we consider the various rocket arrangements with a C...C separation of 5.8 Å, then arrangement (e) will have a Br...Br separation of 5.8 Å which agrees with the separation in the pair distribution function. The F...F separation will vary from 5.8 Å to 6.4 Å. If we examine the F...F pair distribution function in this range then it appears fairly flat which indicates that there is free rotation about the C...C axis. The corresponding C...Br separations are 3.9 Å and 7.7 Å. The latter of these is lost in the second shell and the former, although not at the maximum for the first peak, still has a reasonable probability in the distribution function. As with the straddle arrangements, there are several separations that are repeated in other rocket arrangements and so it is only necessary to examine the different separations. Arrangement (f) has a F...F separation of 5.8 Å. Although there appears to be a shoulder on the second peak at this distance, it is still much lower in probability than the other peaks. This arrangement also gives a F...F separation of 4.2 Å as the short F...F separation. Again this separation appears to have low probability in the pair distribution function. The Br...Br separation will be somewhere between 5.8 Å and 6.9 Å, although the longer distance would be expected to reduce the steric interference between the two bromine atoms. The pair distribution function does not seem to reflect this, having a higher probability for 5.8 Å and a low probability for 6.9 Å. The C...Br separations are 5.5 Å and 6.7 Å. The former of these is short of the second peak maximum and the latter has a low probability. The short C...F distance is 4.4 Å which is close to the minimum in the C...F distribution. The short

F...Br distance is 4.2 Å which is very close to the minimum in the pair distribution function. Arrangement (g) has a Br...Br distance of 3.7 Å, which is short of the maximum but still has a reasonable probability. The F...Br distance in this case is 5.2 Å which is close to the second maximum. Arrangement (h) has a Br...Br separation of 8.6 Å which is in the second shell of the distribution. The Br...F separation is 6.4 Å which has a reasonable probability in the pair distribution function. This suggests that the rocket structure (e) is the most likely.

5.4.3 Conclusions

There is plenty of support in the pair distribution functions for arrangements (a) and (e). However neither or these arrangements explain the C...Br separation of 5.8 Å. Although this peak in the pair distribution function has a much lower probability than the first peak, it is nevertheless of significant probability and so must be caused by another arrangement. The other three straddle arrangements all give this separation. However (b) is unlikely because of the lack of evidence for a Br...Br separation of 4.6 Å. Arrangement (d) has a short F...F distance that is less likely than the maximum but cannot be completely discounted, although it does not provide any Br...Br separation within the first shell. Out of these three arrangements (c) is the most likely and provides the greatest agreement with the rest of the distribution peaks. The rocket arrangements (f) and (h) have a low probability due to the lack of evidence for their low F...F separation, but arrangement (g) agrees with the distribution functions.

Considering the potential parameters it is evident that the interaction between bromine atoms is more favourable than between bromine and fluorine atoms, which is more favourable than between fluorine and fluorine atoms. However

counterbalancing this is the fact that bromine atoms are considerably larger than fluorine atoms and so volume minimisation would favour the reverse order of these interactions. These considerations, together with the evidence from the pair distribution functions suggest that bromotrifluoromethane adopts the arrangements (a), (c) and (e) in that order of preference.

5.5 Chlorotrifluoromethane

The neutron scattering experiments on this molecule were performed by Dr. C. Hall and the result shown in his thesis [1]. Positions of the intramolecular separations were found by fitting the intramolecular peaks using Gaussians. Simulation studies of the liquid structure have been performed with a good fit to the experimental data obtained. The simulations have been performed in the same manner as for bromotrifluoromethane with the Lennard-Jones parameters and fractional charges considered as adjustable in order to fit the experimental data.

5.5.1 Results

The experimental pair distribution function for chlorotrifluoromethane is shown in figure 5.16. The intramolecular separations are shown in table 5.9. As in bromotrifluoromethane, the liquid shows very little long range structure with only the first two shells being clearly visible. Again this suggests that the structure is driven by volume minimisation and that the long range coulombic forces are small.

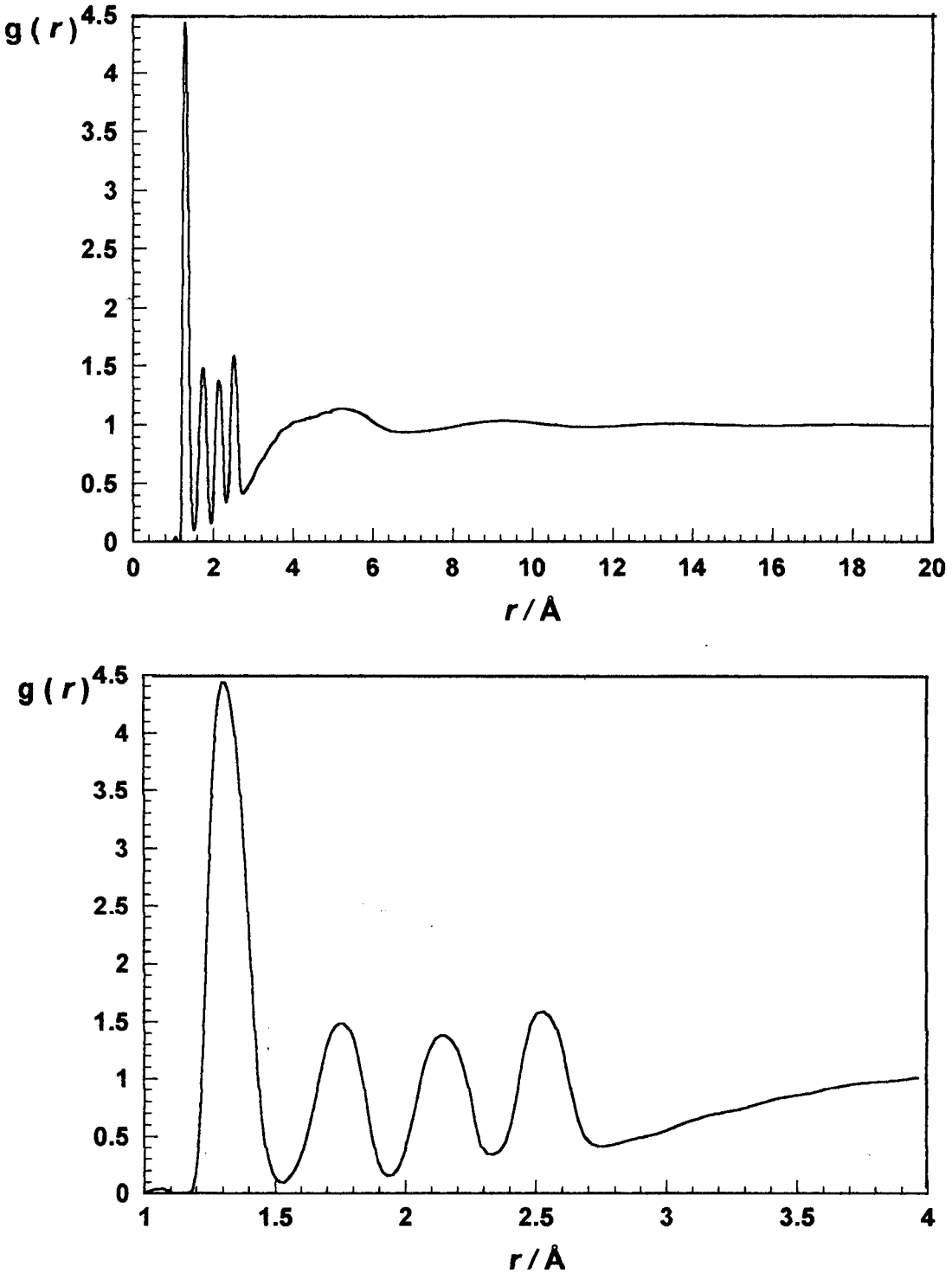

Figure 5.16 Neutron experimental pair distribution function for $CClF_3$ at 153 K

	Distance / Å
C-F (bond)	1.328 ± 0.014
C-Cl (bond)	1.753 ± 0.005
F...F (gem)	2.148 ± 0.005
F...Cl (gem)	2.532 ± 0.005

Table 5.9 Intramolecular structure of $CClF_3$ derived from experimental neutron scattering.

The comparison between the experimental pair distribution function and the pair distribution function obtained by the simulation is shown in figure 5.17. The simulation reproduces the experimental structure well and, as can be seen in table 5.10, correctly predicts the internal energy of the liquid at 153 K.

experiment [5] / $kJmol^{-1}$	simulation / $kJmol^{-1}$
-15.9 ± 0.24	-15.84 ± 0.11

Table 5.10 Comparison between the experimental internal energy and the simulation's configurational energy at 153 K

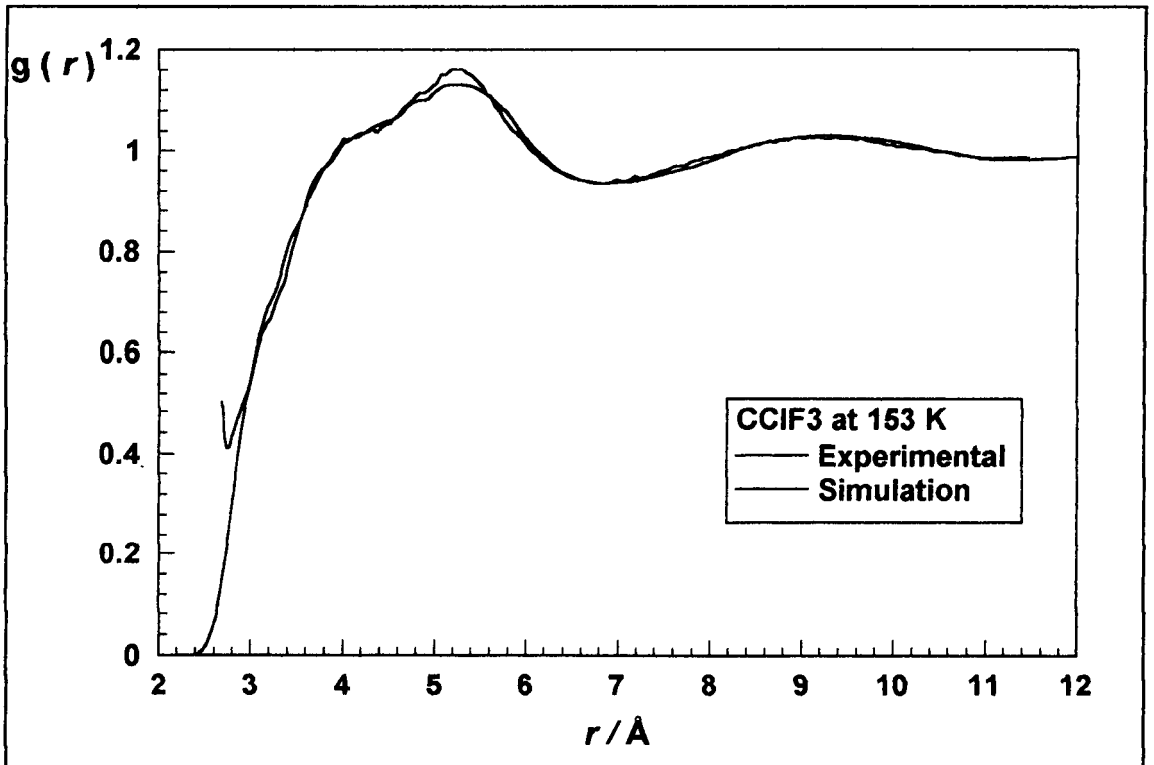

Figure 5.17 Comparison between experimental and simulation pair distribution functions for $CClF_3$ at 153 K

The potential parameters and fractional charges used in the simulation are shown in table 5.11. As in bromotrifluoromethane, the charges are low showing the small contribution they play in the overall structure of the liquid. The polarizability of chlorine is shown in the value of ε. This parameter reflects the range of effect of the polarisability better than a point charge. The values of ε for chlorine are smaller than that for bromine, which is to be expected, as bromine is larger and therefore more polarizable.

	q
C	0.3562
F	-0.1018
Cl	-0.0508

	ε/Jmol^{-1}	σ/Å
C...C	387.4	3.40
C...F	336.0	3.125
F...F	547.0	2.80
Cl...F	450.0	3.10
Cl...C	592.0	3.45
Cl...Cl	1131.1	3.35

Table 5.11 Potential parameters and partial charges used in the simulation of $CClF_3$

The partial pair distribution functions obtained by the simulation are shown in figure 5.18. As can be seen the functions are similar in shape, allowing for the neutron weighting, to those obtained for bromotrifluoromethane, and the analysis reveals a close similarity between the two structures. This is unsurprising as the structure of these liquids is driven by volume minimisation, and each has only one large halogen atom. The possible arrangements for the molecules are the same for bromotrifluoromethane and are shown in figure 5.9

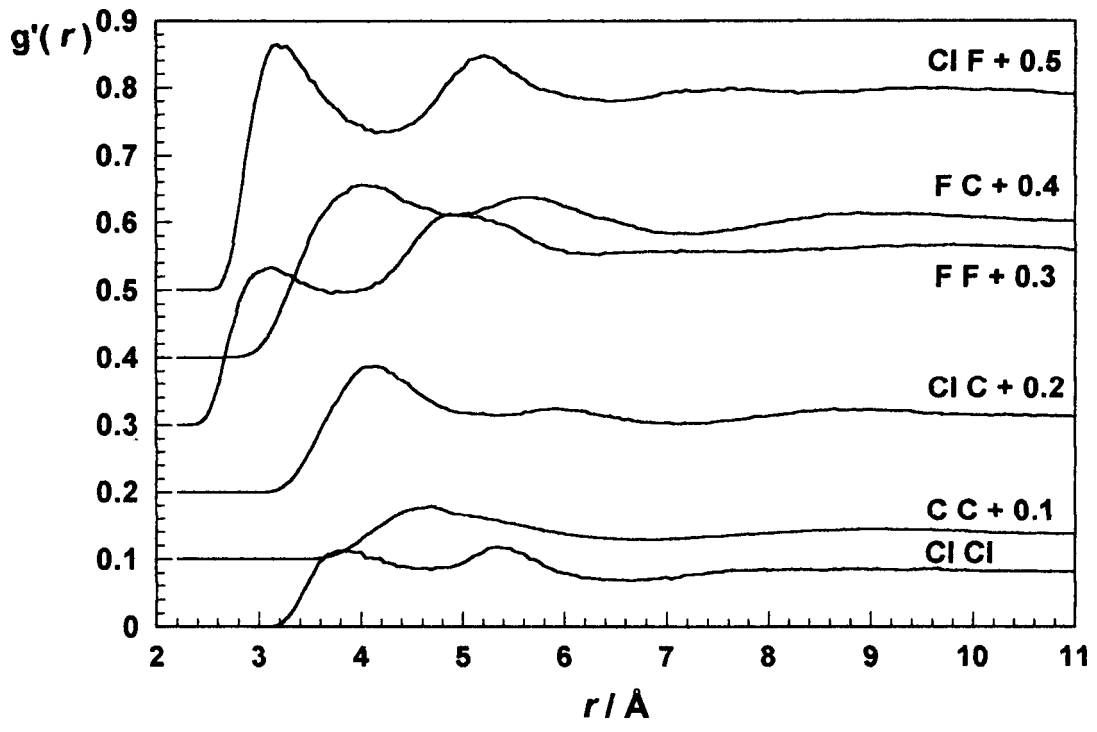

Figure 5.18 The neutron and number weighted partial pair distribution functions for $CClF_3$ at 153 K. The functions have been separated by 0.1 each to aid clarity.

5.5.2 Interpretation

Close examination of the partial pair distribution functions confirms that chlorotrifluoromethane arranges itself in a very similar fashion to bromotrifluoromethane. There is a C...C peak at approximately 4.6 Å with a shoulder at longer *r*. The Cl..Cl distribution shows two peaks, indicating at least two arrangements, with the longer Cl..Cl peak being directly above the C...C shoulder at a distance of 5.5 Å. This would suggest a rocket conformation as shown in figure.5.9(e). Again the associated F...F peaks are smeared suggesting rotation about the C...C axis. The same arguments as before can be used to assign the short Cl...Cl distance (~ 3.7 Å) to the straddle arrangement shown in figure.5.9(a), and the Cl...C

distance of approximately 5.8 Å to the straddle arrangement in 5.9(c). Again there is no evidence for the presence of any other conformation in any appreciable quantity. From the size of the Cl...Cl peaks it would appear that the populations of the 'rocket' and first straddle conformations are approximately equal with the population of the second straddle being smaller.

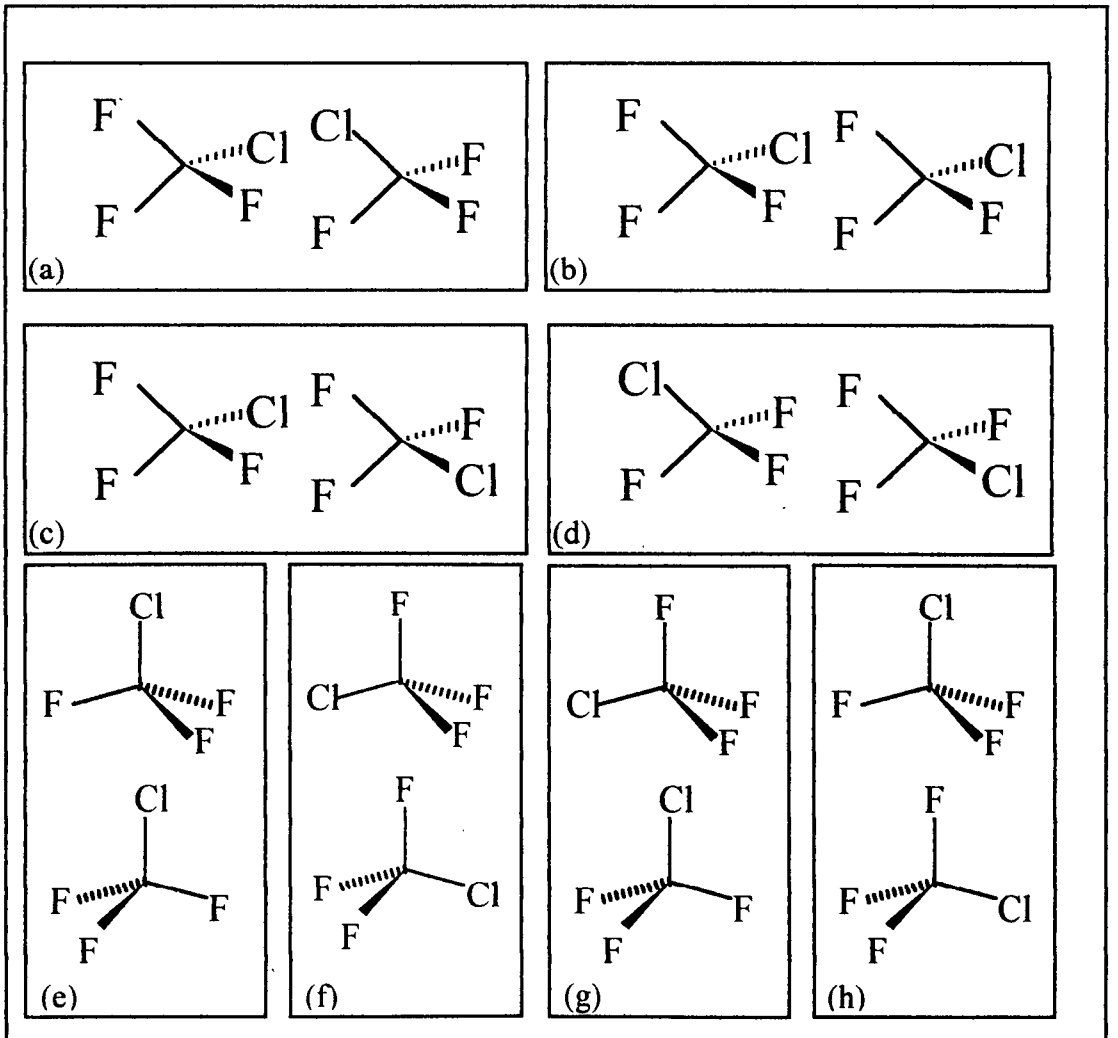

Figure 5.19 Possible arrangements for $CClF_3$

5.5.3 Conclusions

From examination of the simulation results that chlorotrifluoromethane arranges itself in a similar manner in the liquid phase to bromotrifluoromethane and that the most probable configurations are (a), (c) and (e) as shown in figure 5.19.

5.6 Dichloro-difluoromethane

Molecular dynamic simulations were performed to try and reproduce the neutron pair distribution function obtained by Hall et al.[9]. It proved difficult to match the experimental data completely although the final result produces a fair match to the data and the internal energy was reproduced in the simulation. The analysis of the pair distribution function was more difficult, owing to the symmetry of the molecule. However it was possible to rule out various arrangements and draw reasonable conclusions about the way the molecules arrange themselves in the liquid. The conclusions drawn are different to that obtained by C. D. Hall.

5.6.1 Results

The comparison between the neutron pair distribution function and the neutron weighted pair distribution function from the simulation is shown in figure 5.20. It was difficult to match the intermolecular liquid structure for this molecule and the figure shown is the best match obtained in this work, however the match is an improvement on that obtained by Hall et al. [9] The difficulty may be due to the model potential used in the simulation failing to account for the anisotropy in chlorine's potential. However the fit is still reasonable, reproducing the main features of the first shell, and matches the height of the maxima. Table 5.12 shows the configurational energy from the simulation compared to the calculated internal

energy. As can be seen the simulation reproduces the internal energy well and as such can be assumed to be a reasonable portrayal of dichloro-difluoromethane in the liquid phase at this temperature. The potential parameters used in this simulation are shown in table 5.13.

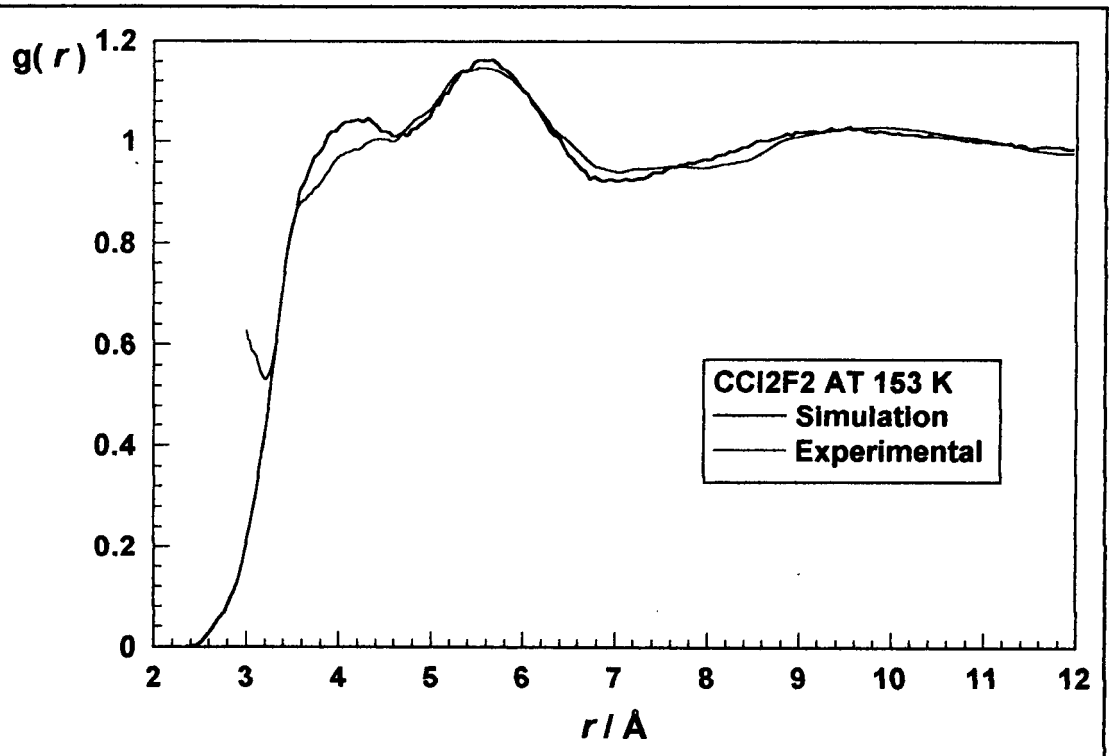

Figure 5.20 Comparison of the pair distribution function obtained by neutron diffraction [7] and molecular dynamics simulation for dichloro-difluoromethane

experiment [5] / kJmol^{-1}	simulation / kJmol^{-1}
-23.1 ± 0.23	-23.74 ± 0.12

Table 5.12 Comparison of experimental internal energy and the configuration energy from the simulation for CCl_2F_2

	q
C	0.18432
F	-0.08352
Cl	-0.00864

	ε/Jmol^{-1}	σ/Å
C...C	613.0	3.40
C...F	336.0	3.125
F...F	347.0	2.80
Cl...F	400.0	3.20
Cl...C	592.0	3.65
Cl...Cl	1131.1	3.35

Table 5.13 Potential parameters and partial charges used in the simulation of CCl_2F_2

The partial pair distribution functions are shown in figure 5.21. As can be seen the C...C distribution has a maximum at 4.8 Å and a shoulder centred at 5.6 Å. There is a minimum in the Cl...Cl distribution at 4.8 Å and a maximum at 5.6 Å. The low *r* peak in the Cl...Cl distribution is at a separation of 3.7 Å. The F...F distribution has maxima at 3.0 Å and 5.2 Å and a minimum at 4.0 Å. The Cl...F distribution has maxima at 3.2 Å and 5.4 Å, and a minimum at 4.3 Å. The Cl...C distribution consists of 1 peak with two shoulders. These are at 4.3 Å, 4.9 Å and 6 Å. The F...C distribution has maxima at 4.0 Å, 4.8 Å and 6.2 Å, and a minimum at 3.2 Å.

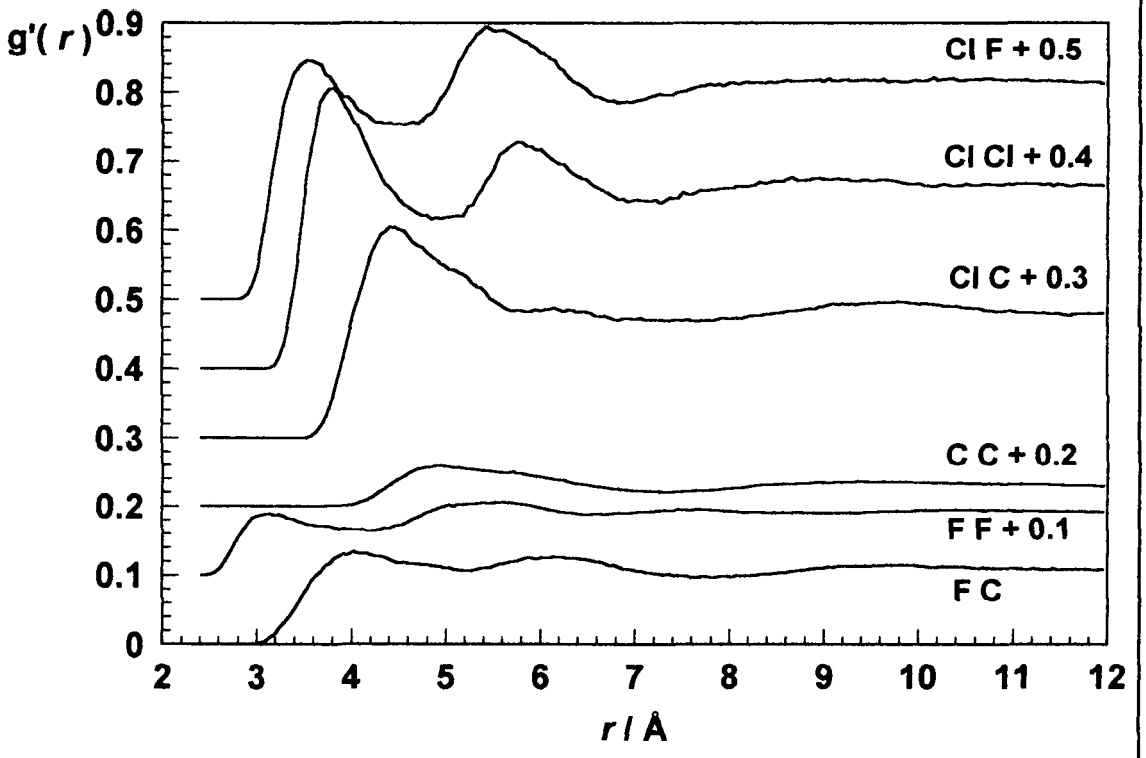

Figure 5.21 The neutron and number weighted partial pair distribution functions for CCl_2F_2. The plots have been separated by 0.1 each to aid clarity.

5.6.2 Interpretation

Figure 5.22 shows the various possible orientations that dichlorodifluoromethane could adopt in the liquid phase.

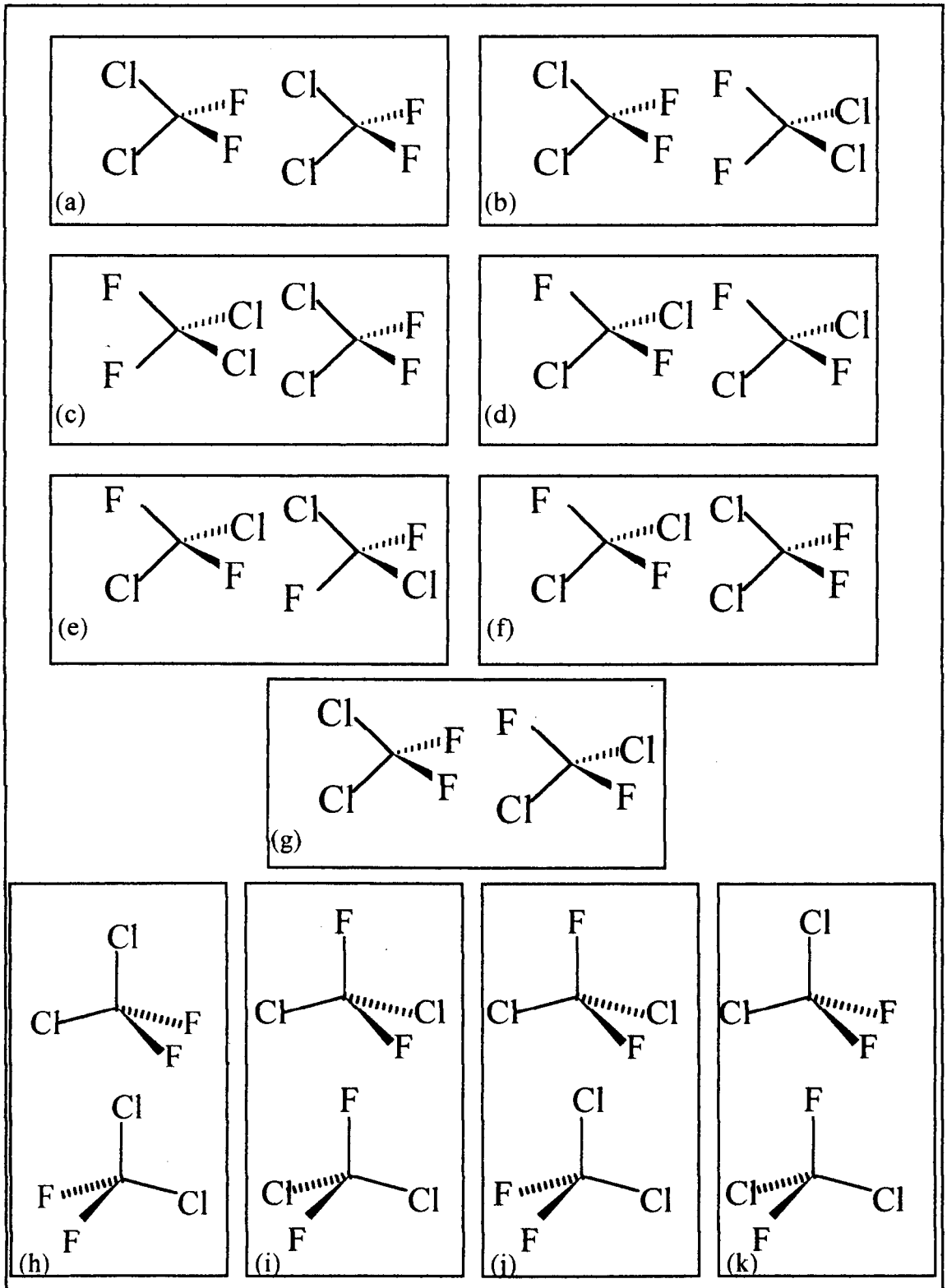

Figure 5.22 Possible orientations of CCl_2F_2 in the liquid phase

(a) - (g) : straddle, (h) - (k) : rocket

As seen previously, the straddle conformation allows the molecular separation to be shorter and so it could be expected that a C...C separation of 4.8 Å would be associated with straddle and a separation of 5.6 Å associated with a rocket conformation. If this is the case then, considering that there is a low probability of a Cl...Cl separation at 4.8 Å, then it would appear that any straddle conformation that gives this separation can be discounted. The arrangements (a), (d) and (f) in figure 5.22 above fall into this category. Of the straddle arrangements, many of the separations are repeated and so it is only necessary to examine a few of them to ascertain the most favourable arrangements. The separation between two Cl atoms facing each other is 3.4 Å, and for two F atoms facing each other, 3.6 Å. The separation between a Cl atom and a F atom facing each other is 3.5 Å. Considering arrangement (a), the distance between the Cl atoms are 4.8 Å and 5.6 Å, and between the F atoms are 4.8 Å and 5.3 Å. The C...Cl distances are 4.05 Å and 6.0 Å and the F...C distances are 4.15 Å and 5.7 Å. Arrangement (a) has already been discounted due to the Cl...Cl separation of 4.8 Å, however many of the other separations are reproduced in the other arrangements. Consider arrangement (b). This has no close Cl...Cl distances and no long F...F distances. The Cl...F separations are 5.10 Å and 6.88 Å which are possible, but this arrangement gives too great a probability for the short F...F at 3.4 Å, when the peak maximum is at 3.0 Å. In fact the short Cl...Cl separation for all the arrangements is really too short and it would seem probable that, as in bromotrifluoromethane and chlorotrifluoromethane, there is some twisting of the molecules to accommodate the size of the chlorine atoms. This would have the effect of lengthening the Cl...Cl distance and shortening the F...F distance. Also, considering the size of the first peak in each of these distributions, and allowing for the contribution from arrangement (h) in the Cl...Cl

peak, it seems likely that there is equal amounts of close F...F and close Cl...Cl in the straddle arrangements. This favours arrangement (e) (arrangement (d) being unfavourable due to the Cl...Cl separation at 4.8 Å.)

Given that there is a high probability of a Cl...Cl separation at 5.6 Å, and the presence of a C...C separation at this distance, it would seem probable that arrangement (h) is present. This is supported by the short Cl...Cl distance in this arrangement, which occurs at 3.6 Å, within the first peak in the Cl...Cl distribution. The remainder of the separations in this arrangement are reproduced in the partial pair distributions from the simulation. The F...F distribution also has a high probability at a separation of 5.6 Å which would support the presence of arrangement (i). However this separation would give a low F...F separation of 4.0 Å, but the F...F distribution has a minimum at this value making this arrangement and arrangement (k) unlikely. Many of the distances in arrangement (j) are the same as for arrangement (h). The separation between the F and Cl atoms that lie on the C...C axis is 5.2 Å, which is present in the Cl...F distribution and so this is another possible arrangement.

5.6.3 Conclusions.

Dichlorodifluoromethane can be simulated using molecular dynamics to reproduce the internal energy and the main features of the experimental liquid structure. The most probable arrangements of the molecules in the liquid phase at 153 K are shown in figure 5.23.

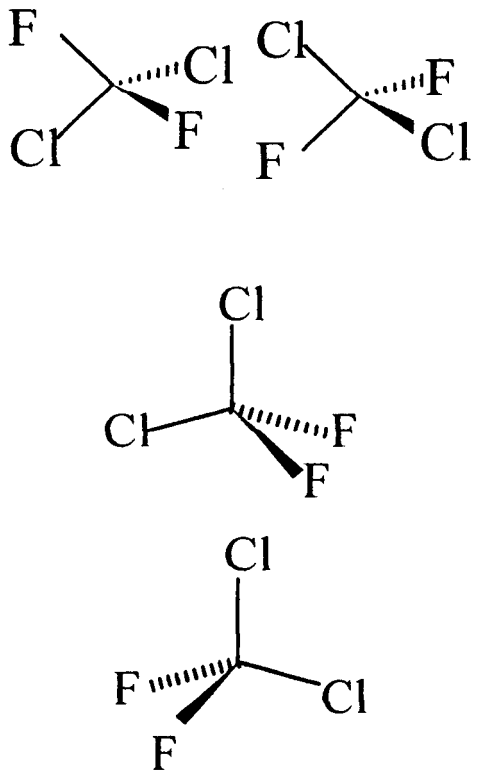

Figure 5.23 Most probable arrangement of molecules in the liquid phase of dichlorodifluoromethane.

5.7 Neutron Diffraction Studies of 1,1,1,2-tetrafluoroethane (R134A)

1,1,1,2-tetrafluoroethane (CF_3CFH_2, R134A) was supplied by ICI at a purity of 99.9%. The experiment was performed at the ISIS facility at Rutherford Appleton Laboratory using the SANDALS diffractometer. The experiment was performed with the assistance of Dr. A. Burgess of I.C.I, and Dr A. Soper of the Rutherford Appleton Laboratory.

The liquid was contained in a cylindrical, thin-walled pressure vessel, constructed of a null-scattering titanium-zirconium alloy. Diffraction data were collected at (200 ± 1) K, (250 ± 1) K, and (300 ± 1) K. The data were analysed using

standard correction routines [4] to obtain the differential cross-sections, and then a fitted Chebyshev polynomial was subtracted from the data to account for the self-scattering.

5.7.1 Results

At this stage only the analysis on the lower temperature has been completed and it is this that has been included here. Figure 5.24 shows the S(Q) obtained from the sample for the lowest temperature, 200 K. Figure 5.25 shows the pair distribution function, g(r), obtained from the S(Q) by using the minimum information method [5] on the data.

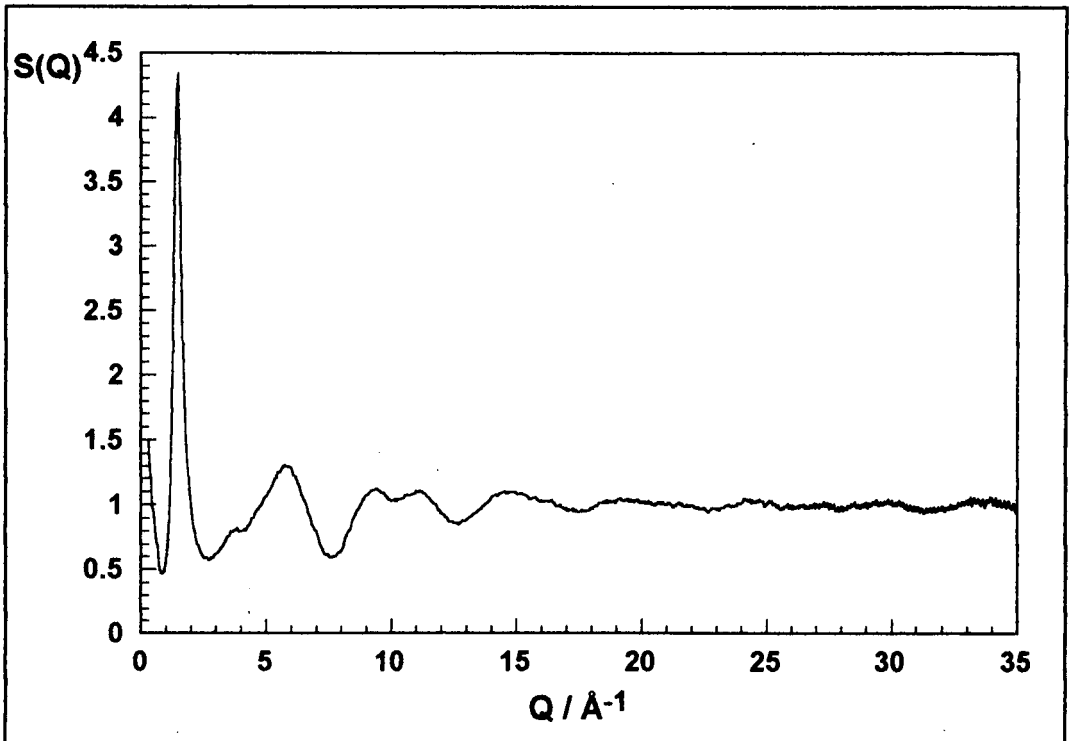

Figure 5.24 S(Q) for 1,1,1,2-tetrafluoroethane at 200 K.

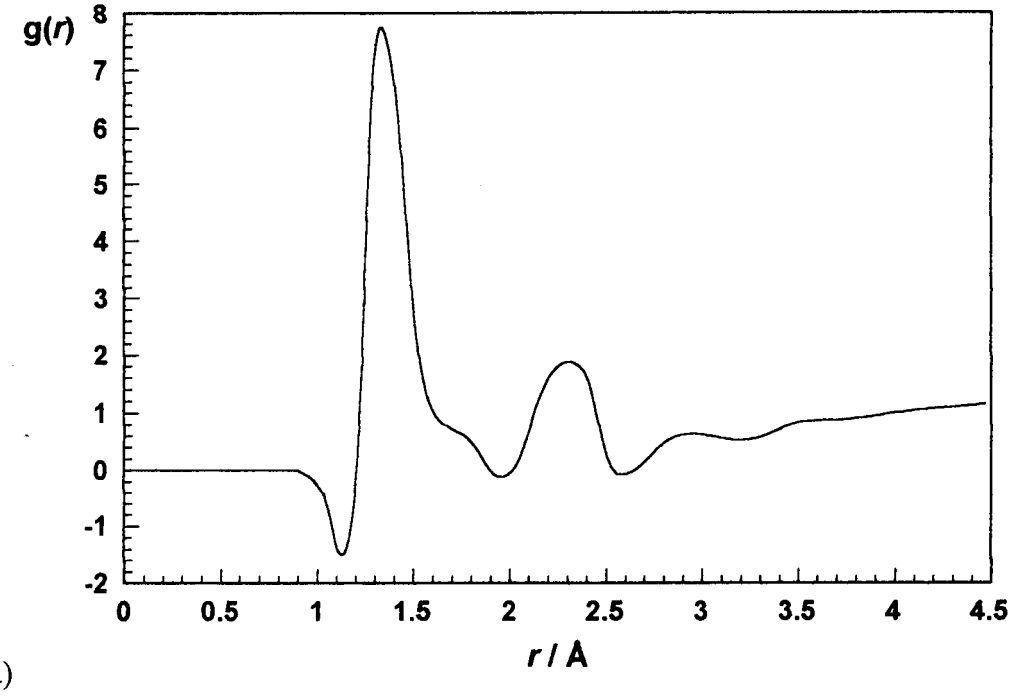

(a)

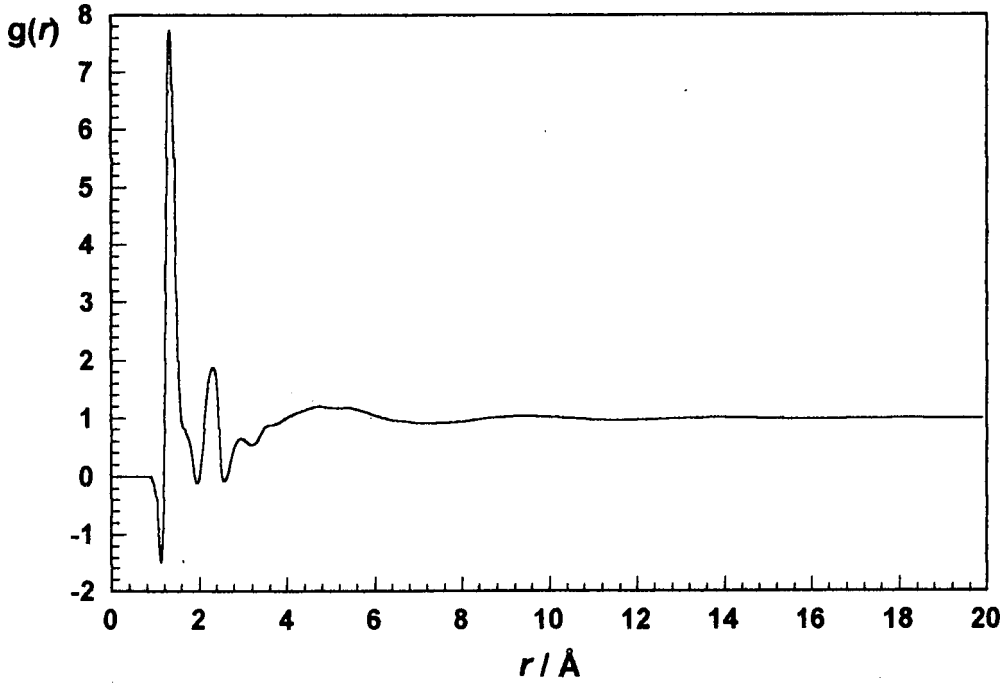

(b)

Figure 5.25 pair distribution function for 1,1,1,2-tetrafluoroethane at 200 K

5.7.2 Interpretation

The negative peak at 1.1 Å and the positive peak at 1.35 Å are due to the average C-H and C-F bond distances respectively. The C-C bond distance would be at 1.5 Å which lies within the first positive peak. The next shoulder at 1.8 Å is probably attributable to the intramolecular H...H distance, with the negative peak at 2.0 Å being the close F...H intramolecular distance. The peak at 2.2 Å will be due to the close F...F intramolecular distance. The peak at 2.4 Å is probably due to the distance between two fluorines that are *cis* to each other on different carbons, and likewise the negative peak at 2.6 Å is probably the *cis* H...F intramolecular distance. Beyond this the intramolecular region and the intermolecular region overlap, making it difficult to assign peaks. Unfortunately we have as yet to perform molecular dynamic simulations on this molecule and this is a project for the near future.

5.8 Neutron Diffraction Studies on 1,1,2,2-tetrafluoroethane (R134)

1,1,2,2-tetrafluoroethane (CF_2HCF_2H, R134) was provided by ICI at a purity >99.9%. The experiment was carried out by with the assistance Dr. K. A. Johnson and Dr. A. Burgess with help from W. S. Howells.

The liquid was contained in a cylindrical, thin-walled pressure vessel, constructed of a null-scattering titanium-zirconium alloy. Diffraction data were collected at 200 ± 1 K, 250 ± 1 K, and 300 ± 1 K. The data were analysed using standard correction routines [4] to obtain the differential cross-sections, and then a fitted Chebyshev polynomial was subtracted from the data to account for the self-scattering.

5.8.1 Results

Again the analysis for this experiment has only been completed at this time for the lower temperature, 200 K. The S(Q) obtained is shown in figure 5.26. This data was transformed into a pair distribution function using the minimum information method of Soper [5]. This g(r) is shown in figure 5.27.

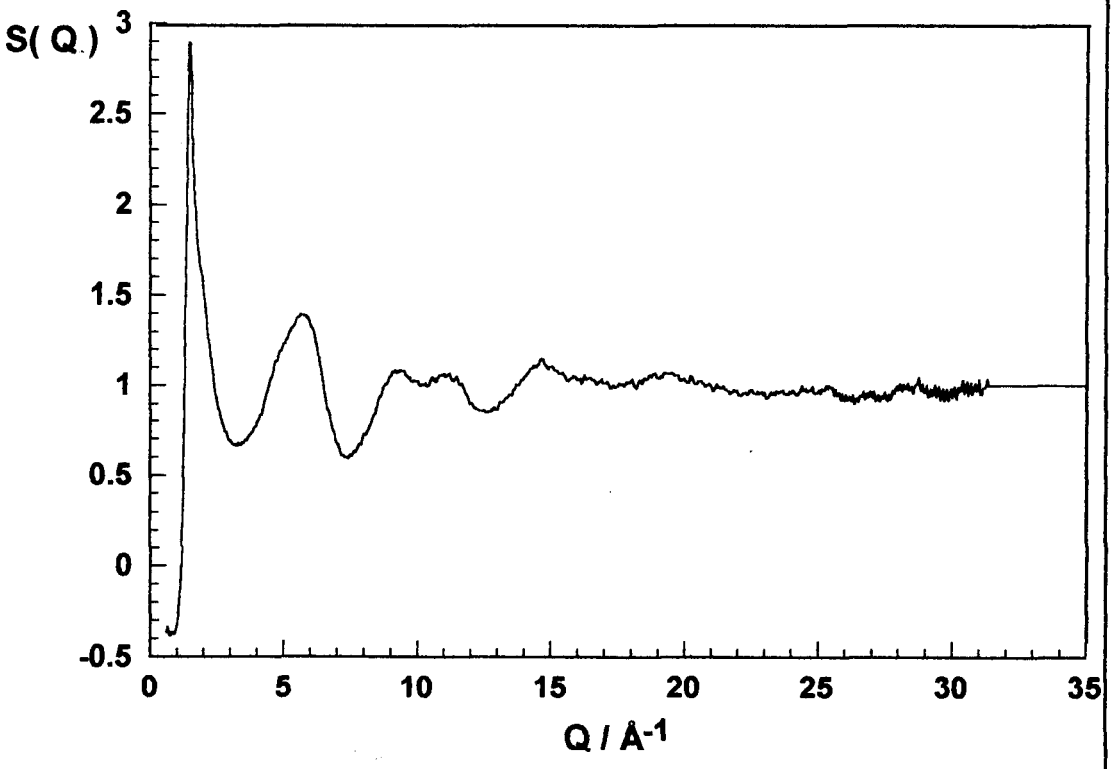

Figure 5.26 S(Q) for 1,1,2,2-tetrafluoroethane at 250 K

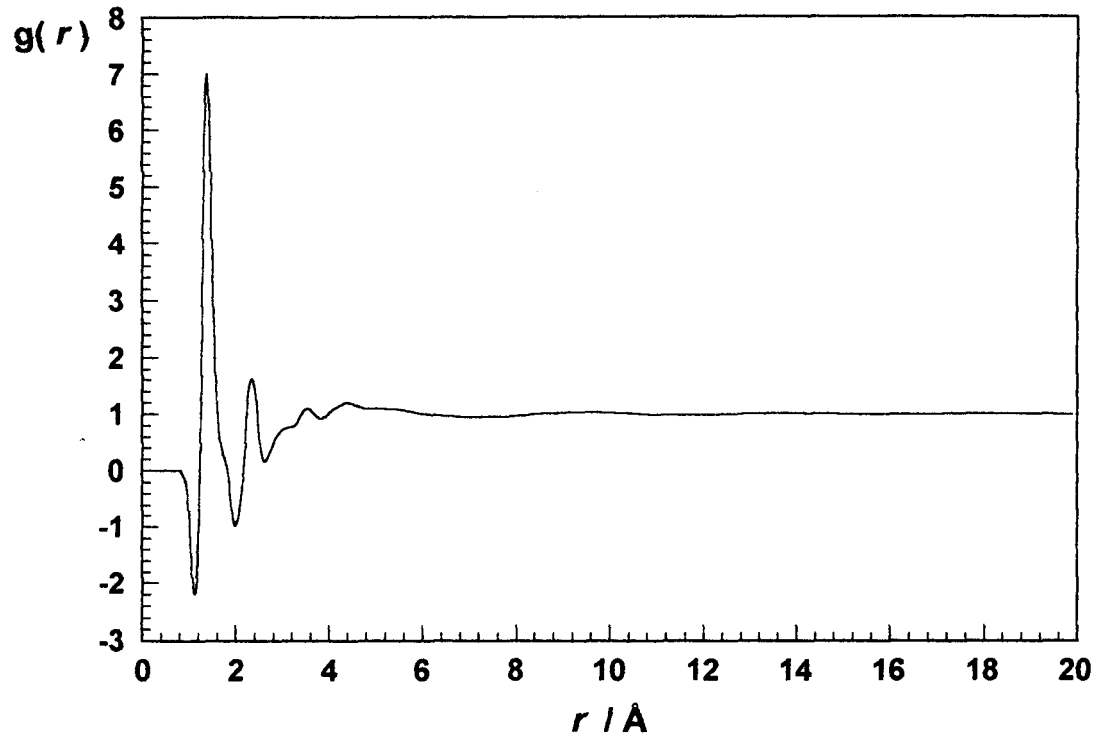

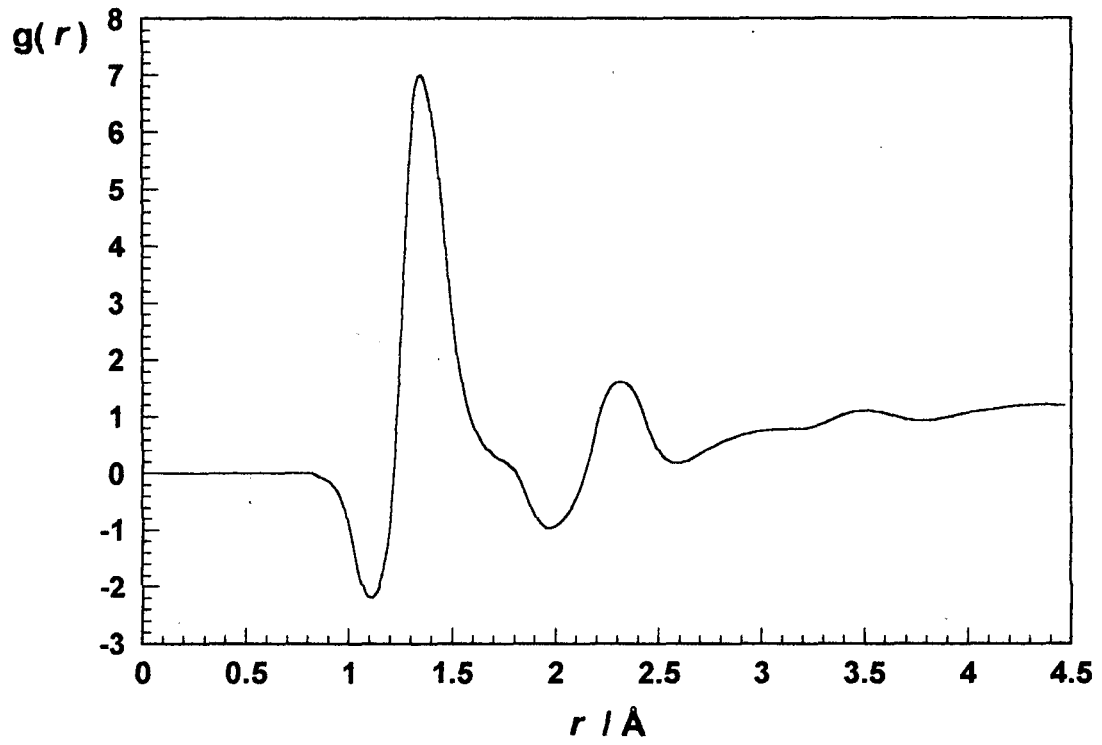

Figure 5.27 pair distribution function from 1,1,2,2-tetrafluoroethane

5.8.2 Interpretation

The negative peak at 1.1 Å is due to the average C-H bond distance. The first positive peak covers both the C-F and C-C bond distance. The C-F bond length is 1.3 Å and the C-C bond length is 1.5 Å. The close F-H distance produces a negative peak at 1.95 Å. The next positive peak is at 2.3 Å and corresponds to the close F-F distance. There is a dip in the distribution function at 2.6 Å which corresponds to the long H-F distance. Beyond this the intramolecular separations are of the same length as the close intermolecular separations, making it difficult to assign peaks.

Molecular dynamics simulations have yet to be performed for this molecule and so an analysis of the intermolecular structure cannot be done at this stage.

---

1 HALL, C.D., *Thesis: Neutron Diffraction and Molecular Dynamics Studies of Fluid Halocarbons*, 1992, *University of Liverpool*

2 MORT, K. A., JOHNSON, K. A., COOPER, D. L., BURGESS, A. N. HOWELLS, W. S.,1997, *Mol. Phys.*, **90**, 415

3 MORT, K. A., JOHNSON, K. A., COOPER, D. L., BURGESS, A. N. HOWELLS, W. S.,1997, *Mol. Phys.*, **90**, 415

4 A. K. Soper, W. S. Howells and A. C. Hannon, 1989, *ATLAS- Analsis of Time-of-Flight Diffraction Data from Liquid and Amorphous Samples*, Ral-89-046 (Chilton, UK: Rutherford Appleton Laboratory).

5 A. K. Soper, 1990, *Neutron Scattering Data Analysis*, edited by M. W. Johnson (Bristol, UK: Institute of Physics).

6 H. J. Bohm, R. Ahlrichs, P. Scharf, and H. Schiffer, 1984, *J. Chem. Phys.*, **81**, 1389

7 T. R. Forester and W. Smith, 1994, DLPOLY: a molecular dynamics program for the simulation of polyatomic molecular liquid mixtures, CCP5 Program Library (Manchester, UK: Daresbury Laboratory).

8 EGELSTAFF, P. A., PAGE, D. I., POWLES, J. G., 1971, *Molec. Phys.*, **20**, 88

9 C. D. Hall, K. A. Johnson, A. N. Burgess, N. Winterton and W. S. Howells, Mol. Phys. 76 (1992) 1061

10 TORRIE, B. H., BINBREK, O. S., 1996, *Mol. Phys.*, **87**, 1007

11 DEZWAAN, J., 1975, *J. Chem. Phys.*, **63**, 422

12 GUEST, M. F., KENDRICK, J., *GAMESS Manual*, Daresbury Laboratory, Warrington, UK.

13 ASHRAE Handbook Fundamentals, 1993 (Atlanta, GA: ASHRAE, Inc.)

Chapter Six

Conclusions and Future Work

Neutron diffraction provides a good method of establishing bulk liquid structure with relative ease. The advances in instruments and analysis techniques make even hydrogenated samples accessible to this method. Molecular dynamics has in the past shown its ability in providing a method for developing potentials by empirically fitting to experimental data. However this project has shown that the combination of both techniques provide a powerful tool in deriving a complete understanding of the liquid structure as well as the intermolecular forces at work within the liquid.

The work has established the structure for several fully halogenated methanes as well as providing a complete understanding of the structure and forces involved in trifluoromethane. Neutron diffraction studies of 1,1,1,2-tetrafluoroethane and 1,1,2,2,-tetrafluoroethane have been performed and the low temperature intramolecular structures have been established. Neutron diffraction has also been performed on difluoromethane, although simulation studies have yet to reproduce the neutron structure.

The problems with simulating difluoromethane need to be investigated, and inadequacies in the potential dealt with. This may mean changing to a more complicated potential function, or the inclusion of multipoles within the forcefield. It would also be interesting to compare the results of a neutron diffraction experiment on deuterated difluoromethane with the hydrogenated, and simulation work.

The higher temperature neutron data analysis of the fluorinated ethanes, when completed, will provide, with the data already analysed, a good set of data for comparisons with molecular dynamics simulations. The range of temperatures will be able to provide a test of the potential as was seen with the deuterated trifluoromethane work.

The potentials already developed could now be implemented in other molecular dynamics simulations to investigate a range of dynamic and thermodynamic data.

It would be interesting to extend the work into mixtures and non-aqueous solutions as an aid to the understanding of solvation effects. Once the potentials have been developed for the pure liquids, the problem would be in calculating the cross-terms for the intermolecular potentials, and again, neutron diffraction results on these mixtures will help in the fitting process.